

3376

NATIONAL LIBRARY

BIBLIOTHÈQUE NATIONALE

OTTAWA



OTTAWA

NAME OF AUTHOR... William D. Ellis

TITLE OF THESIS... A Study of Ligand Binding

to Horseradish Peroxidase

.....

UNIVERSITY... University of Alberta

DEGREE... Ph.D. YEAR GRANTED... 1968

Permission is hereby granted to THE NATIONAL LIBRARY OF CANADA to microfilm this thesis and to lend or sell copies of the film.

The author reserves other publication rights, and neither the thesis nor extensive extracts from it may be printed or otherwise reproduced without the author's written permission.

(Signed) *William D. Ellis*

PERMANENT ADDRESS:

421 County Road 3, Apt. 511
Hopkins, Minnesota 55343
U.S.A.

DATED... December 23, 1968

THE UNIVERSITY OF ALBERTA

A STUDY OF LIGAND BINDING
TO HORSERADISH PEROXIDASE

by



WILLIAM D. ELLIS

A THESIS
SUBMITTED TO THE FACULTY OF GRADUATE STUDIES
IN PARTIAL FULFILMENT OF THE REQUIREMENTS FOR
THE DEGREE OF DOCTOR OF PHILOSOPHY

DEPARTMENT OF CHEMISTRY

EDMONTON, ALBERTA


JULY, 1968

UNIVERSITY OF ALBERTA
FACULTY OF GRADUATE STUDIES

The undersigned certify that they have read,
and recommend to the Faculty of Graduate Studies
for acceptance, a thesis entitled
A STUDY OF LIGAND BINDING
TO HORSERADISH PEROXIDASE
submitted by WILLIAM D. ELLIS, in partial fulfilment
of the requirements for the degree of Doctor of
Philosophy.



H. B. Dunford, Supervisor



R. G. Cavell



R. U. Lemieux



J. A. Flambeck



C. M. Kay



G. G. Hammes, External Examiner

Date JULY 30, 1968

ABSTRACT

The kinetics of the reversible binding of cyanide by ferric horseradish peroxidase was studied at 25.0° and an ionic strength equal to 0.11 over the pH range 4.2 to 11.3 by means of a stopped-flow apparatus. Analysis of the pH dependence of the bimolecular rate constants is consistent with the presence of three heme-linked ionizable groups on peroxidase with pK values of 4.1, 6.4 and 10.8. It is not possible to distinguish whether HCN or CN⁻ is the attacking species but the bound form of the ligand appears to be the cyanide ion.

The optical rotatory dispersion of horseradish peroxidase and its cyanide, fluoride and hydroxide complexes was studied in the spectral region from 215 mμ to 450 mμ, and that of the azide complex from 350 mμ to 450 mμ. The effect that splitting the heme from the protein of peroxidase has on the optical rotatory dispersion in the 215 mμ to 450 mμ region was also studied. Results of measurements of the reduced mean residue rotation at 233 mμ lead to the conclusion that there are no significant changes in gross protein conformation upon the binding of ligands to peroxidase, but that the splitting of the heme causes a reduction of the helical content of the protein. Pure peroxidase was estimated to have 43 % α-helical content, which was reduced to 33 % α-helical content when the heme was split from

the protein. Results of studies in the Soret region indicate that the binding of various ligands does not cause an alteration of the geometry of the heme with respect to the protein moiety.

The equilibrium constants for the formation of the hydroxide complex of ferric horseradish peroxidase were determined spectrophotometrically at 25.0° for seven values of ionic strength over the range 0.02 to 0.20 and also at 18.0° and 35.0° with $\mu = 0.11$. The results, which were analyzed on the assumption that the hydroxide complex is formed by the ionization of a water molecule in the sixth coordination position of the heme ferric iron, lead to the conclusion that two isozymes of peroxidase are present in the preparations of horseradish peroxidase which were used. The isozymes differ in that they have different values for the pK of peroxidase-hydroxide complex formation. The effective charge on the aquo species of the predominant isozyme is indicated to be between +2 and +3; its dissociation constant is $(2.1 \pm 0.2) \times 10^{-11}$ M and the thermodynamic parameters for its ionization are $\Delta G^\circ = 14.6 \pm 0.1$ kcal/mole; $\Delta H^\circ = 7.8 \pm 0.1$ kcal/mole; $\Delta S^\circ = -22.6 \pm 1.0$ entropy units at 25° and zero ionic strength. Results of temperature-jump relaxation kinetic experiments indicate that the rate constant for the combination of a proton with the peroxidase-hydroxide complex is greater than $1.3 \times 10^{10} \text{ M}^{-1} \text{ sec}^{-1}$ at 31°.

The NMR halide ion probe technique was shown to be a

very sensitive method for detecting the binding of Cl^- and Hg^{2+} to proteins. There appears to be only a small amount of chloride ion binding to horseradish peroxidase and to its apoprotein in basic aqueous solutions, but the binding increases markedly as the pH is lowered, indicating that the chloride ion is binding non-specifically to positively charged regions on the protein. Hg^{2+} was found to bind to myoglobin in increasing amounts as the pH was raised above 7, indicating that it may be binding to regions of negative charge on the protein. Use of the halide ion probe technique as a means of detection for HgCl_2 titrations resulted in the finding that there is one reactive sulfhydryl group in peroxidase. The nature and number of the sulfhydryl groups of hemoglobin and catalase were also investigated.

ACKNOWLEDGMENTS

It is a pleasure to acknowledge the support of Dr. H.B. Dunford, the supervisor of this work.

Discussions with Dr. D. Dolman, Dr. J.A. Plambeck, Dr. J.S. Martin and Dr. R.B. Jordan, with the technical staff, and with my fellow graduate students were of great help throughout the course of this investigation.

The financial assistance provided by an Izaak Walton Killam Memorial Fellowship, the University of Alberta, and the National Research Council of Canada is gratefully acknowledged.

TABLE OF CONTENTS

CHAPTER 1. INTRODUCTION	1
General Introduction to the Nature of Peroxidase, Its Occurrence and Isolation	1
Ligand Binding to Horseradish Peroxidase	7
CHAPTER 2. APPARATUS FOR THE STUDY OF FAST REACTIONS IN SOLUTION	12
Stopped-Flow Apparatus	13
History and Principles	13
Description of the Apparatus	14
Performance of the Apparatus	26
Temperature-Jump Apparatus	29
History and Principles	29
Description of the Apparatus	33
Performance of the Apparatus	35
Combination Apparatus Table	38
CHAPTER 3. THE KINETICS OF CYANIDE BINDING BY FERRIC HORSERADISH PEROXIDASE	41
Experimental	41
Results	43
Discussion	57
CHAPTER 4. THE EFFECT OF LIGAND BINDING AND ACID SPLITTING ON THE OPTICAL ROTATORY DISPERSION OF HRP	76
Introduction	76
Experimental	79
Results	81
Discussion	87
CHAPTER 5. THE EFFECTS OF TEMPERATURE AND IONIC STRENGTH ON THE FORMATION OF THE HYDROXIDE COMPLEX OF HRP	92
Introduction	92

Experimental	93
Results	96
Discussion	99
CHAPTER 6. STUDIES ON HEME PROTEINS USING THE NMR HALIDE ION PROBE TECHNIQUE	115
Theory	115
Experimental	117
Results	120
Discussion	129
LITERATURE CITED	136
APPENDIX I. COMPUTER PROGRAMS	143
APPENDIX II. PURIFICATION OF HRP USING SEPHADEX GELS	173

LIST OF TABLES

I	Spectral and magnetic properties of HRP and ferri-HRP ligand complexes.	8
II	Response time constants for the photomultiplier circuit.	37
III	Rate data for the binding of cyanide by peroxidase at 25°C.	52
IV	Equilibrium data for the binding of cyanide by peroxidase at 25°C.	53
V	Rate and equilibrium constants obtained from analysis of equations 23 and 24 (mechanisms III and IV).	63
VI	Rate and equilibrium constants of simplified versions A and B of mechanism V.	70
VII	Rate and equilibrium constants of simplified versions C and D of mechanism V.	71
VIII	Reduced mean residue rotation at 233 mμ for horseradish peroxidase, its hydroxide, cyanide, fluoride and azide complexes, and for split HRP.	84
IX	Summary of results of computer analysis of experimental titration data using eq 6.	102
X	Thermodynamic constants for the ionization of water, and water coordinated to various Fe ^{III} complexes, at 25.0°.	114
XI	Purification of crude HRP on a G-75 Sephadex column.	176
XII	Purification of crude HRP on a CM Sephadex column.	176
XIII	Further purification of G-75 purified HRP on a CM column.	177

LIST OF FIGURES

1	Protohematin IX.	4
2	Absolute absorption spectra of ferri-HRP and its fluoride, azide and cyanide complexes.	9
3	Absolute absorption spectra of ferri-HRP, its hydroxide complex, and of ferro-HRP.	10
4	Block diagram of stopped-flow apparatus.	15
5	Photomultiplier circuit.	17
6	Power supply for photomultiplier circuit.	18
7	Spectral sensitivity of optical detection system.	21
8	Photograph of stopped-flow apparatus.	22
9	Stopped-flow mixing and observation section.	24
10	Plot of $-\log A$ ferricyanide <u>vs.</u> apparent reaction time (stopped-flow dead time test).	30
11	Schematic diagram of temperature-jump system.	34
12	Temperature-jump cell.	36
13	Apparatus table.	39
14	Typical oscilloscope trace showing the progress of the reaction between HRP and cyanide.	45
15	Test of second-order--first-order kinetics.	51
16	Plot of $\log k'_1$ <u>vs.</u> pH for the binding of cyanide by HRP.	54
17	Plot of $\log k'_{-1}$ <u>vs.</u> pH for the dissociation of the HRP-CN complex.	55
18	Plot of $\log K_d$ <u>vs.</u> pH for the HRP-CN complex.	56
19	Test of mechanism for HCN and CN^- binding to peroxidase with no heme-linked acid groups.	60
20	Plot of the left side of eq 38 <u>vs.</u> $[H^+]$ used to test the validity of mechanism VA for the binding of cyanide by HRP over the pH range 4.2 to 8.1.	74

21	ORD curves of HRP and split HRP in the UV region.	82
22	ORD curves in the visible region for HRP and its fluoride, cyanide and hydroxide complexes.	85
23	ORD curves in the visible region for the azide complex of HRP and for HRP which has had the heme group partially and totally split from the protein.	86
24	Plot of ΔA vs. $\Delta A[H^+]$ for a spectrophotometric titration of pure horseradish peroxidase at 25.0° and $\mu = 0.14$.	98
25	Plot of ΔA vs. pH for a spectrophotometric titration of pure horseradish peroxidase at 25.0° and $\mu = 0.14$.	101
26	Plot of $\log K_{c1}$ vs. $0.509\left(\frac{\sqrt{\mu}}{1+\sqrt{\mu}} - 0.20\mu\right)$ showing the ionic strength dependence of K_{c1} at 25.0° .	110
27	Plot of $\log K_{c2}$ vs. $0.509\left(\frac{\sqrt{\mu}}{1+\sqrt{\mu}} - 0.20\mu\right)$ showing the ionic strength dependence of K_{c2} at 25.0° .	111
28	Plot of $\log K_{T2}$ vs. $1/T$ for experiments performed at $\mu = 0.11$.	113
29	Representative NMR spectra.	119
30	Plot of line broadening vs. pH for HRP and apo-HRP.	122
31	Curve showing the titration of HRP with $HgCl_2$.	124
32	Curve showing the titration of hemoglobin with $HgCl_2$.	125
33	Curve showing the titration of catalase with $HgCl_2$.	126
34	Curve showing the titration of myoglobin with $HgCl_2$.	127
35	Plot of line broadening vs. pH for myoglobin plus $HgCl_2$.	128

CHAPTER 1. INTRODUCTION

The organization of this thesis reflects the fact that a number of different projects were undertaken in the course of the author's research. Hence, the thesis consists of several chapters, each of which is meant to be complete in itself with regard to an introduction, experimental details, and discussion of the results for each research problem.

However, since the major part of the research was carried out on the enzyme horseradish peroxidase (abbreviated to HRP), the following chapter is included to acquaint the reader with the nature and physical properties of HRP.

General Introduction to the Nature of Peroxidase, Its Occurrence and Isolation

Peroxidase is an enzyme which catalyzes oxidations in the presence of hydrogen peroxide and has been given the following designation by the Enzyme Commission of the International Union of Biochemistry¹: 1.11.1.7 Donor: H₂O₂ Oxidoreductase. It is much less specific in its action than many enzymes, with known substrates including leuco-dyes, phenols, indole, aromatic amines, ascorbic acid, and some inorganic ions such as iodide. A discussion of specific oxidative reactions involving peroxidase and a review of the theories of the mechanism of its enzyme action are found elsewhere², and will not be discussed further here.

Peroxidases are present in human saliva, leucocytes, animal thyroid tissue, milk, and many higher plants. Henceforth the material in this chapter will specifically refer to the peroxidase obtained from its most common source, horseradish roots.

The first isolation of HRP, in partially purified form, was carried out by Bach and Chodat in 1903³. It was crystallized by Theorell in 1942 using electrophoretic techniques⁴. Other, simpler methods of preparing pure HRP have been described by Keilin and Hartree⁵ and by Paul⁶. HRP is now available commercially in various degrees of purity from a number of firms.

HRP is known to consist of a number of components which vary in peroxidatic activity, amino acid composition, and spectral properties. The first evidence of these multiple components, or isozymes, was found by Theorell, who isolated a form of HRP which he called peroxidase I or paraperoxidase⁷. Since that time, studies on peroxidase isozymes have been made by Jermyn and Thomas⁸ and by Klapper and Hackett⁹. Recently, a thorough and detailed study of the physical and chemical properties of the isozymes was reported by Shannon, Kay and Lew^{10, 11}.

Structure and Physical Properties

HRP has a molecular weight of 40,200¹², and an isoelectric point of 7.2¹³. It is thermally stable for 15 min.

at 63°, and for weeks at room temperature¹⁴. Elemental analysis shows HRP to contain 47.0 % carbon, 7.25 % hydrogen, 13.2 % nitrogen, 0.43 % sulfur, 0.127 % iron, and 32 % oxygen¹³. It has been found that about 18 weight percent of HRP is carbohydrate material^{10,13}, and although the nature of the linkage to the protein is not known, the composition of the carbohydrate has been studied^{9,10}. The protein moiety contains 287 amino acid residues¹³; the sequence of these has not been determined, but qualitative and quantitative amino acid analyses have been published by a number of workers^{9,10,15,16}.

HRP is a member of the family of heme proteins, which also includes hemoglobin, myoglobin, and catalase. The common feature of these proteins is that they all contain as a prosthetic group protohematin IX, shown in Figure 1. Hemoglobin and catalase contain four heme groups and HRP and myoglobin each contain one heme group. The hematin nature of HRP was established by Keilin and Mann¹⁷, and the importance of the heme group was demonstrated by Theorell who found that neither the protein nor the prosthetic group independently has peroxidatic activity¹⁸. In its natural form, the iron in the heme group of HRP is in the ferric state. It can be reduced with sodium hydrosulfite, but is re-oxidized in the presence of oxygen. The reduction potentials of HRP, determined at 30° by Harbury, were found to range from -0.1002 at pH 3.95 to -0.3372 at pH 11.25¹⁹.

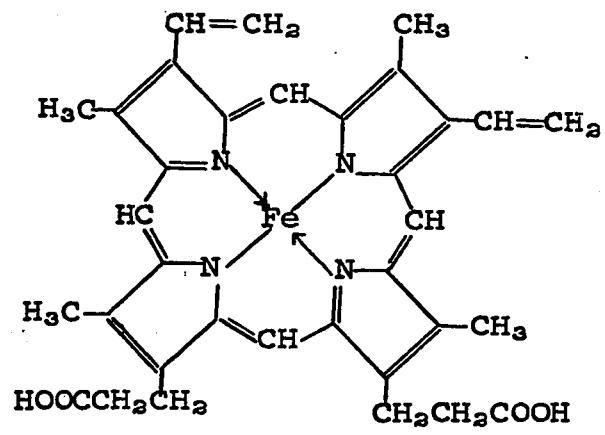


Figure 1. Protohemin IX

The heme group is bound to the protein by several types of bonds, with the nature of those bonds being best known for myoglobin, since its crystal structure has been determined in detail by X-ray studies. The heme of myoglobin is located in a cleft of the protein with the vinyl groups of the porphyrin ring buried in a hydrophobic region and the propionic acid groups bonded to the surface by either hydrogen bonds or salt linkages²⁰. It has been established that a histidine residue and water occupy the fifth and sixth coordination positions of the heme iron, with another histidine residue hydrogen bonded to the water²¹. X-ray studies on a number of high-spin ferric porphyrins have shown that in all cases, the iron atom is displaced greater than 0.3 Å out of the plane of the nitrogen atoms, presumably because the high-spin ferric iron has an electronic structure which gives it too large an effective size to be accommodated in the plane of the nitrogen atoms²². For myoglobin, this displacement is toward the bound histidine²⁰.

To date there has been no X-ray crystallographic work reported for HRP, so evidence regarding the nature of the heme - protein forces is mostly based on a comparison of the properties of HRP with those of hemoglobin and myoglobin. There has been a considerable amount of speculation in regard to the identity of the ligands occupying the fifth and sixth positions on the heme iron of HRP. On the basis of a comparative study of the reduction potentials, magnetic

moments, and spectra of the heme proteins, Brill and Williams concluded that HRP is "an amino-carboxylate, or less probably, an amino-water complex"²³. However, Brill later discussed the formation of HRP-ligand complexes in terms of the ligand replacing water in the sixth position²⁴, a scheme also proposed by Nicholls²⁵. Additional support for the belief that water is in the sixth position is obtained from a study of the temperature dependence of the spectra of HRP at various values of pH⁵. Nicholls and Brill both disagreed with the views of George and Lyster, who postulated that the heme of HRP is in a protein crevice with protein residues bound in both the fifth and sixth positions²⁶. Recently, Brill and Sandberg concluded from a difference spectroscopy study in the 210-280 m μ region that histidine must be in the fifth position of HRP²⁷.

Early titration data from the work of Theorell and Paul implicated the propionic acid groups of the porphyrin in the binding of the heme to the protein of HRP²⁸. This has been substantiated by experiments performed by Maehly, who showed that protohematin IX-dimethylester and protoporphyrin IX-dimethylester (no iron present in the ring) do not bind to the apoprotein but that free protoporphyrin IX does bind to apo-HRP²⁹.

A detailed study of the splitting of HRP into heme and protein has been reported in a series of papers by Maehly³⁰⁻³². HRP is stable between pH 4.2 and 11.4. The rate of the

splitting reaction depends on $[H^+]^2$ or $[OH^-]^2$, thus it increases markedly when the pH is lowered or raised outside the range of stability. The half-time of the splitting reaction is about one minute at either pH 2.5 or 13. At low pH, the splitting is reversible and takes place in four spectroscopically distinguishable steps; at high pH, only one step is observed and the splitting is irreversible. The splitting reaction at low pH occurs faster at any given pH in the presence of ligands which bind to the sixth position of the iron of HRP. As the heme is split from the protein, there is an accompanying loss of peroxidatic activity, which is regained if the solution is neutralized to allow the heme and protein to recombine.

Ligand Binding to HRP

The heme proteins perform their biological functions by interaction with ligands, such as in the transport of oxygen by hemoglobin. Although magnetic and spectral evidence indicates that the iron of the heme is involved, the most positive proof is obtained from X-ray crystallographic studies, which show that for myoglobin, the ligand is found in the sixth coordination position of the iron, having replaced the water molecule normally present in that position^{21, 22}. It is generally accepted that ligands bind to the sixth position for all other heme proteins as well.

A number of ligands bind to ferri-HRP with accompanying

changes in the spectral and magnetic properties of the enzyme. Figures 2 and 3, taken from the work of Keilin and Hartree⁶, show the absorption spectra of ferri- and ferro-HRP and the hydroxide, cyanide, azide, and fluoride complexes of ferri-HRP. The positions of the absorption peak maxima, along with their corresponding molar absorptivities⁵ are summarized in Table I, which also lists the magnetic moments of the various species as determined by Theorell^{3,4}.

Table I

Spectral and Magnetic Properties of HRP
and Ferri-HRP Ligand Complexes

<u>species</u>	<u>wavelengths (mμ) of absorption maxima and corresponding values of $\epsilon \times 10^{-4}$</u>			<u>magnetic moment</u>
ferri-HRP	642(0.284)	497(1.003)	403(9.10)	5.45 B.M.
ferro-HRP	556(1.122)	-	437(7.73)	5.19 B.M.
HRP-OH	574(0.686)	545(0.864)	416(8.85)	2.66 B.M.
HRP-F	612(0.693)	488(0.755)	404(13.00)	5.90 B.M.
HRP-CN	538(1.020)	-	423(9.39)	2.65 B.M.
HRP-N ₃	635(0.170)	534(0.820)	416(11.40)	-

The ferric iron in both HRP and HRP-F appears to be in a high-spin form, whereas for HRP-OH and HRP-CN it is low-spin. In addition to the complexes listed in Table I, ferri-HRP has been shown to react with hydrogen sulfide, with the resulting complex having a magnetic moment of 2.40 Bohr Magnetons^{3,4}. Nitric oxide forms complexes with both ferri- and

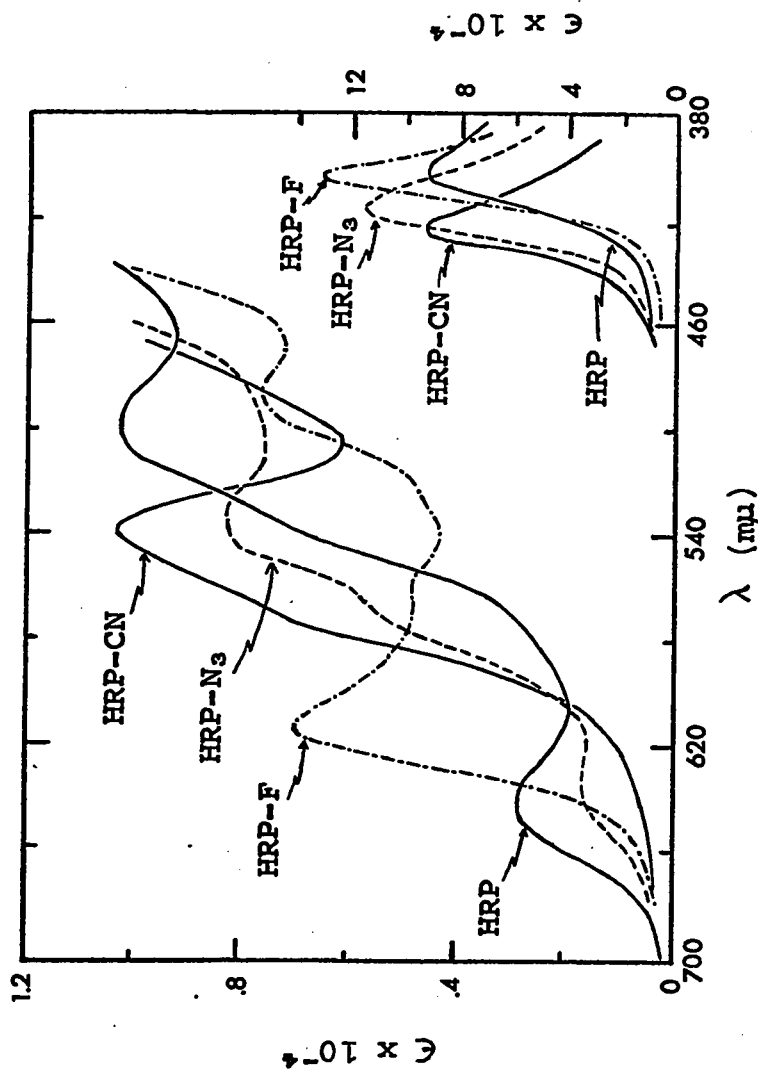


Figure 2. Absolute absorption spectra (molar absorptivity vs. wavelength) of ferri-HRP and its fluoride, azide and cyanide complexes.

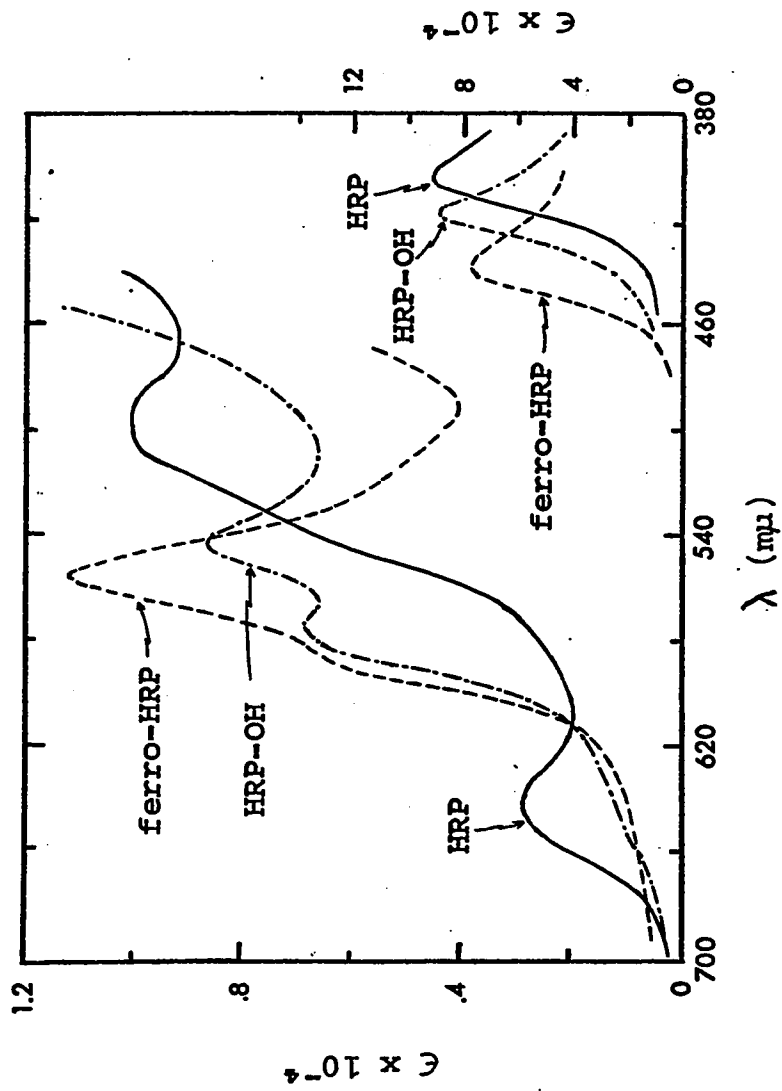


Figure 3. Absolute absorption spectra (molar absorptivity vs. wavelength) of ferri-HRP, its hydroxide complex and of ferro-HRP.

ferro-HRP; stable complexes are also formed by ferro-HRP with carbon monoxide³⁵ and with cyanide³⁶.

Early quantitative studies on ligand binding by ferri-HRP included the investigations by Theorell³⁴ and by Chance³⁷ on the effect of pH on the equilibrium constant of the reaction between HRP and fluoride, and Chance's kinetic and equilibrium study of the reaction of HRP with cyanide at two values of pH³⁸. There has been a great deal of speculation as to whether the attacking and/or bound form of the ligand is the neutral species or the anion^{34-36, 39, 40}. In 1967, Dunford and Alberty reported a temperature-jump kinetic study of fluoride binding to HRP and showed that the variation of the apparent bimolecular rate constants with pH could be explained by a mechanism involving the fluoride ion attacking two forms of HRP⁴¹. The two forms differ only by the presence of a proton on a heme-linked ionizable group with a pK of 4.0, with the fluoride ion binding faster to the protonated species.

It was felt that a similar study of the binding of cyanide to HRP over a wide pH range might yield additional information about the nature of ligand binding to HRP. Hence, after the construction of the apparatus described in the next chapter, such a project was initiated.

CHAPTER 2.

APPARATUS FOR THE STUDY OF FAST REACTIONS IN SOLUTION

The title of this chapter raises a question: how fast is a "fast reaction"? Caldin⁴² has defined a fast reaction as "... a reaction that is fast relative to the time required for mixing and observation by conventional methods." By Caldin's own admission, this definition is imprecise, but serviceable. If one considers the conventional method of mixing reagents in a cuvet and taking a reading on a spectrophotometer, a fast reaction would then be one with a half-time of less than a few seconds. To study such a reaction, one needs a special apparatus. By constructing an apparatus designed to mix reagents rapidly, one can study reactions with a minimum half-time of a few milliseconds. For even faster reactions, one must use a method which avoids mixing altogether. Such a method is the temperature-jump technique, which is one of the relaxation methods proposed by Eigen⁴³, all of which involve taking a reversible reaction system which is at equilibrium and suddenly perturbing the equilibrium so that the reaction will then proceed until a new position of equilibrium is established. The time taken to reach the new position of equilibrium can be related to the rate constants of the forward and reverse reactions. The use of relaxation techniques makes it possible to study reactions with half-times as small as a few

microseconds.

This chapter contains a discussion of the construction and performance of two types of apparatus for the study of fast reactions in solution: a stopped-flow apparatus and a temperature-jump apparatus.

Stopped-Flow Apparatus

History and Principles

Rapid mixing and flow techniques date back to 1923 when Hartridge and Roughton constructed an apparatus which achieved mixing times of one millisecond⁴⁴. Because of the slow response time of the detection instrumentation available then, time resolution was achieved by a continuous flow procedure in which the freshly mixed solution passed down an observation tube and the composition of the reaction mixture was determined at various cross sections by optical, thermal, or electrical analysis. If the flow velocity is kept constant, the distance from the mixing chamber will correspond to a time equal to the distance divided by the velocity.

The stopped-flow method was developed by Chance in 1940⁴⁵, but has only come into widespread use since Gibson's modifications in 1952⁴⁶. This method involves rapid mixing and flow of mixed reactants to an observation chamber. The flow is stopped quickly and the progress of the reaction in

the observation chamber is followed by some appropriate method. The stopped-flow technique has several advantages over the continuous flow method, including the fact that the observation is independent of the rate and character of flow down the observation tube. Also, very small volumes of reactants can be used, and a permanent record of the progress of the reaction throughout its entire course can be obtained.

Description of the Apparatus

Ideas for the design of the stopped-flow apparatus were obtained from the papers of Gibson⁴⁷ and of Sturtevant⁴⁸ and from examination of Dr. R. A. Alberty's stopped-flow at the University of Wisconsin, which was built by D. A. Ver Ploeg⁴⁹. The primary innovation introduced in the model described in this chapter involves a new design for the mixing chamber and observation section. A block diagram of the apparatus is shown in Figure 4.

A spectrophotometric detection system is used which consists of a Bolex Ace 50 watt projection lamp; a Bausch and Lomb No. 33-86-26-07 High Intensity Model 5 grating monochromator with a Bausch and Lomb quartz collective lens No. 1; a cylindrical lens made from a Fisher plastic thermometer magnifier; an R.C.A. Model 1P28 photomultiplier in a circuit with an emitter follower output; and a Tektronix 535A oscilloscope with a Type D high gain differential

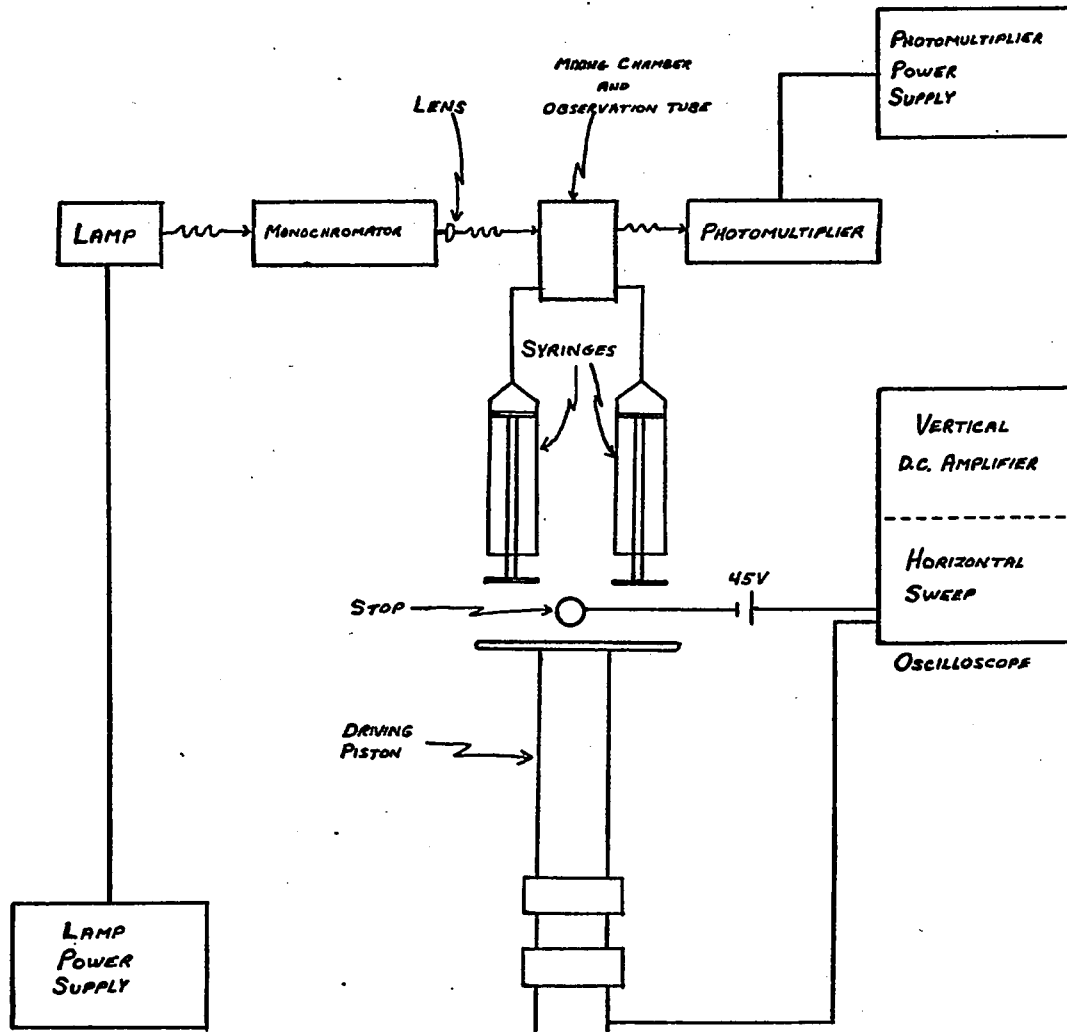
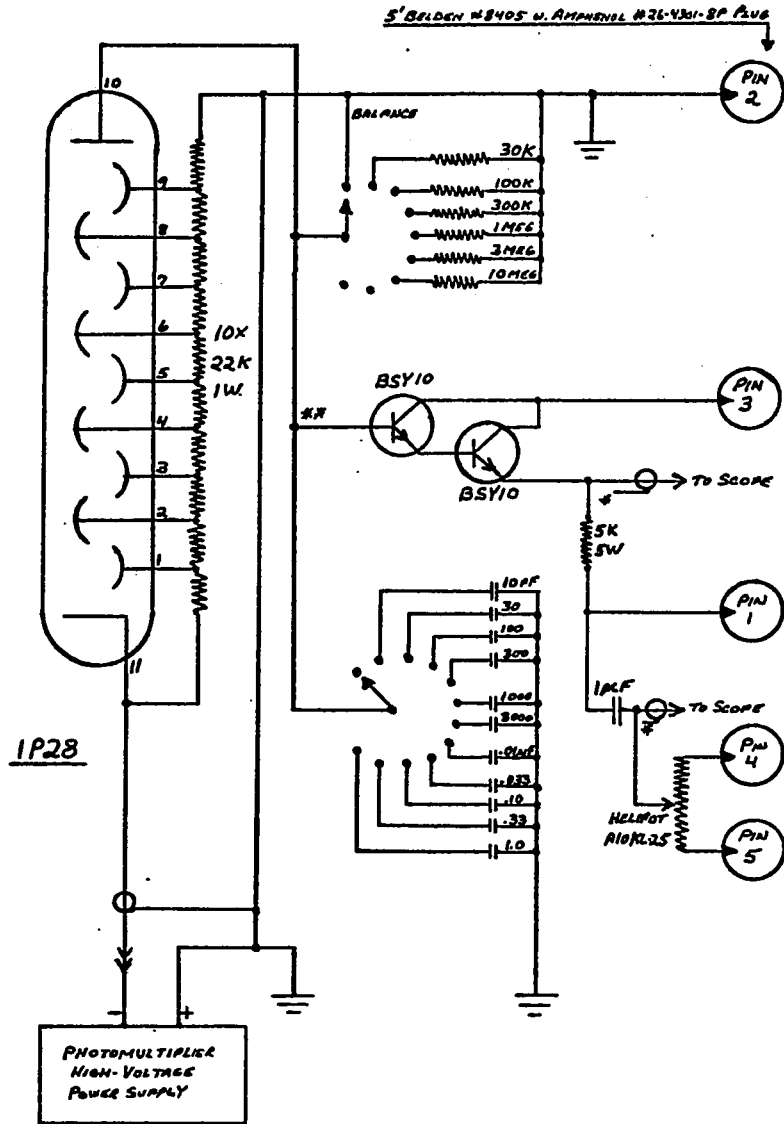


Figure 4. Block diagram of stopped-flow apparatus.

plug-in preamplifier. A Hewlett-Packard Harrison Model 6264A dc power supply for the tungsten lamp provides eight volts with 0.01 % line and load regulation and 500 μ V ripple. Photomultiplier voltage is obtained from a Hewlett-Packard Harrison Model 6110A dc power supply. Experimental traces are photographed with a 35 mm camera mounted on the oscilloscope with a Beattie-Coleman Polexa adapter.

The photomultiplier circuit is shown in detail in Figure 5 and its power supply unit in Figure 6. These two circuits, built by the University of Alberta Chemistry Electronics Shop, contain a number of useful features. The sensitivity can be varied by selecting a value of load resistance ranging from 30 k Ω to 10 M Ω . In order to filter the noise from the output signal, an RC circuit of the appropriate time constant can be introduced by combining the load resistor with a variable capacitance ranging from 0 to 1 μ F. The circuit also contains a zero offset control to provide various amounts of bucking voltage to the photomultiplier output. This allows the initial photomultiplier signal to be nulled and thus provides a convenient means for observing a small signal change which is imposed upon a larger signal.

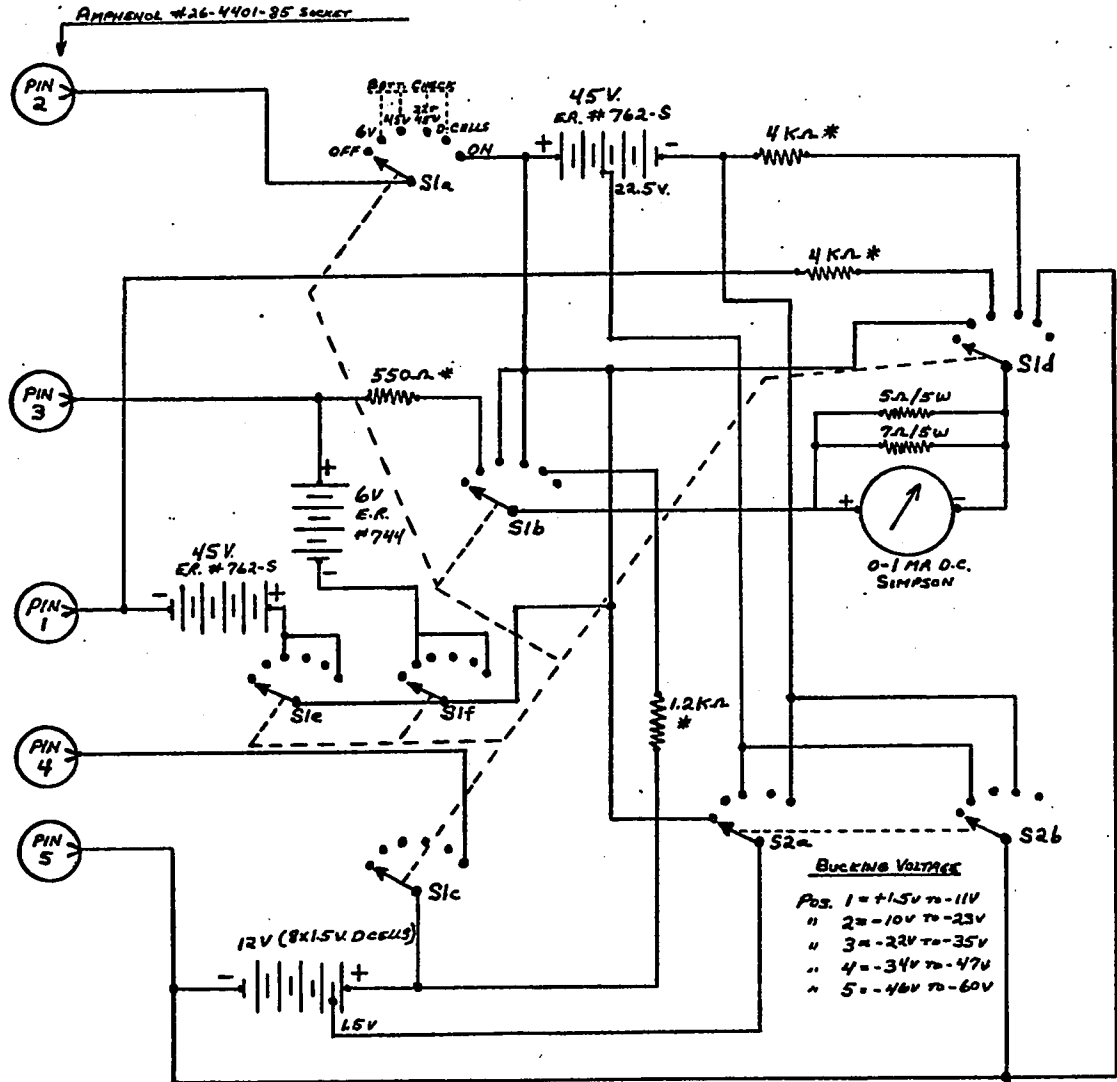
In the case of an experiment involving a reaction which proceeds slowly enough that an oscilloscope sweep rate of slower than 0.1 sec/cm can be used, the procedure for obtaining a record of the oscilloscope trace is very simple.



*grounded at oscilloscope

**this lead to be kept as short as possible (unshielded)

Figure 5. Photomultiplier circuit



*These resistors are selected so that the meter reads in "Batt. O.K." sector (0.6-0.8 ma) while batteries are under load.

Figure 6. Power supply for photomultiplier circuit

The appropriate sweep rate is chosen and the sweep is set for free-running operation. When the trace appears on the left side of the oscilloscope screen, the camera shutter is opened and the driving piston of the stopped-flow apparatus is pushed in quickly. When the reaction reaches equilibrium, as evidenced by no further change in trace voltage with time, the camera shutter is closed. For faster reactions, a trigger is necessary. As shown in Figure 4, the trigger consists of a 45 V battery in a circuit which is completed when the driving piston hits the stop. Generally it is important to observe the first portion of the trace and to be able to establish unequivocally the point corresponding to zero reaction time. These aims are best achieved if a small wire is attached to the stop in such a manner that the piston face brushes the wire just before hitting the stop. Thus, the oscilloscope is triggered at such a time that the last portion of the flow, and hence, the first part of the reaction are always observed.

The overall spectral sensitivity of the detection system is a function of the relative spectral composition of the lamp, the transmittance curve of the monochromator grating, and the spectral response of the photomultiplier. It is important to know the spectral sensitivity of the system, since a reaction is often encountered which can be followed at more than one wavelength of light. If one selects a wavelength corresponding to a high sensitivity,

then a lower photomultiplier voltage can be used to get the same output voltage, and a reduction of photomultiplier voltage results in a decrease of shot noise and hence in a better signal-to-noise ratio. Such a sensitivity curve for the detection system described above is shown in Figure 7. It was obtained by filling the stopped-flow observation tube with water and measuring the output voltage of the photomultiplier vs. wavelength. A calibrated oscilloscope was used for the voltage measurements.

The stopped-flow device itself is best described in conjunction with a photograph of the apparatus, Figure 8. The main body measures 10.5 cm x 43 cm and is made of Plexiglas, painted black to keep out stray light. The driving piston (A) is made of brass, and it slides through two Plexiglas collars. The stopping pin (B) is made of stainless steel and it seats 1.5 cm into the main body of the apparatus. There are five positions for the stop, spaced 1.05 cm apart. The thermostated compartment (C), shown with the top off, is 4.0 cm deep. It contains the two 1.0 ml driving syringes (D) which lead to Hamilton three-way valves (E). The valves are positioned so that reactants can flow into the driving syringes from thermostated 5.0 ml reservoir syringes (F) or from the driving syringes through Teflon tubing to the mixing and observation chamber (G). From there the used reaction mixture passes to the 2.0 ml collection, or back-up syringe (H).

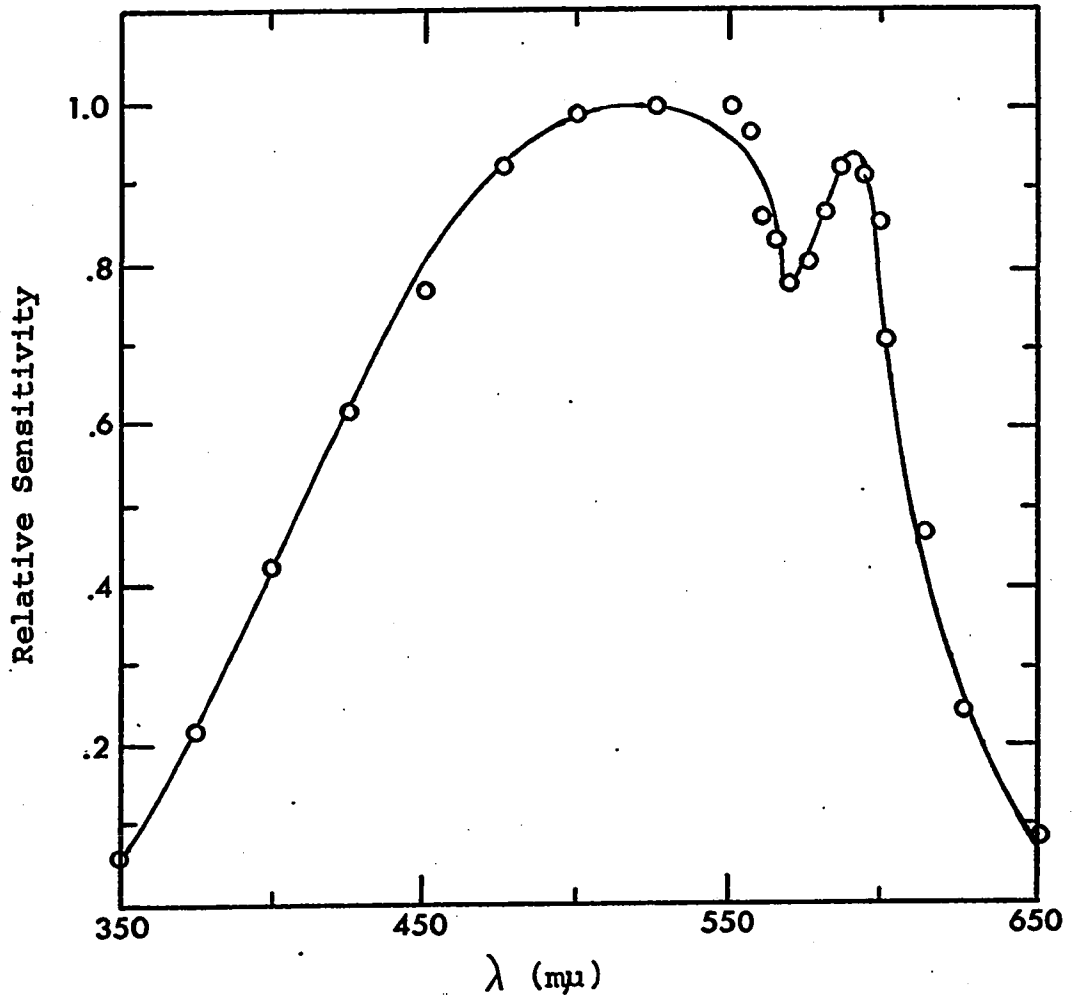


Figure 7. Spectral sensitivity of optical detection system

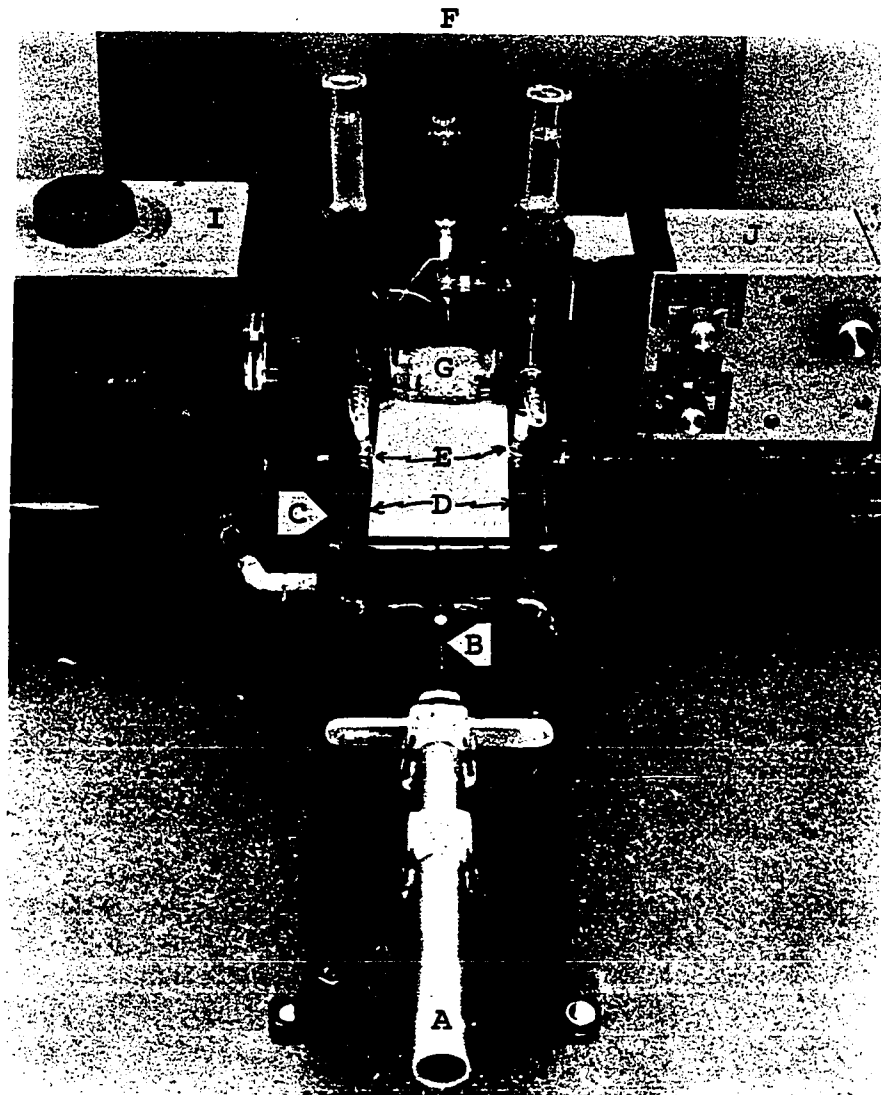


Figure 8. Photograph of Stopped-Flow Apparatus
Key: A, driving piston; B, stopping pin; C, thermostated compartment; D, driving syringes; E, three-way valves; F, reservoir syringes; G, mixing and observation chamber; H, back-up syringe; I, monochromator; J, photomultiplier.

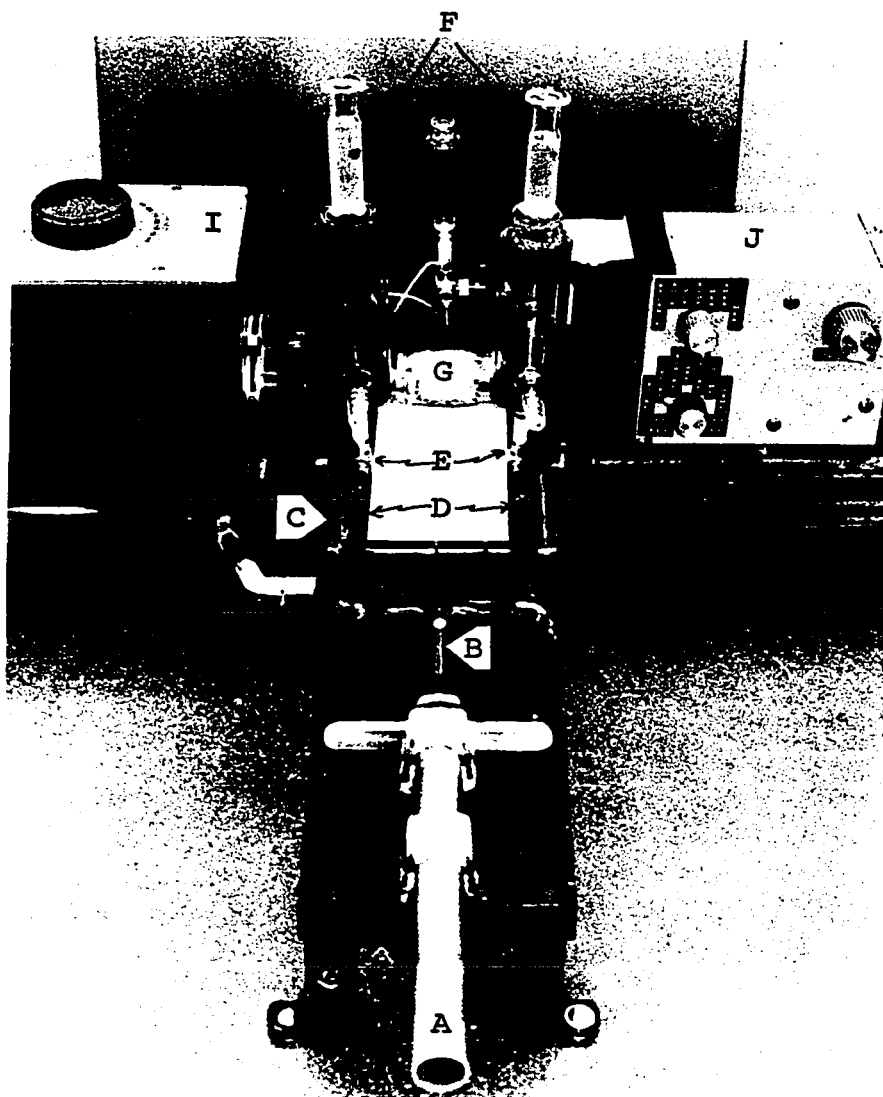


Figure 8. Photograph of Stopped-Flow Apparatus

Key: A, driving piston; B, stopping pin; C, thermostated compartment; D, driving syringes; E, three-way valves; F, reservoir syringes; G, mixing and observation chamber; H, back-up syringe; I, monochromator; J, photomultiplier.

This syringe provides a small back pressure to help overcome the inertia of the driving syringes. Another Hamilton three-way valve allows the back-up syringe to be emptied easily, or bypassed if desired. Also shown in the photograph are the monochromator (I) and the box housing the photomultiplier circuit (J).

The heart of the stopped-flow apparatus is the mixing and observation section. Figure 9A, drawn to scale, shows a top exploded view of this section, which consists of a series of wafers and light ports, all made of Plexiglas. The arrows show the paths of the reactants. The two halves of this section are identical except that the effluent tube is located in one of the "B" wafers rather than the center. The light ports are hollow Plexiglas rods with a 0.95 cm o.d. and a 0.55 cm i.d. They are glued to wafer A on one side and on the other side attach to the thermostated compartment by means of Plexiglas nuts. Wafer A contains a viewing window made from a rod of General Electric type 104 fused quartz, 5 mm in diameter and 2.0 cm in length. The ends of the rod are ground and polished to a plate glass finish. The window is held in place by epoxy resin. Because the Teflon tubing cannot be glued in place, a special connection is necessary; it is designed so that the flared tubing fits over a stainless steel fitting which is glued into the Plexiglas. The tubing is held snugly in place by a hollow threaded steel rod. The length of the observation

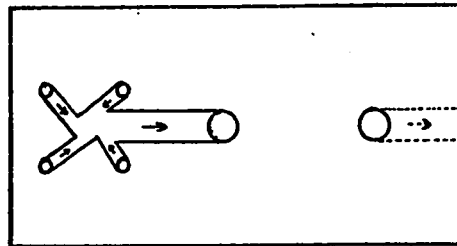
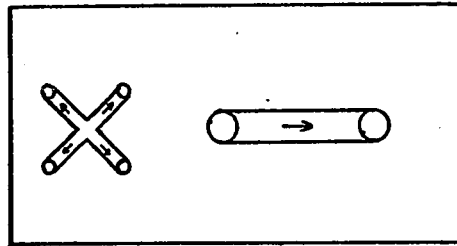
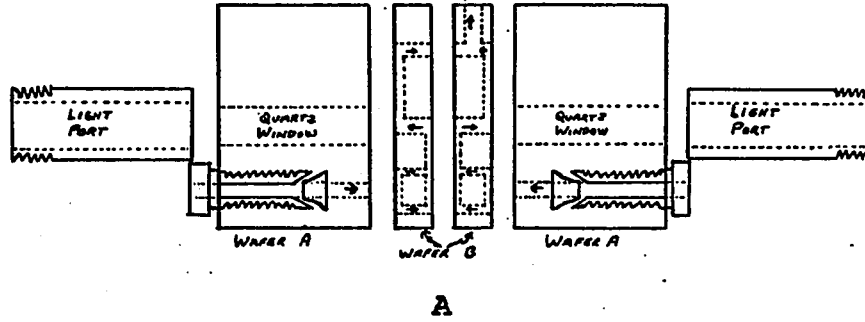


Figure 9. Stopped-flow mixing and observation section. A. Exploded top view, to scale. B. Outside face of wafer B. C. Inside face of wafer B. B and C are enlarged by a factor of two.

tube, i. e. two times the width of a B wafer, is 1.067 cm.

The two faces of wafer B are illustrated, enlarged by a factor of two, in Figures 9B and 9C. Solution containing one of the reactants flows into the center of the splitter shown in the drawing of the outside face. The solution is then split into four portions which pass through the wafer and meet head-on with the streams of the other reactant solution. This constitutes the first stage of mixing. The four freshly mixed portions flow down the inside face of the wafer and mix a second time when they meet tangentially at the center cavity. From there the solution passes through a channel to the center of the observation tube, where it splits to fill the observation tube. The line of flow continues out of the observation tube to the back of the mixing-observation section and then into a stainless steel hypodermic needle which connects to the three-way valve at the back of the apparatus.

The wafers are held together by four screws, one placed above and one below the tubing inlets and the other two at corresponding positions at the rear of the section. Under high pressure driving, a few small leaks appeared from between the wafers. These were stopped by coating the whole mixing-observation section with General Electric silicone rubber.

Performance of the Apparatus

The first performance criterion a stopped-flow apparatus must meet is that it must have the ability to flush old solution completely from the observation chamber. For the apparatus described above, the total volume of the mixing chamber and observation tube is about 0.07 ml and the volume delivered by the movement of the driving piston from one stop to the next is 0.4 ml. Thus, since at least four volumes of fresh solution sweep out the observation tube before the portion which will be observed enters, it is expected that only a negligible amount of old solution would remain behind. This expectation is borne out by experiments using colored solutions and photometric detection which showed that no detectable old solution remained in the observation chamber when a portion of fresh solution was injected.

Another performance criterion is the time resolution, which depends on two factors: the mixing time and the time for flow from the mixing chamber to the observation tube, the latter being the "dead time". The mixing time is usually fast compared to the dead time, and this can be confirmed by performing a simple experiment. Since an acid-base reaction is instantaneous on the stopped-flow time scale, any change in transmittance with time after an acid and base are mixed in the presence of an indicator must be due to incomplete mixing at the beginning. For this test, one syringe was filled with a dilute solution of brom cresol green

indicator in base form, and the other with a solution of pH 2.0 buffer. The indicator changes from blue to yellow as the solution becomes acidic through the pH range 3.8-5.4. The monochromator was set at 620 m μ , which is the wavelength corresponding to the maximum of the absorption peak of the base form of the indicator, the reactants mixed and the resulting oscilloscope trace was photographed. Inspection of the photograph showed that the solution was greater than 98 % mixed by the time the solution was stopped in the observation chamber. Thus, the time resolution was shown to depend primarily on the dead time of the apparatus.

The dead time of the apparatus can be calculated if the flow rate and volume of the mixing chamber and observation tube are known exactly. If these are not known, the dead time can be found easily by experiment*. The point on the experimental oscilloscope trace corresponding to the time that the flow is stopped is the apparent $t=0$. The true $t=0$ exists when the reactants are mixed, so it is the time between the true and apparent $t=0$ which must be determined. The reaction studied to determine this time was the redox reaction between ascorbate and ferricyanide. It was followed at 422 m μ , the maximum of the absorption peak of

*The author is indebted to members of Dr. G. G. Hammes' group at Cornell University for helpful discussions regarding this experiment.

ferricyanide. A solution of $2 \times 10^{-4}M$ potassium ferricyanide was mixed with excess ascorbate and photographs were taken of the resulting oscilloscope traces. Three experiments were performed using the same ferricyanide concentration, but each with a different ascorbate concentration. As long as the ascorbate is kept in excess so that the reaction is pseudo-first-order, it is not necessary to know the exact ascorbate concentrations to carry out the analysis.

Photographs of the oscilloscope traces provided a record of photomultiplier circuit output voltage vs. time. This output voltage is proportional to the current at the anode of the photomultiplier tube, which is in turn proportional to the intensity of light incident upon the photocathode. If I_0 and I are the light intensities with solvent only and with solvent plus absorbing compound, respectively, and V_0 and V are the corresponding voltages which are produced, then: $V/V_0 = I/I_0$; but $I/I_0 = T$, the transmittance, so V/V_0 is also equal to the transmittance. To analyze the results of the dead time determination experiments, the oscilloscope screen was calibrated in terms of transmittance using solutions whose transmittances were known from measurement on a Beckman DU spectrophotometer. Points were read from the photographs with the aid of a photographic enlarger, converted to transmittance and then absorbance readings.

For a first-order reaction:

$$-\log c = -\log c_0 + \frac{kt}{2.303} \quad (1)$$

where c_0 and c are the initial concentration and the concentration at time t of the first-order reactant. Since by Beer's law, $A \propto c$, a plot of $-\log A$ vs. t should yield a straight line with an intercept at $-\log A_0$. Figure 10 contains such plots for the dead time test, with $-\log A$ of ferricyanide plotted vs. apparent time for the three different concentrations of ascorbate. If no reaction had taken place at the apparent $t=0$, the three lines should have intersected at that point, since the true c_0 of ferricyanide and hence, the true $\log A_0$, would be the same for the three experiments. This was not observed, as shown in Figure 10. Extrapolation of the three lines back to the point where they intersect, and thus at which they do represent equal values of $-\log A_0$, allows determination of the true $t=0$. From Figure 10, it can be seen that the true $t=0$ occurs approximately ten msec before the apparent $t=0$, so the dead time of the apparatus is about ten msec. The small locus of intersection indicates that although the driving piston was pushed by hand, the flow rate achieved was quite reproducible. It is expected that a shorter dead time would be possible if the driving piston were driven pneumatically to increase the flow rate.

Temperature-Jump Apparatus

History and Principles

The general theory of relaxation methods is treated in

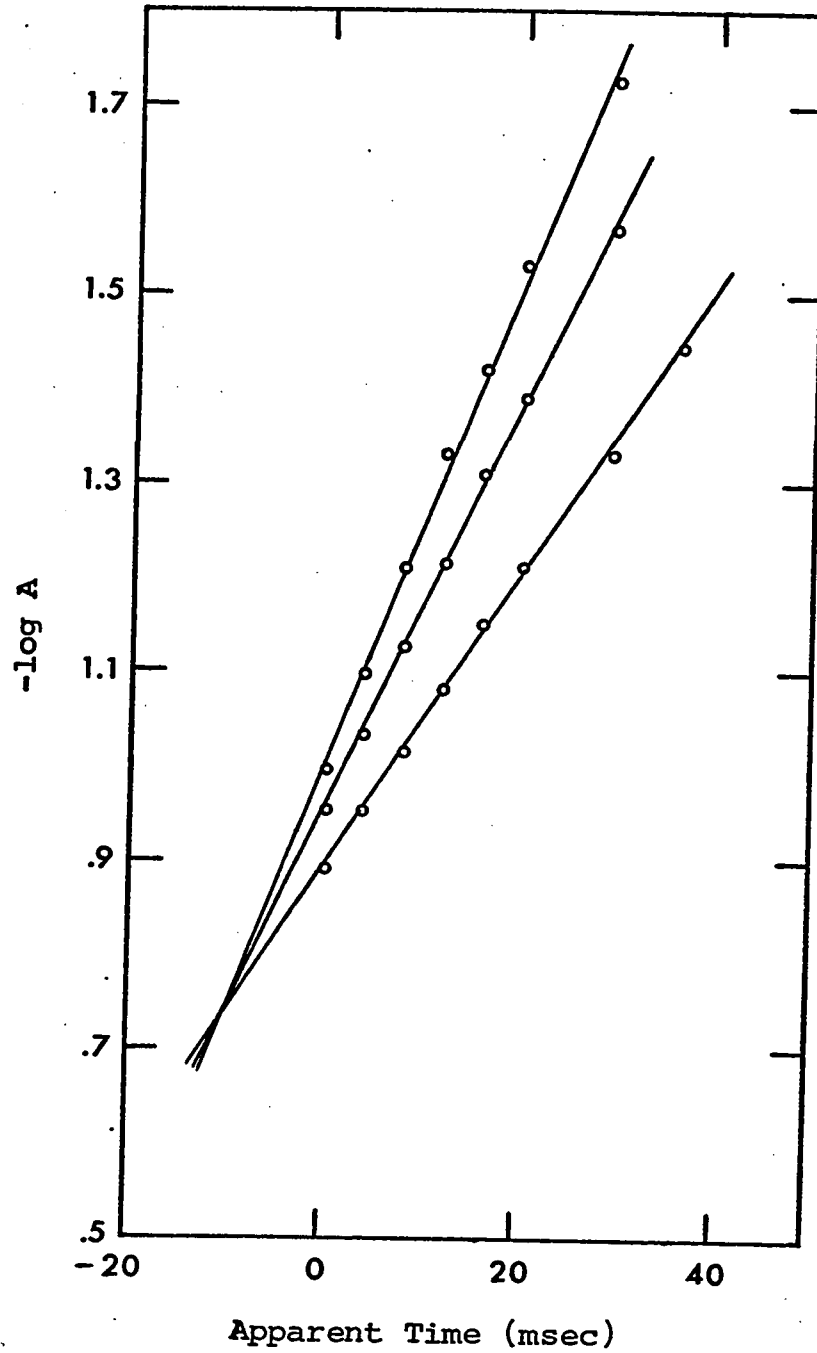


Figure 10. Plot of $-\log A$ of ferricyanide vs. apparent reaction time. The negative value of time at which the lines intersect is the dead time of the stopped-flow apparatus.

detail elsewhere⁵⁰⁻⁵², so this section will deal only with the temperature-jump method and apparatus.

The temperature-jump method was first proposed by Eigen in 1954⁴³, and a description of the first operational instrument appeared five years later⁵³. Since that time, the use of this technique has grown very rapidly, and has found widespread use in the study of inorganic and biochemical reactions.

The thermodynamic basis for the temperature-jump method is expressed by a form of the Gibbs-Helmholtz equation:

$$\left(\frac{d \ln K}{dT}\right)_p = \frac{\Delta H^\circ}{RT^2} \quad (2)$$

From eq 2 it can be seen that the constant pressure equilibrium constant of a reaction will change upon a perturbation of the temperature, provided the reaction being studied has a non-zero standard enthalpy. A reaction which has a very small value of ΔH° can often be studied by coupling it to one which has a greater value of ΔH° .

The temperature rise is obtained by discharging a capacitor through a solution containing the reactants at equilibrium. There is no spark or flash through the solution; the rise in temperature is due to a Joule heating of the solution. This heating may be likened to the heating caused by an IR drop across a resistor. In the solution, the energy is distributed among the translational, vibrational, and rotational degrees of freedom in a time which is much faster

than the time required for the discharge of the capacitor⁵⁴. Since ions must be present to carry the current, the solution is usually made 0.1 M in some inert electrolyte such as potassium nitrate.

The magnitude of the temperature rise, ΔT , can be estimated by assuming that all the energy stored in the capacitor is transferred to the solution, and is given by:

$$\Delta T = \frac{CV^2}{2\rho vk} \quad (3)$$

where C is the capacitance in farads, V is the voltage on the capacitor in volts, ρ is the solution density in g/cm³, v is the volume of liquid heated, in cm³, and k is the specific heat capacity of the solution in J/g deg. A typical temperature-jump apparatus is designed to produce temperature increases of two to ten degrees.

The temperature-jump method is applicable over a wide time scale. The lower limit is determined by the time required to heat the solution. This is usually expressed in terms of a heating time constant, τ_0 . If the inductance of the capacitor and the circuit capacitance, inductance, and resistance are assumed to be negligible, τ_0 may be calculated from the equation:

$$\tau_0 = \frac{1}{2} RC \quad (4)$$

where R is the resistance of the solution and C is the capacitance of the capacitor. The values of τ_0 for various temperature-jump instruments range from 0.1 μ sec to 10 μ sec⁵⁵.

The upper time limit for the apparatus is of the order of one second. This limit is associated with the cooling of the solution between the electrodes by convection currents from the bulk solution.

Description of the Apparatus

The temperature-jump apparatus described here is modeled after the one used by Dr. R. A. Alberty and co-workers at the University of Wisconsin⁵⁶.

The detection system used with the instrument is like the one illustrated in Figure 4 and described in the preceding section, but with the cylindrical lens replaced by a spherical lens from a Parr Instrument Co. buret meniscus magnifier. This lens was chosen because it fit conveniently into the light port of the temperature-jump cell thermostating jacket.

A schematic diagram of the temperature-jump circuit is shown in Figure 11. A Plastic Capacitors, Inc. 50 kV, 5 ma High Voltage Power Supply Model HV-500-502M coupled with a Superior Powerstat No. 10B is used to charge a Plastic Capacitors, Inc. LK500-104ZND, 0.1 μ F, 50 kV capacitor. The capacitor is discharged through an EG and G Inc. Spark Gap Model GP14B by triggering the spark gap with an EG and G Inc. Trigger Module Model TM-11. The oscilloscope is triggered by means of a signal inductively produced in a coil around the lead from the capacitor. A second temperature-jump

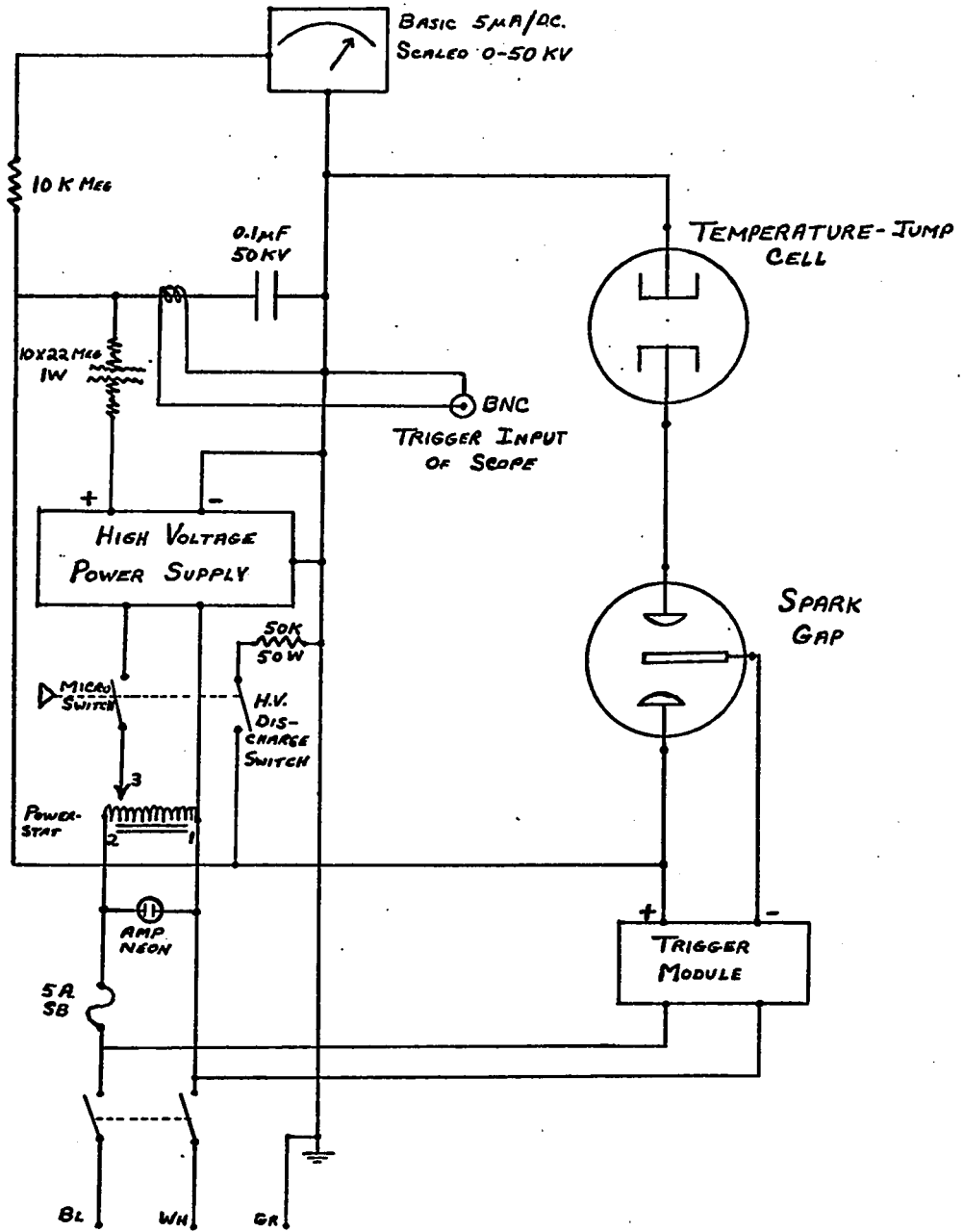


Figure 11. Schematic diagram of temperature-jump system

apparatus was built which differed from the one described above in that the spark gap was constructed by the University of Alberta Chemistry Electronics Shop and the high voltage is supplied by a Spellman High Voltage Power Supply Model 2040.

The features of the temperature-jump cell are illustrated in Figure 12, a side sectional view of the cylindrical cell, drawn to scale. The main body of the cell is made of Plexiglas, the base of Colorlith, the windows of quartz rod as described in the preceding section, and the top and electrodes of stainless steel. All corners of the electrodes were rounded and the surfaces polished to prevent arcing. The volume of solution contained between the electrode faces is 1 cm^3 , and experiments can be performed using as little as 5 ml total solution in the cell.

The cell is fitted snugly into a brass thermostating jacket; the cell and jacket are both surrounded by a light-tight canister. The high voltage connection is made by the banana plug at the bottom of the cell, and the top electrode is connected to ground.

Performance of the Apparatus

The resistance of the cell containing 0.11 M KNO_3 , measured with a bridge circuit, is 133 ohms. Using this value in eq 4, along with a capacitance of 0.1 μF , the heating time constant for the apparatus is calculated to be

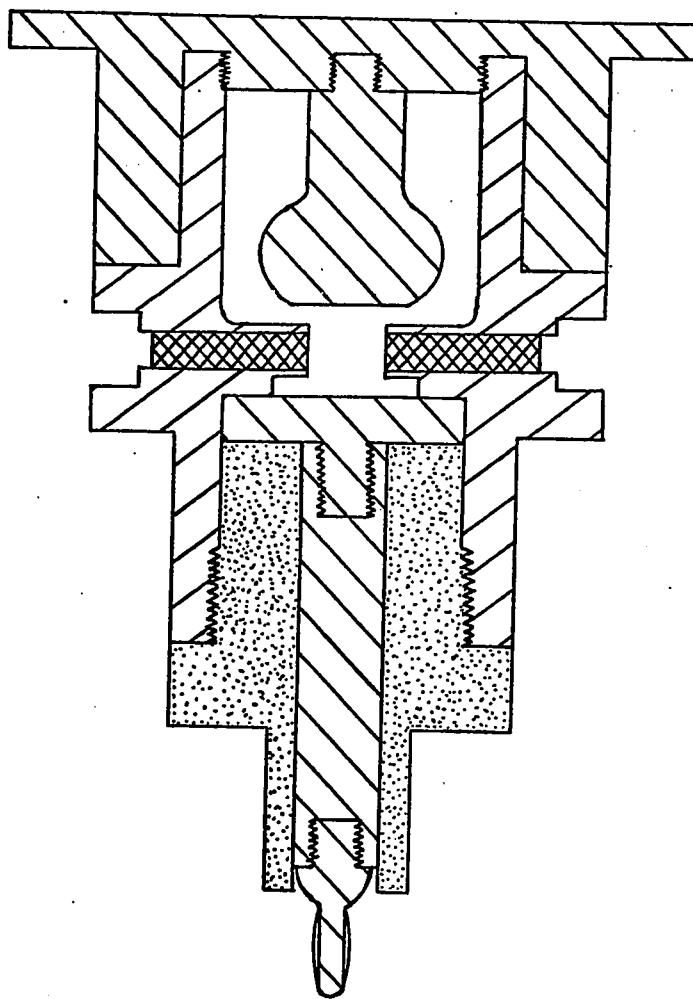


Figure 12. Temperature-jump cell

Key: \\\ stainless steel
 // plexiglas
 XXX quartz
 . . . colorlith

7 μ sec. Although this figure represents the minimum relaxation time which can be studied using this apparatus, one must also consider the response time of the photomultiplier circuit. The response time of the circuit depends on the values of the residual circuit capacitance, the filtering capacitance, and the load resistance. Values of the circuit response time constant, \mathcal{T}_c , were determined experimentally. A xenon flash lamp with a flash decay time constant of 3 μ sec was placed in front of the photomultiplier tube. With the filtering capacitance set at zero, photographs of oscilloscope traces of the photomultiplier circuit response following a lamp flash were taken at each setting of the load resistor. \mathcal{T}_c was obtained from inspection of the photographs, and was taken to be the time required for the output voltage to decay to two-thirds of the maximum value caused by the lamp pulse. Table II contains values of \mathcal{T}_c for the various values of load resistance in the photomultiplier circuit.

Table II

Response Time Constants for the Photomultiplier Circuit

<u>Load Resistance</u>	<u>\mathcal{T}_c, μsec</u>
30 k Ω	3
100 k Ω	5
300 k Ω	12
1 M Ω	30
3 M Ω	60
10 M Ω	125

The theoretical expression for the temperature rise of the solution, given by eq 3, can be simplified for the usual conditions of operation for this apparatus. With v equal to 1 cm^3 , C equal to $0.1 \text{ } \mu\text{F}$, and values of k and ρ taken as 4.18 and 1.0, the corresponding values for water, eq 3 becomes:

$$\Delta T = 1.19 \times 10^{-8} v^2 \quad (5)$$

The validity of eq 5 was checked by another worker in this laboratory⁵⁷ using buffers of known ΔH° and a pH indicator according to the method described by Czerlinski⁵⁸. Experimental values of ΔT agreed within 5 % of the values predicted by eq 5.

Combination Apparatus Table

Because both the stopped-flow and temperature-jump instruments use the same detection system, it was felt that it would be convenient to be able to use the two instruments interchangeably. Two identical tables were built for this purpose. Figure 13 is a photograph of one of the tables, set up for the stopped-flow apparatus, labeled "C" on the photograph. The frame of the table is constructed of 2" angle iron, with additional support from the electronic component cabinet on the left side. The top of the table and the shelf on the right bottom are made of 3/4" Colorlith. The lamp (A), monochromator (B) and photomultiplier (D) are held by clamps which slide along an optical bench (E) made

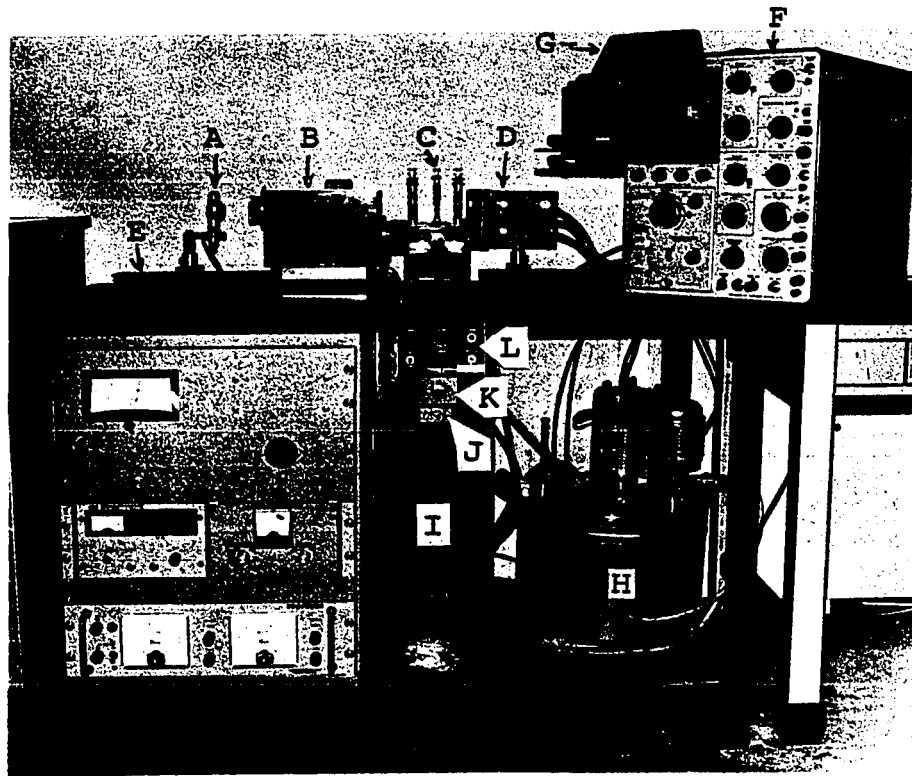


Figure 13. Apparatus Table

Key: A, lamp; B, monochromator; C, stopped-flow apparatus; D, photomultiplier; E, optical bench; F, oscilloscope; G, camera and adapter; H, constant temperature bath; I, box containing capacitor and spark gap; J, trigger output; K, high voltage discharge switch; L, trigger module. The cabinet on the left contains the various power supplies.

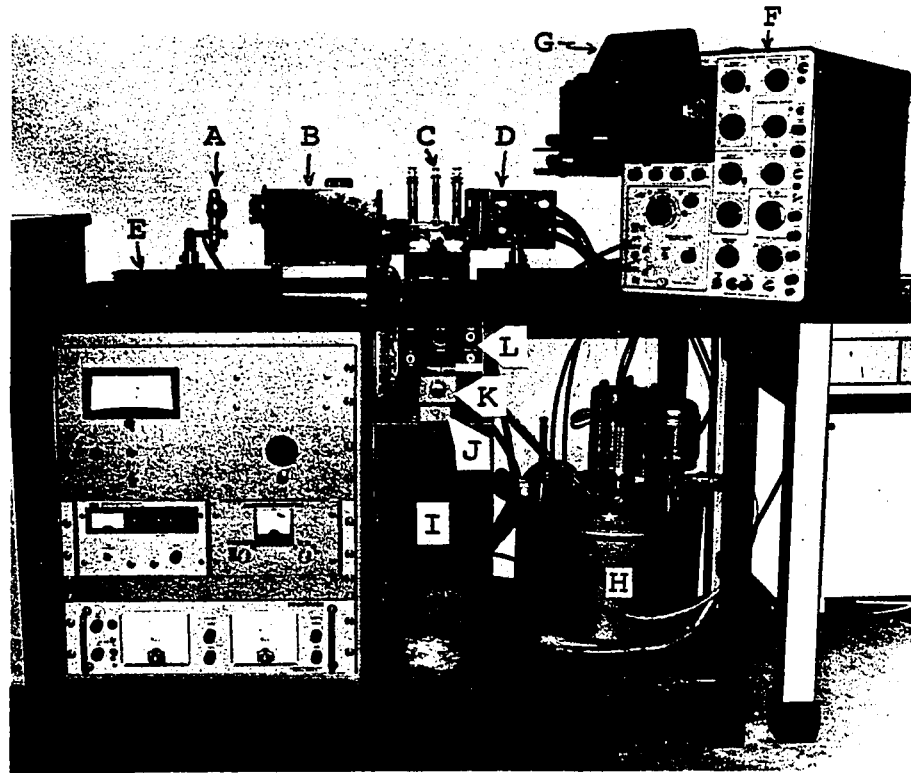


Figure 13. Apparatus Table

Key: A, lamp; B, monochromator; C, stopped-flow apparatus; D, photomultiplier; E, optical bench; F, oscilloscope; G, camera and adapter; H, constant temperature bath; I, box containing capacitor and spark gap; J, trigger output; K, high voltage discharge switch; L, trigger module. The cabinet on the left contains the various power supplies.

of two pieces of 1" angle iron spaced 3/4" apart. Details of the optical bench and mounting arrangement can be seen in more detail in Figure 8. Also shown in Figure 13 are the oscilloscope (F), camera and adapter (G) and constant temperature bath (H). The capacitor and spark gap are contained in the metal box (I), located behind the trigger output (J), high voltage discharge switch (K) and trigger module (L). The cabinet contains the various power supplies and the batteries for the photomultiplier zero offset control. Conversion from a stopped-flow apparatus to a temperature-jump apparatus is simply a matter of unbolting the one, replacing it with the canister housing the temperature-jump cell, and checking the alignment of the optical system, a procedure which takes only a few minutes.

of two pieces of 1" angle iron spaced 3/4" apart. Details of the optical bench and mounting arrangement can be seen in more detail in Figure 8. Also shown in Figure 13 are the oscilloscope (F), camera and adapter (G) and constant temperature bath (H). The capacitor and spark gap are contained in the metal box (I), located behind the trigger output (J), high voltage discharge switch (K) and trigger module (L). The cabinet contains the various power supplies and the batteries for the photomultiplier zero offset control. Conversion from a stopped-flow apparatus to a temperature-jump apparatus is simply a matter of unbolting the one, replacing it with the canister housing the temperature-jump cell, and checking the alignment of the optical system, a procedure which takes only a few minutes.

CHAPTER 3. THE KINETICS OF CYANIDE BINDING
BY FERRIC HORSERADISH PEROXIDASE

A study of the kinetics of cyanide binding to HRP* might be expected to yield fundamental information about the nature of the active site in peroxidase. An early study of this reaction at pH 4.2 and 6.2 showed little change in the value of the forward rate constant⁸. This chapter contains a report of a study of this reaction at nineteen values of pH, ranging from 4.21 to 11.31.

Experimental

Kinetic measurements were made using the stopped-flow apparatus and spectrophotometric detection system described

*Abbreviations used in this chapter: HRP or P, ferric horseradish peroxidase; RZ, purity number, after Theorell and Maehly¹⁴; μ , ionic strength; CN and PCN, all ionizable species of cyanide and complex; HP and H₂P, protonated forms of peroxidase; [F], [CN], and [PCN], equilibrium concentrations of all forms of peroxidase, cyanide, and complex; [P]₀ and [CN]₀, initial concentrations of all forms of peroxidase and cyanide; K₁, dissociation constant of ligand; K_d, dissociation constant of peroxidase-cyanide complex; k_i and k₋₁, apparent second-order binding rate constant and apparent first-order dissociation rate constant.

in Chapter 2. Auxiliary absorbance measurements and spectrophotometric equilibrium constant determinations were made on a Beckman DU spectrophotometer. The cell compartment of the DU and the stopped-flow apparatus were both thermostated at 25.0 ± 0.1 °C. A Beckman expanded scale pH meter was used for all pH measurements.

HRP (analytical reagent grade, RZ = 2.9, lot 6485206 and purified grade, RZ = 0.9) was obtained from the Boehringer-Mannheim Corp., N. Y. Reagent grade potassium cyanide (Fisher) was used without further purification. The concentrations of stock KCN solutions were determined by titration with a standard silver nitrate solution using potentiometric determination of the end point. Below pH 8, possible loss of HCN was minimized by using solutions of cyanide which were less than 10^{-4} M and by keeping them in tightly closed vessels which contained only a small volume of air. All solutions were made from conductivity water.

Solutions of HRP and cyanide were each made to the desired pH using buffer of ionic strength equal to 0.01 and sufficient potassium nitrate so that the total ionic strength was constant at μ equal to 0.11. Concentrations of HRP and cyanide were varied at different pH values in such a manner that the experimental absorbances ranged from 0.25 to 0.50, which is in the region of minimum error due to instrumental uncertainty⁵⁹. The total HRP concentration was typically 5×10^{-6} M, while the total cyanide concentration ranged

from about 5×10^{-6} M to 1×10^{-4} M over the pH range in which experiments were performed.

The buffer systems employed at various pH ranges were: acetate below pH 5.5, cacodylic acid between pH 5.5 and 7.0, tris-nitric acid between pH 7.0 and 9.0, borate between pH 8.0 and 10.0, glycine between pH 9.0 and 11.0, and potassium hydroxide above pH 11. Each buffer was checked for possible complexing with HRP by examining the spectrum of HRP at a particular pH in the presence and absence of buffer. In addition, experiments were repeated with two or more different buffers in all overlapping regions. In all cases, experiments at the same pH but with different buffers gave results agreeing within experimental error.

HRP and its complexes are known to undergo splitting at extremes of pH³⁰. Experiments at the pH extremes were performed with sufficient rapidity that the decrease in absorbance of HRP at 403 m μ during the experiment was less than 1%. Above pH 10 problems in pH control were encountered because of absorption of carbon dioxide from the atmosphere. These were overcome by using freshly boiled water for solutions and by passing nitrogen over any vessel open to the air during the preparation of solutions.

Results

The equation for the reaction studied is that for

second-order-first-order reversible kinetics*:



The course of the reaction can be followed conveniently using light of wavelength 422 mμ, which was found to correspond to the maximum of the Soret absorption peak of the HRP-CN complex (this value differs slightly from Keilin and Hartree's assignment of 423 mμ for the same maximum⁵). A photograph of a typical oscilloscope trace showing a record of photomultiplier output voltage vs. time is reproduced in Figure 14. Values of these quantities were read from an enlargement of the picture and the results were converted to concentration of the HRP-CN complex vs. time in the manner described below.

As pointed out in Chapter 2, the photomultiplier output voltage is proportional to the transmittance of the solution in the stopped-flow observation chamber. If the reaction is slow compared to the mixing time, as is the case with the reaction of cyanide with HRP, one can assume that the point on the trace corresponding to t=0, henceforth designated TP, represents the transmittance of pure HRP only since effectively no reaction has occurred. Similarly, the

*The symbols \rightleftharpoons are used for reactions occurring at measurable rates and \rightleftharpoons for reactions in which equilibrium is assumed to be maintained⁶⁰.

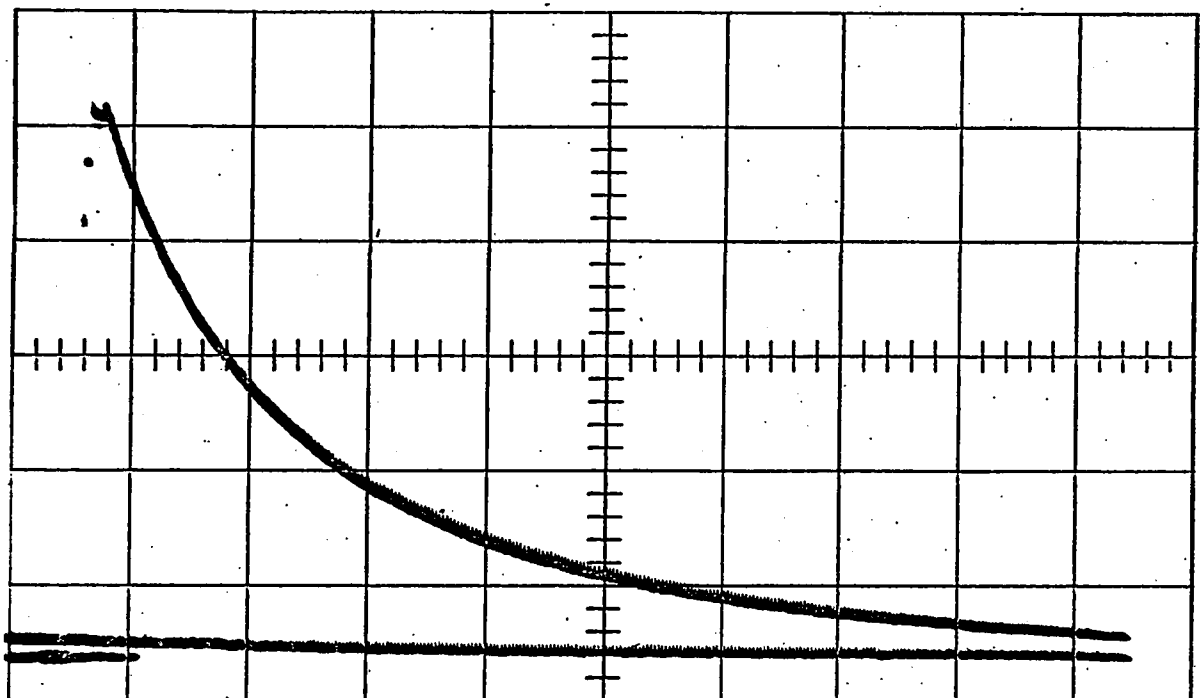


Figure 14. Typical oscilloscope trace showing the progress of the reaction between HRP and cyanide. Horizontal scale: 500 mv/division; vertical scale: 0.5 sec/division.

voltage output when the reaction reaches equilibrium corresponds to the transmittance of the reaction mixture, T_E . One can measure T_P simply by taking a portion of the stock peroxidase to be used in the stopped-flow experiment, diluting by a factor of two, and measuring the transmittance of the solution on a Beckman DU spectrophotometer. Similarly, a 1:1 mixture of stock HRP and ligand solutions can be measured on a DU to yield T_E . In both cases, a small correction must be made to take into account the fact that path length in the DU is 1.000 cm, and the path length in the stopped-flow apparatus is 1.067 cm. The transmittance at any time, $T(t)$, can then be calculated by linear interpolation. If a photograph of an experimental trace is projected onto graph paper and the point T_P is set equal to 0,0 one can obtain numerical readings from the graph paper, $R(t)$, as a function of time, and also a numerical reading, R_E , which corresponds to T_E for the reaction. One can then write the interpolation equation:

$$T(t) = T_P - \left(\frac{R(t)}{R_E}\right)(T_P - T_E) \quad (2)$$

The values of $T(t)$ can be converted to corresponding absorbance values by:

$$A(t) = \log[1.0/T(t)] \quad (3)$$

We now have values for total absorbance vs. time for the course of the reaction. However, the total absorbance at 422 m μ has contributions from both HRP and HRP-CN and, at any time during the course of the reaction, is given by:

$$A_T = (\epsilon_p [P] + \epsilon_c [PCN])1.067 \quad (4)$$

where ϵ_p and ϵ_c are the molar absorptivities of HRP and HRP-CN at 422 m μ , and 1.067 the path length in the stopped-flow observation chamber. From eq 1, we can introduce into eq 4 the expression

$$[P] = [P]_o - [PCN] \quad (5)$$

which results in

$$A_T = 1.067(\epsilon_p [P]_o + (\epsilon_c - \epsilon_p)[PCN]) \quad (6)$$

ϵ_c was found to be constant over the pH range used in this study; however, ϵ_p varied considerably at pH values above 9.5 due to the shift in the Soret peak of HRP upon formation of its hydroxide complex. Equation 6 can be simplified with additional auxiliary absorbance measurements. Another portion of the stock HRP solution is taken and added to an equal volume of cyanide solution of sufficient concentration that 100 % PCN is formed, and the absorbance of the solution is measured to yield a term designated AC. Knowing AC and AP (the absorbance corresponding to TP), an equation can be written which expresses ϵ_p in terms of ϵ_c . For a path length of 1.00 cm:

$$AP = \epsilon_p [P]_o \quad (7)$$

$$\text{and} \quad AC = \epsilon_c [P]_o \quad (8)$$

Equations 7 and 8 can be combined to give:

$$\epsilon_p = \frac{AP \epsilon_c}{AC} \quad (9)$$

Now, substituting eq 7 and 9 into eq 6:

$$A_T = 1.067 \left(AP + \epsilon_c \left(1 - \frac{AP}{AC} \right) [PCN] \right) \quad (10)$$

Equation 10 can be rearranged to give the final desired equation which gives [PCN] at any time:

$$[PCN] = \frac{A_T - 1.067AP}{1.067\epsilon_c \left(1 - \frac{AP}{AC} \right)} \quad (11)$$

For each experiment which was performed, duplicate solutions were made up for the measurement of each of AP, AC and TE; these values were measured and the average of the determinations calculated. After the stopped-flow experiment was performed, values of RE and R(t) vs. time were read from the photographs of the oscilloscope traces with the aid of a photographic enlarger. Data consisting of the values of AP, AC, TE, RE and R(t) and the corresponding times, along with a value of $\epsilon_c = 9.39 \times 10^4 \text{ M}^{-1}\text{cm}^{-1}$ as determined by Keilin and Hartree⁵, were used with a computer program consisting of eq 2, 3, and 11 to yield values of [PCN] vs. time. Once [PCN] is known as a function of time for the course of the reaction, one can proceed with the analysis of the data from the photographs of the oscilloscope traces.

The differential rate equation corresponding to eq 1 is:

$$\frac{d[PCN]}{dt} = k_1[P][CN] - k_{-1}[PCN] \quad (12)$$

The apparent rate constants were obtained by direct use of eq 12, but with $d[PCN]/dt$ approximated by $\Delta[PCN]/\Delta t$; i.e., by taking a chord over a short interval as equal to the tangent at the center of that interval. Using this

approximation, along with the average concentration of PCN complex within the interval, $[PCN]_{av}$, eq 12 becomes:

$$\frac{\Delta[PCN]}{\Delta t} = k_1^i ([P]_o - [PCN]_{av})([CN]_o - [PCN]_{av}) - k_{-1}^i [PCN]_{av} \quad (13)$$

In order that the chords would be good approximations of tangents, the following technique was used: $\Delta[PCN]/\Delta t$ was determined over short intervals of time in the early stages of the reaction when the rate was changing rapidly with time, and then at increasingly larger intervals as the reaction approached equilibrium. Values of k_1^i and k_{-1}^i could then be obtained from eq 13 when experimental data consisting $\Delta[PCN]/\Delta t$ and the corresponding $[PCN]_{av}$ was used with a nonlinear least-squares computer program. A copy of this program is found in Appendix I. Fifteen to twenty points from each experimental trace were used to help ensure a valid analysis. Generally three oscilloscope traces were analyzed for each experiment and average values of k_1^i and k_{-1}^i were determined.

Although eq 12 can be integrated when $[P]_o \neq [CN]_o$, the resultant equation is complex⁴⁹. For the case where $[P]_o = [CN]_o$, the integrated form of eq 12 is⁵¹:

$$\frac{[PCN]}{([CN]_o^2 - [PCN]^2)} \ln \frac{[PCN]([CN]_o^2 - [PCN][PCN])}{[CN]_o^2([PCN] - [PCN])} = k_1^i t \quad (14)$$

A plot of the left side of this equation vs. time should give a straight line of slope equal to k_1^i and an intercept of zero. Unfortunately, eq 14 suffers from two disadvantages: it does not yield k_{-1}^i and it can be used only if

$[P]_0$ equals $[CN]_0$. A plot of the left side of eq 14 vs. time for an experiment at pH 6.5 where $[P]_0$ was equal to $[CN]_0$ is shown in Figure 15. The resulting value for k'_1 , agreed within 5 % of the value obtained using the computer analysis of eq 13.

The experimental rate constants obtained at each pH studied are presented in Table III. Found in Table IV are values of the dissociation constants for the HRP-CN complex obtained in two different ways: direct spectrophotometric determination and calculation from $K_d = k'_{-1}/k'_1$. The spectrophotometric determination consisted of determining $[PCN]$ for an equilibrium mixture of HRP and cyanide and using eq 15, below, for calculation of the equilibrium constant.

$$K_d = \frac{([P]_0 - [PCN])([CN]_0 - [PCN])}{[PCN]} \quad (15)$$

Plots of the logs of k'_1 , k'_{-1} and K_d vs. pH are shown in Figures 16, 17 and 18, respectively.

Most of the work was done using crude HRP; runs at pH 4.2, 5.5 and 8.5 were repeated using pure HRP. The results obtained from the pure HRP agreed within 10 % of the corresponding results using crude HRP. As will be discussed further in Chapter 5, the possible presence of isozymes^{10, 11} in the commercial HRP used does not affect significantly the observed kinetic results of this study or their interpretation.

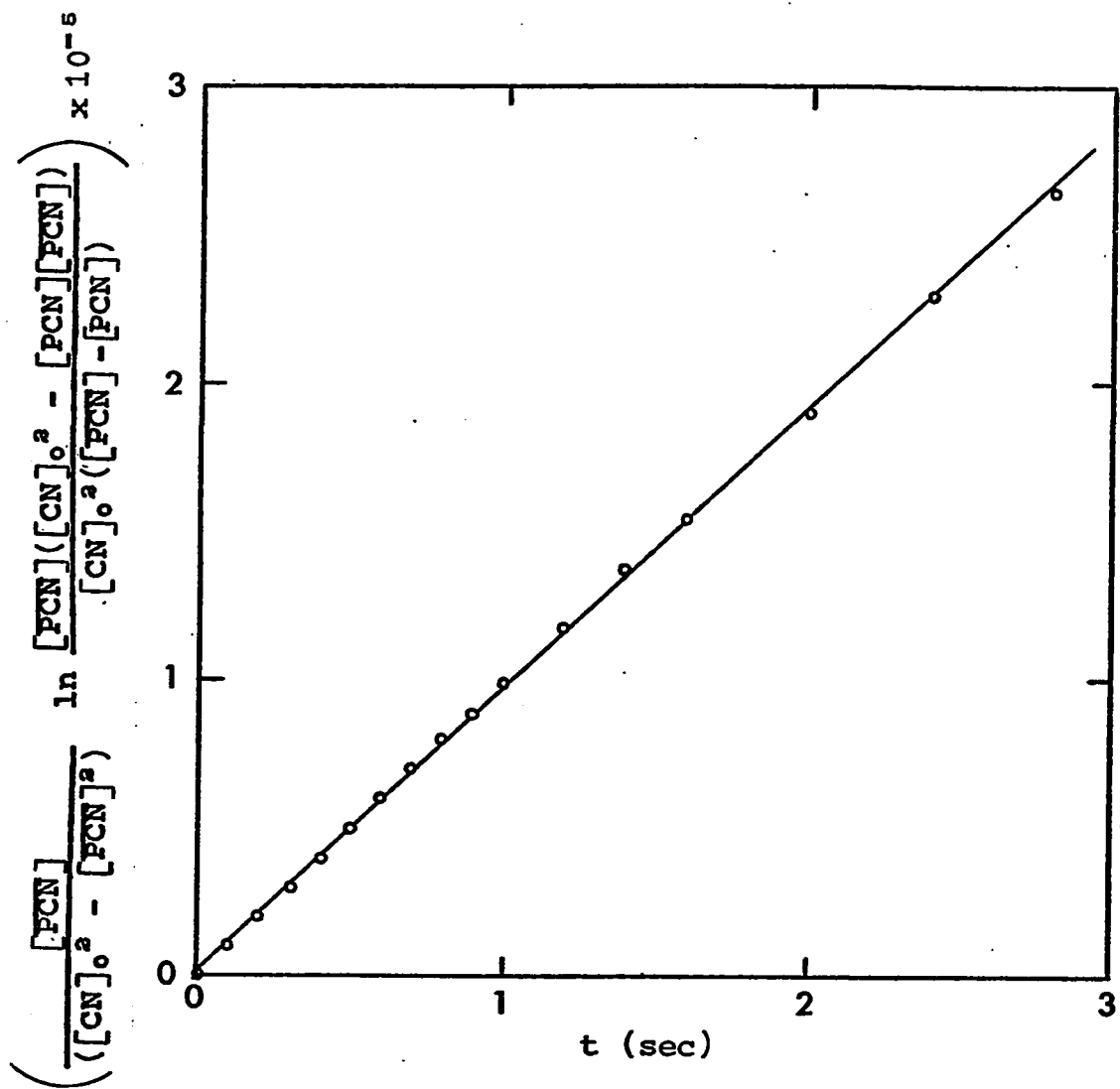


Figure 15. Test of reversible second-order-first-order kinetics. The left side of eq 14 is plotted vs. time using data for the reaction of HRP with cyanide at pH 6.5. The slope is equal to k_1 .

Table III

Rate Data for the Binding of Cyanide by Peroxidase at 25°C.

Experimental Rate Constants With Standard Deviations		
pH	k_1 ($M^{-1}sec^{-1}$)	k_{-1} (sec^{-1})
4.21	$(6.1 \pm 0.3) \times 10^4$	$(1.7 \pm 0.2) \times 10^{-1}$
4.46	$(7.3 \pm 0.3) \times 10^4$	$(1.7 \pm 0.2) \times 10^{-1}$
4.96	$(8.8 \pm 0.5) \times 10^4$	$(1.9 \pm 0.2) \times 10^{-1}$
5.50	$(1.2 \pm 0.1) \times 10^5$	$(1.9 \pm 0.2) \times 10^{-1}$
5.94	$(1.0 \pm 0.1) \times 10^5$	$(1.8 \pm 0.3) \times 10^{-1}$
6.50	$(9.7 \pm 0.5) \times 10^4$	$(2.0 \pm 0.2) \times 10^{-1}$
7.05	$(9.8 \pm 0.5) \times 10^4$	$(2.8 \pm 0.3) \times 10^{-1}$
7.47	$(9.4 \pm 0.5) \times 10^4$	$(2.9 \pm 0.3) \times 10^{-1}$
8.11	$(7.2 \pm 0.4) \times 10^4$	$(2.9 \pm 0.3) \times 10^{-1}$
8.55	$(6.6 \pm 0.4) \times 10^4$	$(2.9 \pm 0.2) \times 10^{-1}$
8.98	$(4.6 \pm 0.3) \times 10^4$	$(3.2 \pm 0.2) \times 10^{-1}$
9.39	$(2.4 \pm 0.2) \times 10^4$	$(2.9 \pm 0.2) \times 10^{-1}$
9.84	$(1.0 \pm 0.1) \times 10^4$	$(2.3 \pm 0.1) \times 10^{-1}$
10.10	$(5.9 \pm 1.1) \times 10^3$	$(2.6 \pm 0.3) \times 10^{-1}$
10.33	$(3.4 \pm 0.3) \times 10^3$	$(1.9 \pm 0.2) \times 10^{-1}$
10.48	$(2.2 \pm 0.2) \times 10^3$	$(2.0 \pm 0.2) \times 10^{-1}$
10.73	$(1.0 \pm 0.1) \times 10^3$	$(1.3 \pm 0.1) \times 10^{-1}$
11.05	$(2.7 \pm 0.3) \times 10^2$	$(8.9 \pm 1.2) \times 10^{-2}$
11.31	$(1.0 \pm 0.1) \times 10^2$	$(7.3 \pm 1.0) \times 10^{-2}$

Table IV

Equilibrium Data for the Binding of Cyanide
by Peroxidase at 25°C.

$$K_d = \frac{[P][CN]}{[PCN]}$$

pH	From Kinetic Data	Spectrophotometric Determination*
4.21	$(2.9 \pm 0.4) \times 10^{-6}$	$(2.6 \pm 0.2) \times 10^{-6}$
4.46	$(2.3 \pm 0.3) \times 10^{-6}$	2.1×10^{-6}
4.96	$(2.1 \pm 0.3) \times 10^{-6}$	2.0×10^{-6}
5.50	$(1.7 \pm 0.3) \times 10^{-6}$	$(1.5 \pm 0.2) \times 10^{-6}$
5.94	$(1.7 \pm 0.3) \times 10^{-6}$	1.6×10^{-6}
6.50	$(2.1 \pm 0.2) \times 10^{-6}$	$(1.9 \pm 0.2) \times 10^{-6}$
7.05	$(2.9 \pm 0.3) \times 10^{-6}$	$(2.4 \pm 0.2) \times 10^{-6}$
7.47	$(3.2 \pm 0.4) \times 10^{-6}$	2.7×10^{-6}
8.11	$(4.1 \pm 0.5) \times 10^{-6}$	$(3.5 \pm 0.1) \times 10^{-6}$
8.55	$(4.3 \pm 0.4) \times 10^{-6}$	$(4.0 \pm 0.2) \times 10^{-6}$
8.98	$(7.0 \pm 0.5) \times 10^{-6}$	$(6.3 \pm 0.5) \times 10^{-6}$
9.39	$(1.2 \pm 0.1) \times 10^{-5}$	$(1.2 \pm 0.1) \times 10^{-5}$
9.84	$(2.3 \pm 0.1) \times 10^{-5}$	2.2×10^{-5}
10.10	$(4.5 \pm 0.7) \times 10^{-5}$	$(4.2 \pm 0.7) \times 10^{-5}$
10.33	$(5.7 \pm 0.6) \times 10^{-5}$	5.4×10^{-5}
10.48	$(9.1 \pm 1.4) \times 10^{-5}$	$(8.8 \pm 0.4) \times 10^{-5}$
10.73	$(1.3 \pm 0.2) \times 10^{-4}$	$(1.3 \pm 0.1) \times 10^{-4}$
11.05	$(3.3 \pm 0.6) \times 10^{-4}$	$(3.1 \pm 0.4) \times 10^{-4}$
11.31	$(7.1 \pm 1.2) \times 10^{-4}$	6.6×10^{-4}

*Error limits are average deviations for multiple determinations, no limits given for single determinations.

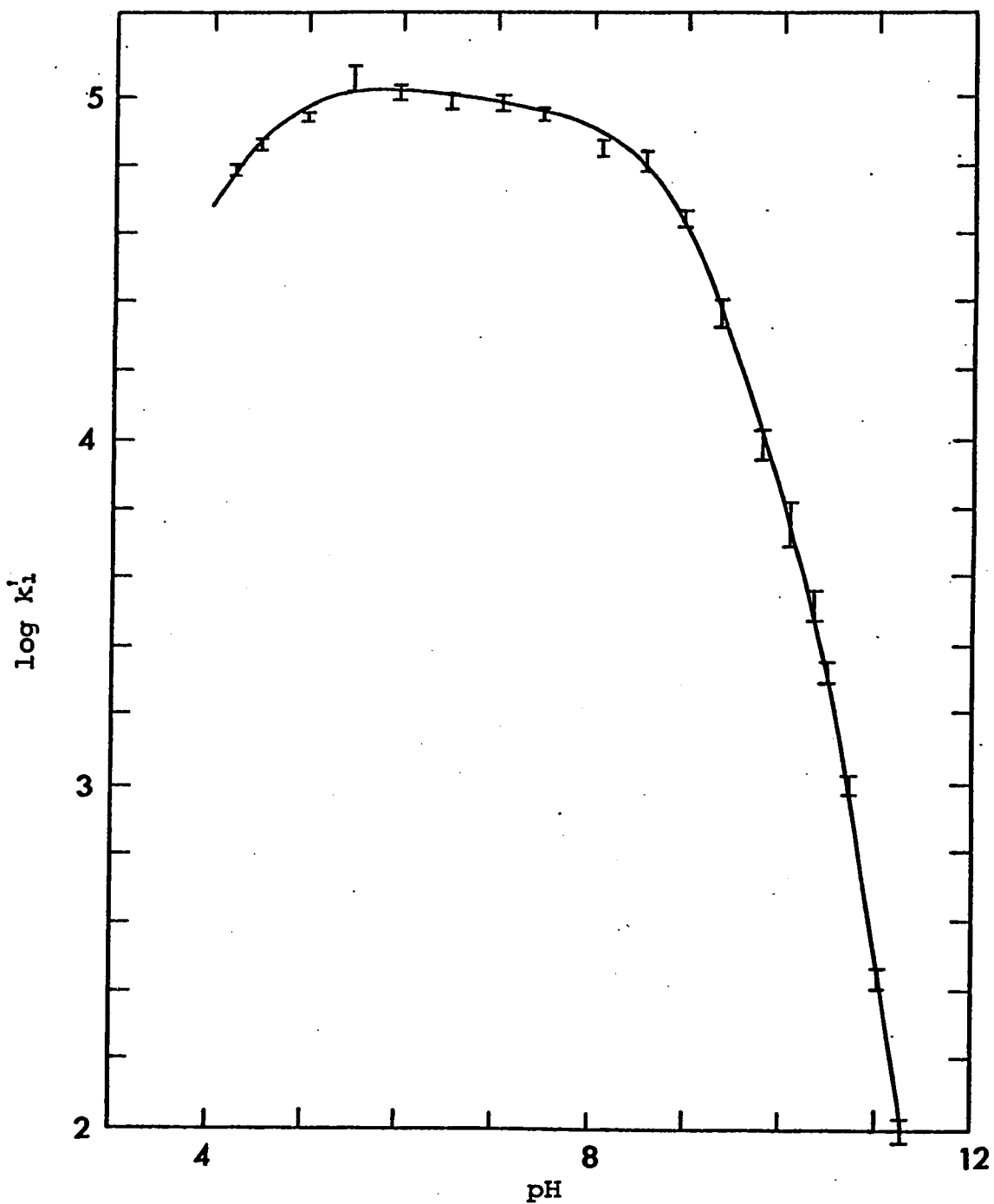


Figure 16. Plot of $\log k_1$ vs. pH for the binding of cyanide by HRP. The solid line is calculated using the best-fit parameters of mechanism V.

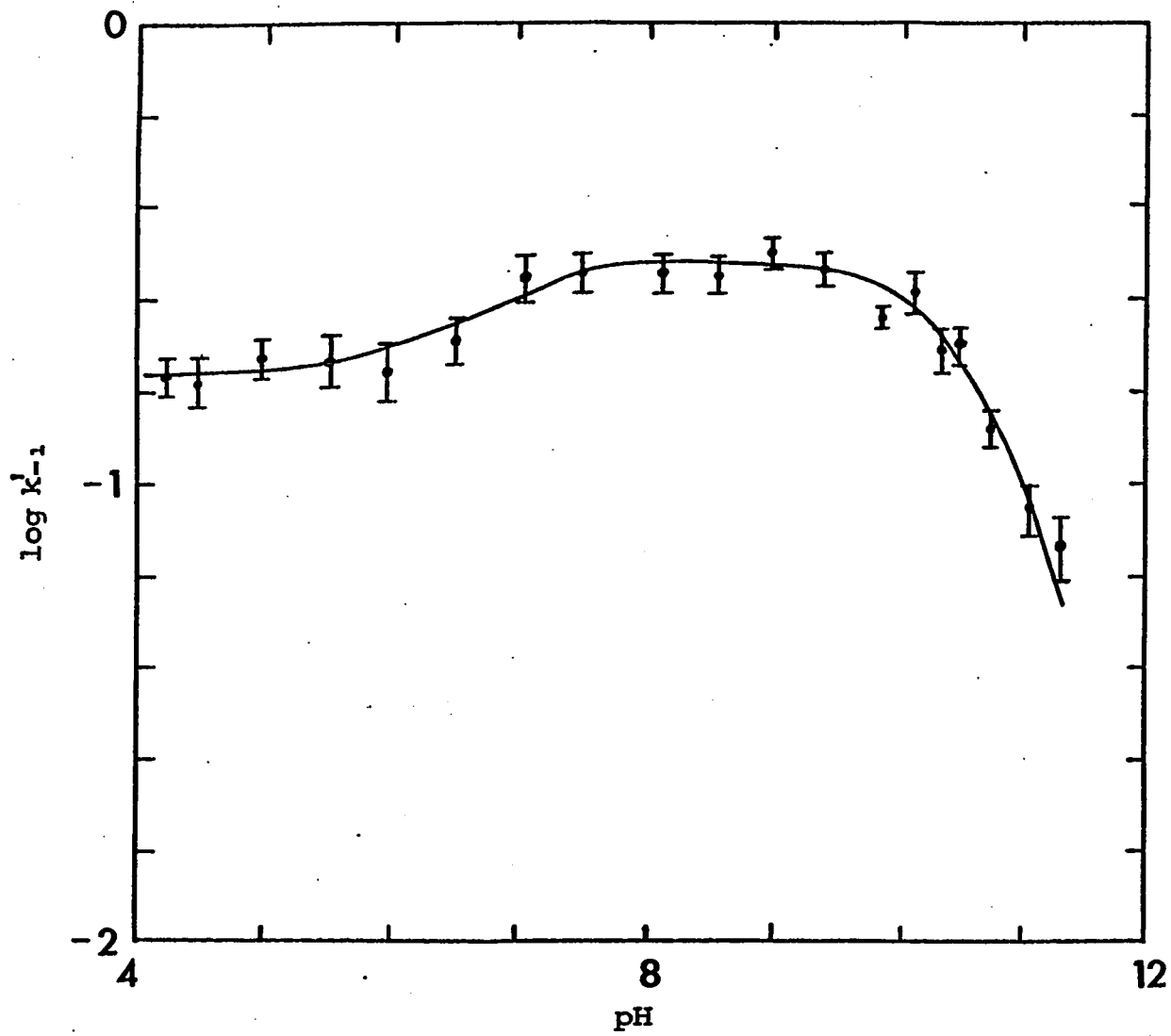


Figure 17. Plot of $\log k'_{-1}$ vs. pH for the dissociation of HRP-cyanide complex. The solid line is calculated using the best-fit parameters of mechanism V.

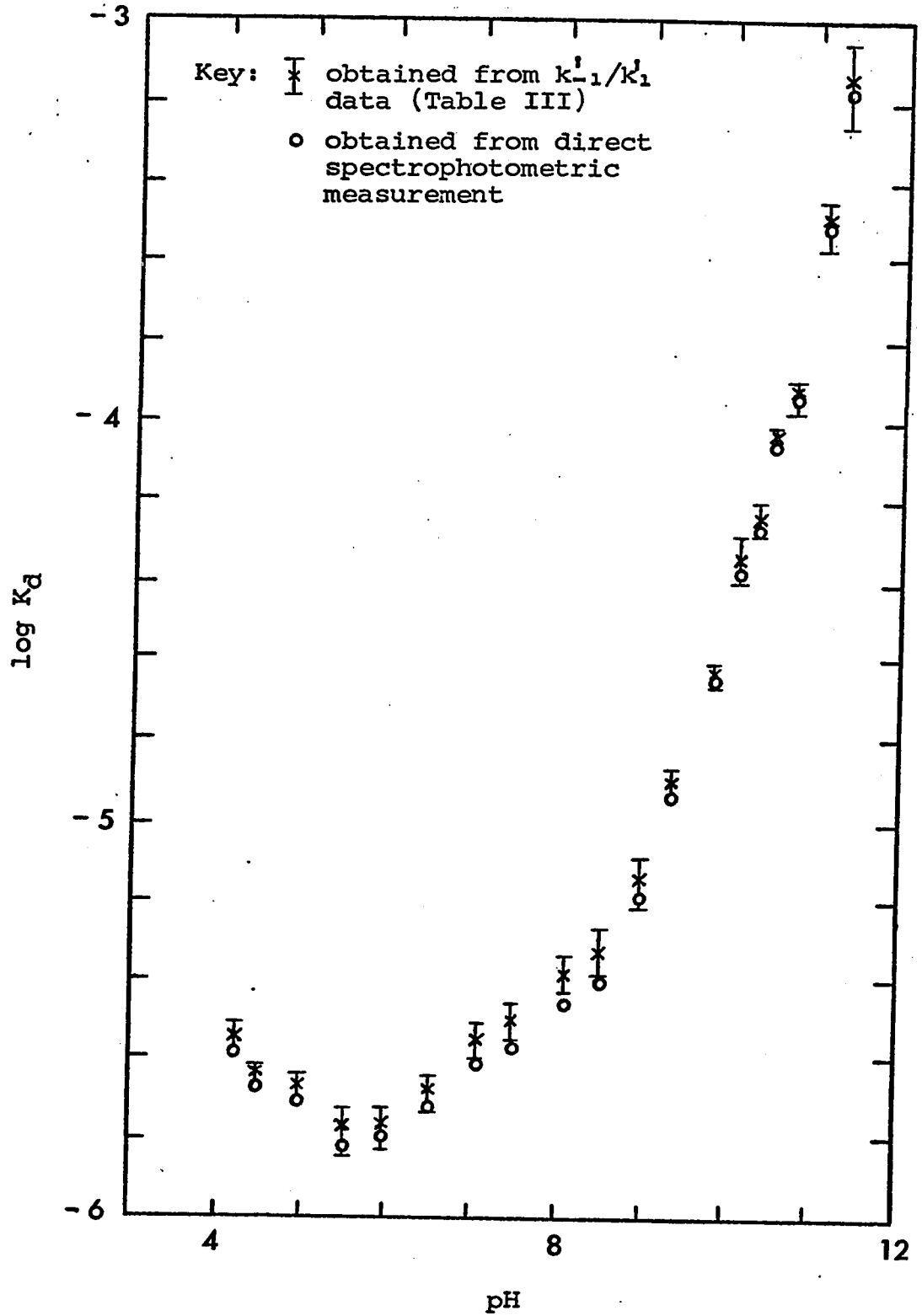
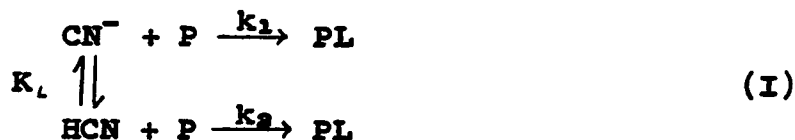


Figure 18. Plot of $\log K_d$ vs. pH for the HRP-CN complex.

Discussion

The pK for the dissociation of hydrocyanic acid is 9.21 at 25°C. and zero μ^{63} . An extended Debye-Hückel equation⁶³ was used to calculate the activity coefficients at μ equal to 0.11 and yielded a corrected pK of 9.0. Since the study was made over a pH range encompassing both sides of this pK, both CN^- and HCN must be considered as possible binding ligands. The first mechanism considered is the binding of cyanide to HRP with no heme-linked ionizable groups*:



The representation of mechanism I contains several simplifying features: hydrogen ions have been omitted, the charges on the proton species are not shown since they are unknown, and the HRP-ligand complex has been designated PL without specifying whether the ligand is bound as HCN or CN^- since this is irrelevant to the analysis of the k_1 data. The form of the complex and the nature of the reverse reaction will

*A heme-linked ionizable group is defined as any ionizable group in HRP which influences the binding of a ligand at the sixth coordination position of the heme ferric iron. This group may be part of either the prosthetic group or protein moiety.

be considered for the analysis of the k_1' data.

For the analysis of the apparent forward rate constant data, it is necessary to have an equation which relates the specific rate constants of mechanism I to k_1' of eq 1. From mechanism I, neglecting the reverse rate term:

$$\frac{d[PL]}{dt} = k_1[P][CN^-] + k_2[P][HCN] \quad (16)$$

Multiplying the right side of eq 16 by

$([HCN]+[CN^-])/([HCN]+[CN^-])$ yields:

$$\frac{d[PL]}{dt} = \frac{k_1[P][CN^-]([HCN]+[CN^-])}{[HCN]+[CN^-]} + \frac{k_2[P][HCN]([HCN]+[CN^-])}{[HCN]+[CN^-]} \quad (17)$$

Introducing the notation $[CN] = [CN^-] + [HCN]$ and rearranging, eq 17 becomes:

$$\frac{d[PL]}{dt} = \frac{k_1[P][CN]}{\frac{[CN^-]}{[CN^-]} + \frac{[HCN]}{[CN^-]}} + \frac{k_2[P][CN]}{\frac{[HCN]}{[HCN]} + \frac{[CN^-]}{[HCN]}} \quad (18)$$

Simplification of eq 18 by use of the ligand dissociation constant $K_L = ([H^+][CN^-])/[HCN]$ leads to the expression:

$$\frac{d[PL]}{dt} = \frac{k_1[P][CN]}{1 + \frac{[H^+]}{K_L}} + \frac{k_2[P][CN]}{1 + \frac{K_L}{[H^+]}} \quad (19)$$

Comparing eq 19 with eq 12 one obtains the desired result, which is:

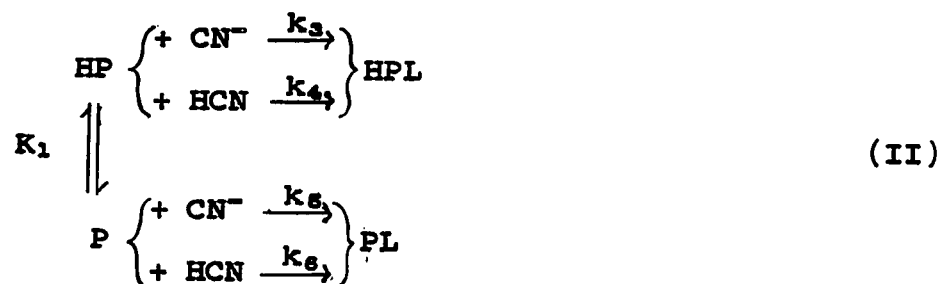
$$k_1' = \frac{k_1}{1 + \frac{[H^+]}{K_L}} + \frac{k_2}{1 + \frac{K_L}{[H^+]}} \quad (20)$$

Equation 20 can be rearranged to the form of a linear equation:

$$k_1' \left(1 + \frac{K_L}{[H^+]}\right) = k_3 + \frac{k_1 K_L}{[H^+]} \quad (21)$$

If mechanism I were valid, a plot of $k_1'(1 + K_L/[H^+])$ vs. $1/[H^+]$ would be linear, with a slope equal to $k_1 K_L$ and an intercept equal to k_3 . As can be seen in Figure 19, this plot is not linear, so mechanism I is not valid.

The next simplest mechanism involves the participation of one heme-linked group:



Total charges on the peroxidase species and the equilibria involving the ligand species have been omitted, although the effect of the dissociation of HCN on the concentration of ligand has been taken into account in the mathematical treatment of the mechanism. A derivation analogous to that used for eq 20 yields for mechanism II:

$$k_1' = \frac{k_3 + \frac{k_4 [H^+]}{K_L} + \frac{k_5 K_1}{[H^+]} + \frac{k_6 K_1}{K_L}}{1 + \frac{K_1}{[H^+]} + \frac{[H^+]}{K_L} + \frac{K_1}{K_L}} \quad (22)$$

Equation 22 can be used with a nonlinear least-squares program to yield the best-fit values of specific rate constants and equilibrium constant for the heme-linked group. Because the k_1' values have a range of 10^9 , the nonlinear least-

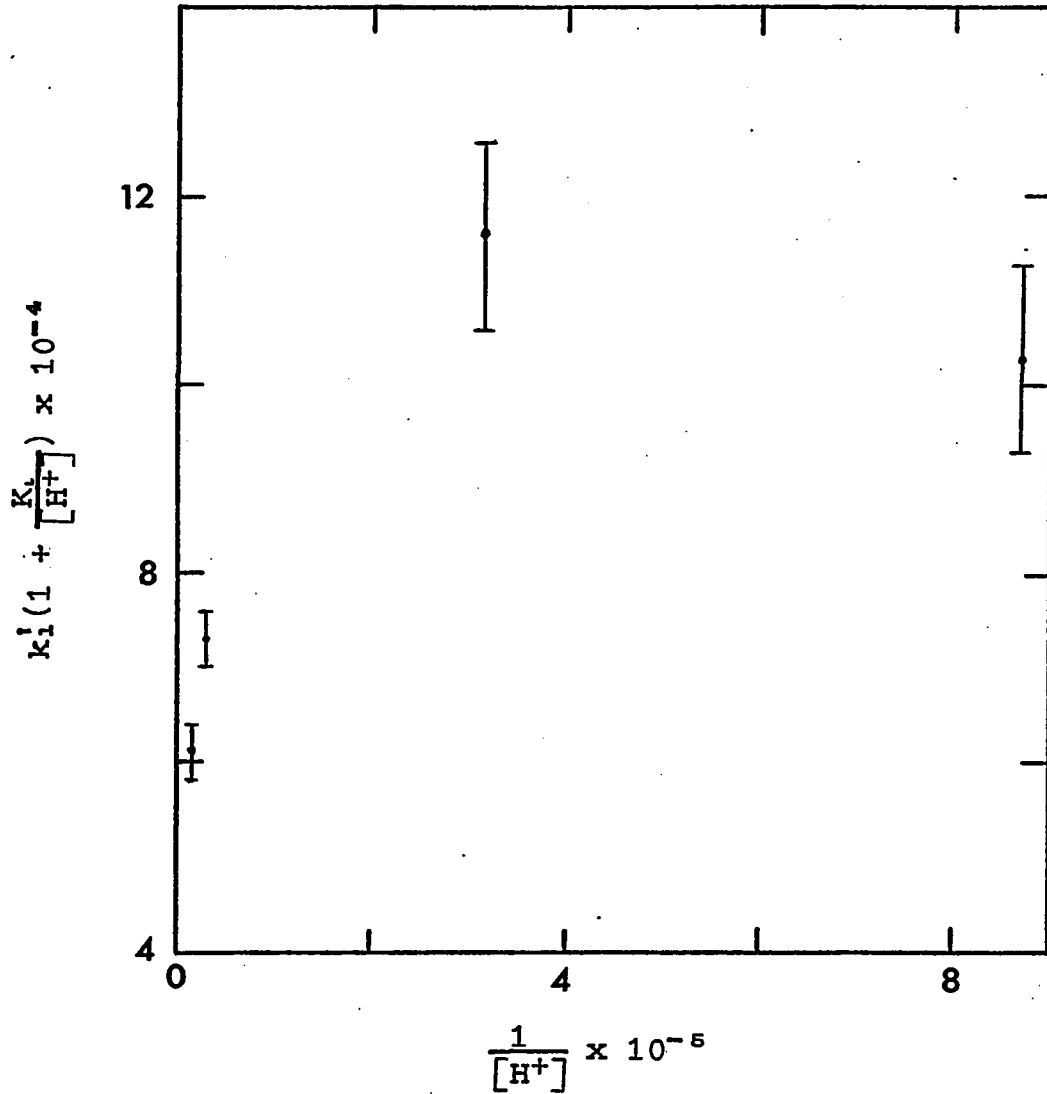
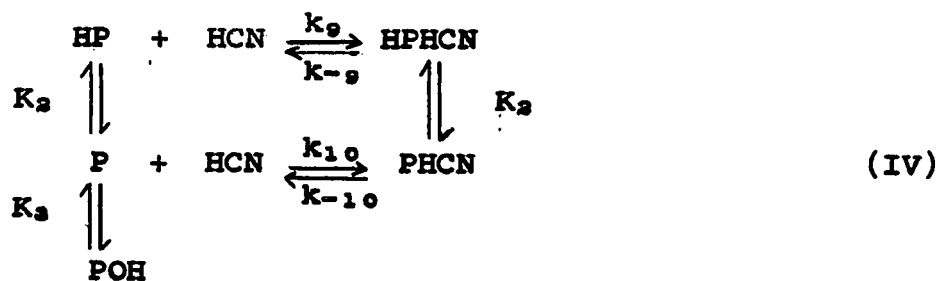


Figure 19. Test of mechanism for HCN and CN^- binding to peroxidase with no heme-linked acid groups (mechanism I). If this mechanism were valid the plot of $k_1^i(1 + K_1/[H^+])$ vs. $[H^+]$ would be linear.



From these mechanisms, one can write the following equations:

$$k_1' \left(1 + \frac{[\text{H}^+]}{K_L}\right) = \frac{k_7}{1 + \frac{K_2}{[\text{H}^+]} + \frac{K_2 K_3}{[\text{H}^+]^2}} + \frac{k_8}{1 + \frac{[\text{H}^+]}{K_2} + \frac{K_3}{[\text{H}^+]}} \tag{23}$$

$$k_1' \left(1 + \frac{K_L}{[\text{H}^+]}\right) = \frac{k_9}{1 + \frac{K_2}{[\text{H}^+]} + \frac{K_2 K_3}{[\text{H}^+]^2}} + \frac{k_{10}}{1 + \frac{[\text{H}^+]}{K_2} + \frac{K_3}{[\text{H}^+]}} \tag{24}$$

$$k_{-1}' = \frac{k_{-7}}{1 + \frac{K_{ac}}{[\text{H}^+]}} + \frac{k_{-8}}{1 + \frac{[\text{H}^+]}{K_{ac}}} \tag{25}$$

$$k_{-1}' = \frac{k_{-9}}{1 + \frac{K_{ac}}{[\text{H}^+]}} + \frac{k_{-10}}{1 + \frac{[\text{H}^+]}{K_{ac}}} \tag{26}$$

Equations 23 and 25 correspond to mechanism III, and eq 24 and 26 correspond to mechanism IV. By proper choice of the values for the adjustable parameters in both eq 23 and 24, a satisfactory fit to the k_1' data is obtained. The best-fit parameters and their standard deviations obtained from non-linear least-squares analysis are shown in Table V. The specific rate constants k_8 and k_9 have effective values of zero, which means that although they might have finite

Table V

Rate and Equilibrium Constants
Obtained from Analysis of Equations 23 and 24

Mechanism III, Eq. 23

$$k_7 = (1.0 \pm 0.1) \times 10^{10} \text{ M}^{-1} \text{ sec}^{-1}$$

$$0 \leq k_8 \leq 20 \text{ M}^{-1} \text{ sec}^{-1}$$

$$K_2 = (1.1 \pm 0.1) \times 10^{-4} \text{ M}$$

$$K_3 = (1.5 \pm 0.4) \times 10^{-11} \text{ M}$$

Mechanism IV, Eq. 24

$$0 \leq k_9 \leq 1 \times 10^4 \text{ M}^{-1} \text{ sec}^{-1}$$

$$k_{10} = (9.6 \pm 0.7) \times 10^4 \text{ M}^{-1} \text{ sec}^{-1}$$

$$K_2 = (1.1 \pm 0.1) \times 10^{-4} \text{ M}$$

$$K_3 = (1.5 \pm 0.4) \times 10^{-11} \text{ M}$$

values, their corresponding terms in eq 23 and 24 do not affect significantly the predicted values of k_1' . They are included, however, because of the discussion below of the principle of detailed balancing. Upper limits on their values, shown in Table V, are estimated by assuming that the corresponding terms in eq 23 and 24 contribute a maximum of five per cent to the predicted values of k_1' .

The predicted value of the pK of the most basic heme-linked group, 10.8, appears to correspond to the pK for the formation of the HRP-hydroxide complex. This pK has been measured at the values ranging from 10.6 to 11.3^{19,34}. Therefore P and POH have been used in mechanisms III and IV to represent HRP with the most acid heme-linked groups ionized, and with water and hydroxide, respectively, in the sixth coordination position of the heme ferric iron.

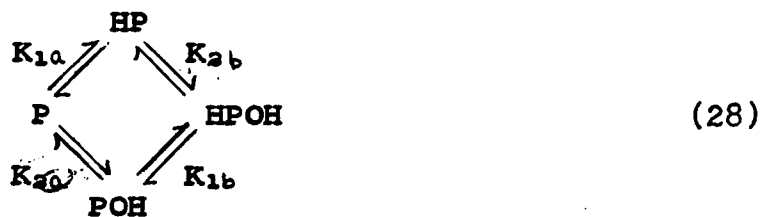
One flaw of mechanisms III and IV is that they allow no simple explanation for the behavior of k_{-1}' at high pH. For the pH region 4.2-9.4, nonlinear least-squares analyses of eq 25 and 26 give the best-fit parameters and their standard deviations: $k_{-7} \equiv k_{-9} = 0.17 \pm 0.02 \text{ sec}^{-1}$;
 $k_{-8} \equiv k_{-10} = 0.30 \pm 0.02 \text{ sec}^{-1}$; $K_{2c} = (1.9 \pm 0.8) \times 10^{-7} \text{ M}$.

Although both mechanisms III and IV can account for the pH dependence of the k_1' data, they are not valid because the principle of detailed balancing is violated. By applying this principle to mechanism III, it can be shown that:

$$k_8 = \frac{k_7 k_{-8} K_{2c}}{k_{-7} K_2} \quad (27)$$

Using reverse rate constant data from above and other data from Table V in the right side of eq 27, one obtains a detailed balance value of $k_8 = (3.0 \pm 1.6) \times 10^7 \text{ M}^{-1} \text{ sec}^{-1}$, while the direct kinetic analysis results in a value of $k_8 \leq 20 \text{ M}^{-1} \text{ sec}^{-1}$. Similar analysis applied to mechanism IV results in $k_8 = (3.1 \pm 1.6) \times 10^7 \text{ M}^{-1} \text{ sec}^{-1}$ compared to $k_8 \leq 1 \times 10^4 \text{ M}^{-1} \text{ sec}^{-1}$. In addition, in the case of mechanism IV, evidence from inorganic chemistry indicates that cyanide complexes of transition metals do not exist with HCN as the bound ligand^{64, 65}. If mechanism IV is revised so the ligand is bound as the anion, it is not possible to fit the k_{-1} data with the equation derived from this version. Thus the mechanisms III and IV must be eliminated.

It should be mentioned here that the protein ionization schemes represented in mechanisms III and IV are also simplifications. That ionization scheme can be more properly written as:



which shows that there are really four ionization constants and four species involved, rather than two ionization constants and three species, as implied in mechanisms III and IV. Following the treatment of Dixon and Webb⁶⁶, K_2 and K_3 ,

the experimentally observable constants, can be considered "molecular" ionization constants and K_{1a} , K_{2a} , K_{1b} and K_{2b} the true group ionization constants. If the two ionizing groups are sufficiently far enough apart that they do not influence each other, then $K_{1a} = K_{1b}$ and $K_{2a} = K_{2b}$. It can be shown⁶⁶ that the relationship between the molecular ionization constants and the group ionization constants is:

$$K_2 = K_{1a} + K_{2a} \quad (29)$$

and
$$K_3 = \left(\frac{1}{K_{1b}} + \frac{1}{K_{2b}} \right)^{-1} \quad (30)$$

If $K_{1a} \gg K_{2a}$, then eq 29 reduces to $K_2 = K_{1a}$ and if $K_{1b} \gg K_{2b}$, then eq 30 reduces to $K_3 = K_{2b}$. Thus, although the kinetic study yields only molecular ionization constants, if these constants differ by more than a factor of 100, they can be taken to represent group ionization constants quite accurately.

Similarly, since the rigorous treatment shows that there are four possible species present rather than the three indicated by the simplified treatment, the meaning of the kinetic assignments must be examined. The binding of a ligand species to HP and POH are unambiguous, but what was represented as binding of a ligand species to P, shown in mechanisms III and IV, could actually be binding to either or both of the species P or HPOH represented in eq 28. This

ambiguity cannot be resolved by use of the kinetic method. The rate expressions for the binding to the species P and HPOH from eq 28 can be written:

$$\text{Rate of binding to P} = k_a[P][L] \quad (31)$$

$$\text{Rate of binding to HPOH} = k_b[\text{HPOH}][L] \quad (32)$$

where [L] represents the ligand concentration. From the equations for the group ionization constants it can be shown that:

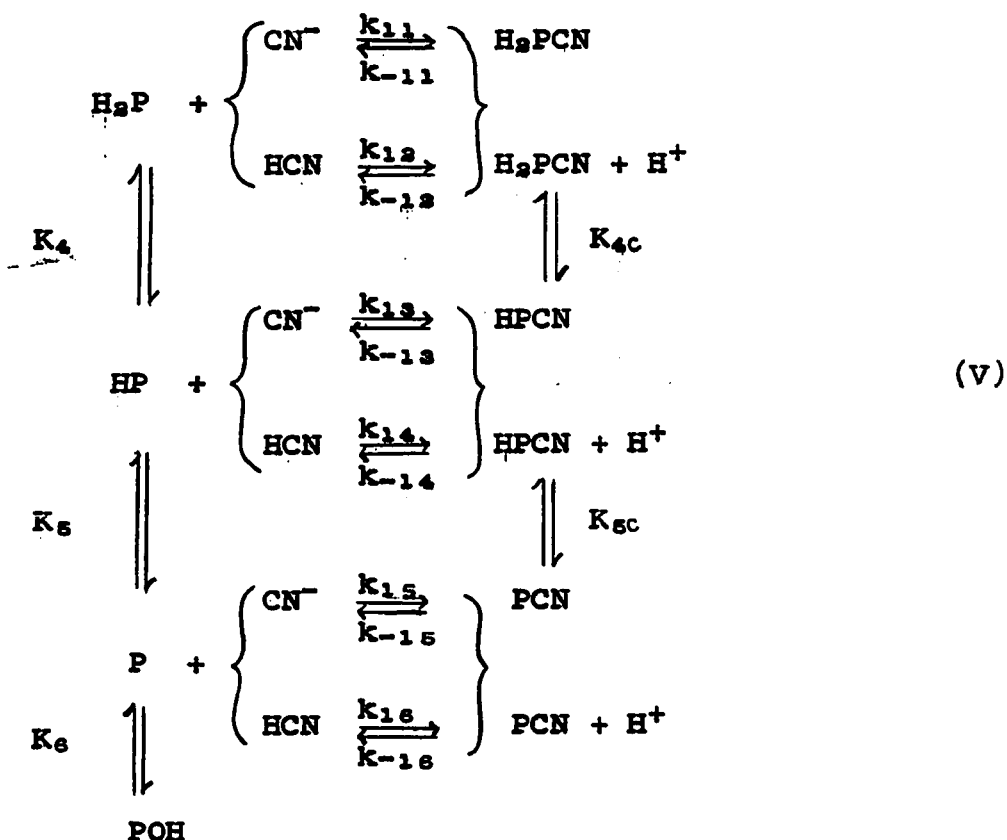
$$\frac{[P]}{[\text{HPOH}]} = \frac{K_{1a}}{K_{2a}} \quad (33)$$

Substituting [HPOH] from eq 33 into eq 32:

$$\text{Rate of binding to HPOH} = k_b\left(\frac{K_{2a}}{K_{1a}}\right)[P][L] \quad (34)$$

Equation 34 is of the same form as eq 31, but with k_a replaced by $k_b(K_{2a}/K_{1a})$. Thus, it is impossible to tell whether the rate constants k_b and k_{10} correspond to k_a , k_b , or a linear combination of the two.

We finally consider mechanism V which involves three heme-linked ionizable groups:



where K_4 , K_5 , K_6 , K_{4c} and K_{5c} are molecular ionization constants. The corresponding rate equations are:

$$\begin{aligned}
 k_1' &= \frac{k_{11} + \frac{k_{12}K_4}{[\text{H}^+]} + \frac{k_{15}K_4K_5}{[\text{H}^+]^2}}{\left(1 + \frac{K_4}{[\text{H}^+]} + \frac{K_4K_5}{[\text{H}^+]^2} + \frac{K_4K_5K_6}{[\text{H}^+]^3}\right) \left(1 + \frac{[\text{H}^+]}{K_L}\right)} \\
 &+ \frac{k_{12} + \frac{k_{14}K_4}{[\text{H}^+]} + \frac{k_{16}K_4K_5}{[\text{H}^+]^2}}{\left(1 + \frac{K_4}{[\text{H}^+]} + \frac{K_4K_5}{[\text{H}^+]^2} + \frac{K_4K_5K_6}{[\text{H}^+]^3}\right) \left(1 + \frac{K_L}{[\text{H}^+]}\right)}
 \end{aligned}
 \quad (35)$$

$$k_{-1}^{\prime} = \frac{k_{-11} + k_{-12}[H^+] + \frac{k_{-13}K_{4c}}{[H^+]} + k_{-14}K_{4c} + \frac{k_{-15}K_{4c}K_{5c}}{[H^+]^2} + \frac{k_{-16}K_{4c}K_{5c}}{[H^+]}}{1 + \frac{K_{4c}}{[H^+]} + \frac{K_{4c}K_{5c}}{[H^+]^2}} \quad (36)$$

Four simplifications of mechanism V and of the corresponding eq 35 and 36 fit the experimental rate data satisfactorily and do not violate the principle of detailed balancing. These simplified versions of mechanism V all contain two pairs of forward and reverse specific rate constant terms. All other terms do not contribute. The forward rate constants for these four simplifications are:

(A) k_{11} , k_{13} ; (B) k_{14} , k_{16} ; (C) k_{13} , k_{14} ; (D) k_{11} , k_{16} .

The various kinetic and equilibrium parameters, obtained from nonlinear least-squares analysis, are listed in Tables VI and VII. The same equilibrium constants for the heme-linked ionizable groups and identical predictions, to four significant figures, of the k_1^{\prime} and k_{-1}^{\prime} data are obtained from the four mechanisms. The values of k_1^{\prime} and k_{-1}^{\prime} computed from the best-fit parameters of the four mechanisms are shown by the solid lines in Figs. 16 and 17, respectively.

The equivalence of the four mechanisms in their fit to the experimental rate data is a result of symmetry properties inherent in the overall mechanism V. Thus the rate of binding of CN^- by H_2P , given by $k_{11}[H_2P][CN^-]$, can be rearranged using the relations $K_4 = [H^+][HP]/[H_2P]$ and $K_L = [H^+][CN^-]/[HCN]$ to give $(k_{11}K_L/K_4)[HP][HCN]$. Similarly

Table VI

Rate and Equilibrium Constants
of Simplified Versions A and B of Mechanism V

Constant	Version	
	A	B
k ₁₁	(7.4±1.3) × 10 ⁹ M ⁻¹ sec ⁻¹	*
k ₁₂	*	*
k ₁₃	(3.8±0.4) × 10 ⁷ M ⁻¹ sec ⁻¹	*
k ₁₄	*	(1.1±0.2) × 10 ⁵ M ⁻¹ sec ⁻¹
k ₁₅	*	*
k ₁₆	*	(9.3±1.0) × 10 ⁴ M ⁻¹ sec ⁻¹
k ₋₁₁	0.17±0.03 sec ⁻¹	*
k ₋₁₂	*	*
k ₋₁₃	0.30±0.03 sec ⁻¹	*
k ₋₁₄	*	(9.4±1.6) × 10 ⁵ M ⁻¹ sec ⁻¹
k ₋₁₅	*	*
k ₋₁₆	*	(1.4±0.1) × 10 ¹⁰ M ⁻¹ sec ⁻¹
K ₄	(7.2±2.0) × 10 ⁻⁵ M	(7.2±2.6) × 10 ⁻⁵ M
K ₅	(4.3±0.6) × 10 ⁻⁷ M	(4.3±4.8) × 10 ⁻⁷ M
K ₆	(1.4±0.4) × 10 ⁻¹¹ M	(1.4±0.4) × 10 ⁻¹¹ M
K _{4c}	(1.8±0.9) × 10 ⁻⁷ M	(1.8±0.9) × 10 ⁻⁷ M
K _{5c}	(2.1±0.8) × 10 ⁻¹¹ M	(2.1±0.8) × 10 ⁻¹¹ M

* signifies a rate constant effectively equal to zero.

Table VII

Rate and Equilibrium Constants
of Simplified Versions C and D of Mechanism V

Constant	Version	
	C	D
k_{11}	*	$(7.4 \pm 1.3) \times 10^9 \text{ M}^{-1} \text{ sec}^{-1}$
k_{12}	*	*
k_{13}	$(3.8 \pm 0.4) \times 10^7 \text{ M}^{-1} \text{ sec}^{-1}$	*
k_{14}	$(1.1 \pm 0.2) \times 10^5 \text{ M}^{-1} \text{ sec}^{-1}$	*
k_{15}	*	*
k_{16}	*	$(9.3 \pm 1.0) \times 10^4 \text{ M}^{-1} \text{ sec}^{-1}$
k_{-11}	*	$0.17 \pm 0.03 \text{ sec}^{-1}$
k_{-12}	*	*
k_{-13}	$0.30 \pm 0.03 \text{ sec}^{-1}$	*
k_{-14}	$(9.4 \pm 1.6) \times 10^5 \text{ M}^{-1} \text{ sec}^{-1}$	*
k_{-15}	*	*
k_{-16}	*	$(1.4 \pm 0.1) \times 10^{10} \text{ M}^{-1} \text{ sec}^{-1}$
K_4	$(7.2 \pm 2.6) \times 10^{-5} \text{ M}$	$(7.2 \pm 2.0) \times 10^{-5} \text{ M}$
K_5	$(4.3 \pm 0.6) \times 10^{-7} \text{ M}$	$(4.3 \pm 4.8) \times 10^{-7} \text{ M}$
K_6	$(1.4 \pm 0.4) \times 10^{-11} \text{ M}$	$(1.4 \pm 0.4) \times 10^{-11} \text{ M}$
K_{4c}	$(1.8 \pm 0.9) \times 10^{-7} \text{ M}$	$(1.8 \pm 0.9) \times 10^{-7} \text{ M}$
K_{5c}	$(2.1 \pm 0.8) \times 10^{-11} \text{ M}$	$(2.1 \pm 0.8) \times 10^{-11} \text{ M}$

* signifies a rate constant effectively equal to zero.

$k_{13}[\text{HP}][\text{CN}^-]$ can be converted to $(k_{13}K_L/K_5)[\text{P}][\text{HCN}]$. The equivalent fit of mechanisms VA and VB to the experimental kinetic data implies that $k_{14} = k_{11}K_L/K_4$, and $k_{16} = k_{13}K_L/K_5$. These relations are obeyed by the data in Table VI. In a similar manner, it can be shown from the k_{-1}^1 data that $k_{-14} = k_{-11}/K_{4c}$ and $k_{-16} = k_{-13}/K_{5c}$. It follows that the four mechanisms, VA - VD, are kinetically indistinguishable. It also follows that appropriate linear combinations of the four mechanisms will provide equally satisfactory fits to the experimental rate data.

As an example of the principle of detailed balancing, it can be shown that:

$$k_{13} = \frac{k_{11}k_{-13}K_{4c}}{k_{-11}K_4} \quad (37)$$

From values from Table VI for the factors in the right side of eq 37, $k_{13} = (3.3 \pm 1.9) \times 10^7 \text{ M}^{-1}\text{sec}^{-1}$ compared to $k_{13} = (3.8 \pm 0.4) \times 10^7 \text{ M}^{-1}\text{sec}^{-1}$ obtained from direct kinetic analysis.

In addition to the four simplified versions of mechanism V discussed above, one other mechanism appears to fit the experimental rate data. It is similar to mechanism VB but involves the formation of a complex with undissociated HCN as the bound form of the ligand. Aside from evidence from inorganic chemistry, it can be eliminated, as was the case with mechanism IV, by applying the principle of detailed balancing.

The four simplifications of eq 35 which fit the experimental data can in turn be simplified in certain pH regions, depending on the relative magnitudes of the various parameters. These simplified equations can be rearranged into linear form to provide an alternative means of calculating some of the parameters, as a check on the nonlinear least-squares analysis. For example, in the pH region 4.21-8.11, the expression for ligand binding according to mechanism VA can be reduced to:

$$k'_1 \left(1 + \frac{[H^+]}{K_L}\right) \left(1 + \frac{[H^+]}{K_4} + \frac{K_5}{[H^+]}\right) = k_{13} + \frac{k_{11}[H^+]}{K_4} \quad (38)$$

A plot of the left side of eq 38 vs. $[H^+]$ for $K_4 = 7.2 \times 10^{-5}$ M and $K_5 = 4.3 \times 10^{-7}$ M is shown in Fig. 20. Linear least-squares analysis of the plot yields the values $k_{11}/K_4 = (1.0 \pm 0.2) \times 10^{14}$ sec⁻¹ and $k_{13} = (3.6 \pm 0.6) \times 10^7$ M⁻¹sec⁻¹. Similarly, for the pH region 8.55-11.31, eq 35 reduces to:

$$k'_1 \left(1 + \frac{[H^+]}{K_L}\right) \left(1 + \frac{K_5}{[H^+]}\right) \left(\frac{K_5}{[H^+]}\right) = k_{13} \quad (39)$$

Using the values $K_5 = 4.3 \times 10^{-7}$ M and $K_6 = 1.4 \times 10^{-11}$ M, calculation of the left side of eq 39 yields a mean value of $k_{13} = (3.9 \pm 0.3) \times 10^7$ M⁻¹sec⁻¹.

The predicted pK value for the most acid heme-linked group, 4.1, is consistent with results of other studies^{28,41}. The pK value of 6.4 does not agree with values of 5.0 and 7.0 reported elsewhere^{28,19} but is in agreement with a re-analysis of the HRP-fluoride kinetics⁶⁷. The value of

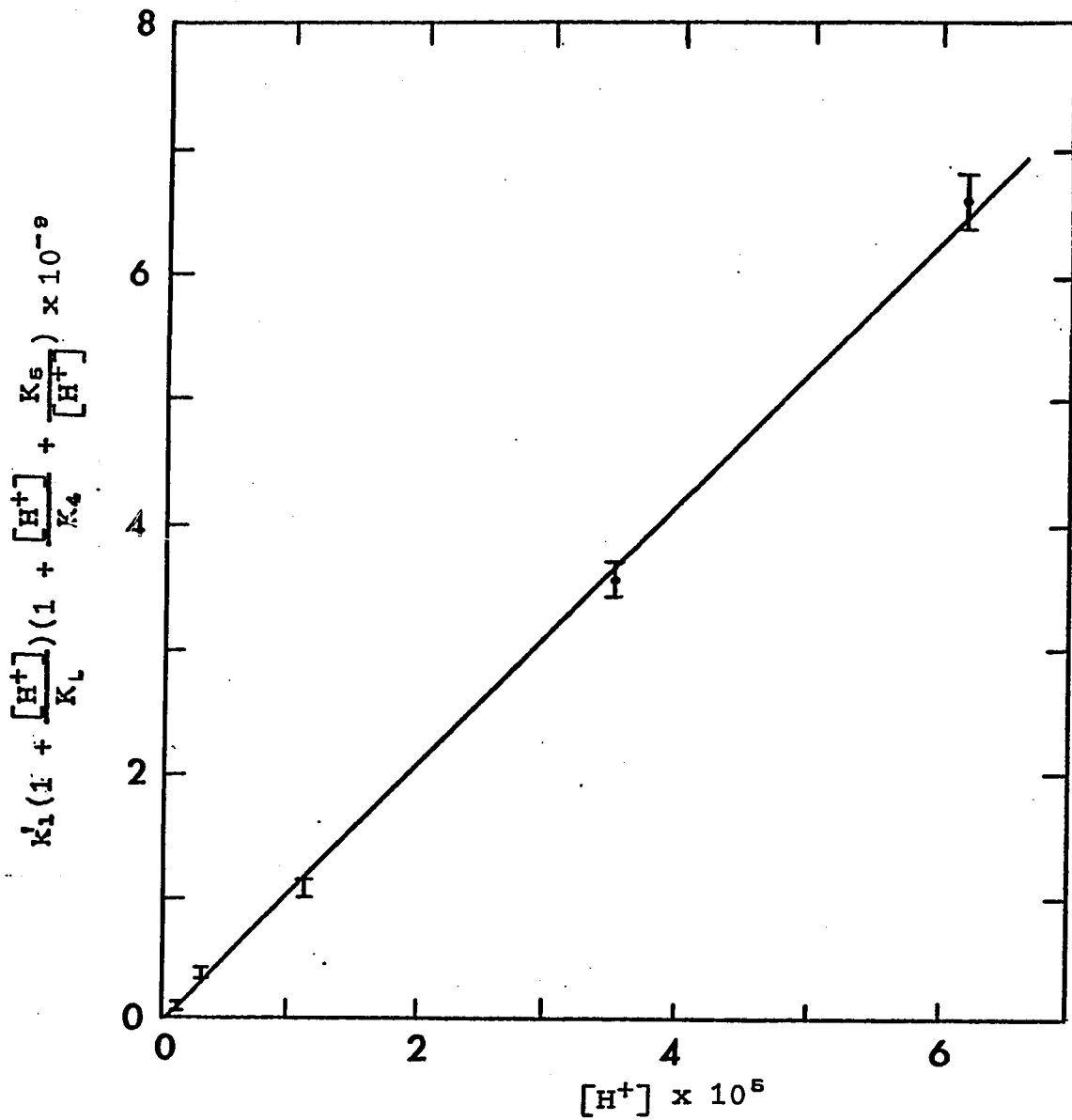


Figure 20. Plot of the left side of eq 38 vs. $[H^+]$ used to test the validity of mechanism VA for the binding of cyanide by HRP over the pH range 4.2 to 8.1.

this intermediate pK obtained from the HRP-cyanide kinetic data is a sensitive parameter. For example, it is changed from a value of 6.4 to 7.2 by arbitrarily changing the value of pK_1 from 9.0 to 9.1. On the other hand the pK values of 4.1 and 10.8 are only changed by 0.1 for the same change in pK_1 .

The values of the equilibrium constants of the heme-linked groups are shifted to smaller values as a result of the binding of the ligand. This shift is in the direction expected if the bound ligand is negatively charged⁶⁸.

Large values of k_{11} and k_{-16} are obtained from mechanism V, raising the question of whether these values might exceed the diffusion-controlled limit, which for a second-order specific rate constant for an enzyme-ligand reaction is of the order of $10^{10} \text{ M}^{-1}\text{sec}^{-1}$ ⁶⁹. Within the error limits of the various parameters required for computing the diffusion-controlled limit, k_{11} and k_{-16} do not exceed this value. Therefore, mechanisms VA, VB and VD cannot be eliminated on this basis.

In summary, the cyanide kinetic results indicate the presence of three heme-linked groups with pK values of 4.1, 6.4 and 10.8 on horseradish peroxidase. They also indicate that the anion form of the ligand exists in the peroxidase-ligand complex, but it is impossible to distinguish which, if either, form of the ligand dominates the binding reaction. The same ambiguity exists as to the reactivities of the various peroxidase species.

CHAPTER 4. THE EFFECT OF LIGAND BINDING AND ACID SPLITTING
ON THE OPTICAL ROTATORY DISPERSION OF HRP

Introduction

A beam of plane-polarized light may be considered to be made up of two circularly polarized rays, one whose vector rotates clockwise and one counterclockwise as the beam advances. A medium containing asymmetric molecules transmits the two components with unequal velocity, *i. e.*, it has different refractive indices for the two circularly polarized rays. If neither ray is absorbed, the two rays have a resultant which is a plane-polarized ray, but whose vibration is in a plane which has been rotated with respect to that of the incident ray. The plane of polarization of the resultant moves through a steadily increasing angle as the beam passes through the medium. The amount of rotation is measured as the angle between the incident and emergent beams, and is normally expressed as specific rotation, $[\alpha]_{\lambda}$, which is given by:

$$[\alpha]_{\lambda} = \frac{\alpha_{\lambda}}{lw} \quad (1)$$

where α_{λ} is the angular rotation of the sample in degrees using light of wavelength λ , l is the path length in decimeters, and w is the number of grams of solute in one ml of solution. Since the indices of refraction are dependent on wavelength, different wavelengths of light are rotated

different amounts, giving rise to the phenomenon known as optical rotatory dispersion*.

If the medium also absorbs the two circularly polarized components unequally, the emergent light beam is elliptically polarized and the medium exhibits circular dichroism. The combined phenomena of optical rotation and circular dichroism occurring in the wavelength region corresponding to an optically active absorption peak is known as a Cotton effect. The ORD curve of a Cotton effect is a symmetrical curve shaped like a derivative of an absorption peak and is centered at a wavelength corresponding to the maximum of the absorption peak. The maximum of a Cotton effect curve is known as the peak, and the minimum as the trough. When the peak occurs at a wavelength longer than that of the maximum of the absorption curve, the Cotton effect is termed "positive", and when it is at a shorter wavelength, the Cotton effect is "negative".

Cotton effects have been classified into two groups. Using the terminology suggested by Blout⁷⁰, "intrinsic Cotton effects" reflect the optical rotatory power of the protein proper, and "extrinsic Cotton effects" are generated

*Abbreviations used in this chapter: ORD, optical rotatory dispersion; CD, circular dichroism; HRP, HRP-CN, HRP-F, HRP-OH, HRP-N₃, ferric horseradish peroxidase and its cyanide, fluoride, hydroxide, and azide complexes, respectively; PGA, poly- α -L-glutamic acid.

by a local chromophoric site on the protein or by a chromophoric molecule interacting with an asymmetric site on the protein. A good review of the use of extrinsic Cotton effects for the study of interactions between proteins and biologically important molecules such as coenzymes, substrates, inhibitors, and prosthetic groups containing metals has been written by Ulmer and Vallee⁷¹.

In 1961 Simmons, et al.⁷² proposed that the trough at 233 m μ in the ORD spectra of many proteins was conformation dependent and that its depth provided a measure of the α -helical content of the protein. Although there is some debate as to whether one can calculate accurately the absolute amount of α -helical structure using Simmons' method^{73, 74}, it is certainly a sensitive tool for measuring changes in protein conformation.

Recently this method has been used to study the effect of ligand binding on the conformation of heme proteins. It has been found that while myoglobin and catalase show no change in helical content upon the binding of ligands^{75, 76, 76}, and while hemoglobin shows no change upon the binding of most ligands⁷⁷, hemoglobin seems to undergo an 8.5 % decrease in helicity upon binding of oxygen⁷⁸. A similar study carried out on HRP would be expected to show if it behaves like most cases involving heme proteins, or whether a gross conformational change takes place upon the binding of ligands. Any conformational changes which might occur

when the prosthetic group is split from the protein could also be observed by an ORD study.

Ulmer and Vallee⁷⁹ have shown from a study of the ORD of HRP, catalase, and their cyanide complexes that the extrinsic Cotton effects apparent in the Soret region reflect the orientation of the heme with respect to the protein. Their work has been extended to include the fluoride, azide, and hydroxide complexes of HRP and HRP solutions in which the heme is partially or completely removed from the protein.

Experimental

Analytical reagent grade HRP (RZ = 2.9, lot 6485206) was obtained from the Boehringer-Mannheim Corp., N. Y., and was dialyzed against water and centrifuged before use. Hemin of White Label grade was obtained from Eastman Organic Chemicals. Inorganic chemicals were reagent grade and were used without further purification. HRP concentrations were determined from absorbance measurements at 403 and 497 m μ using a Beckman DU spectrophotometer and literature values for the molar absorptivities⁵. Typical concentrations of HRP used were 2.5×10^{-6} M for ORD measurements in the UV region and 1.5×10^{-5} M for measurements in the visible region. All pH measurements were made with a Beckman expanded scale pH meter. ORD spectra were obtained at room temperature using a Jasco Model ORD/UV-5 recording spectrometer set at a scan rate of 1.7 m μ /min.

Absorption spectra of solutions were obtained using a Perkin Elmer model 202 recording UV-visible spectrophotometer. For all solutions used in this study, the maximum absorbance was less than two in the wavelength regions of interest. This procedure was followed to help ensure that the ORD spectra obtained were not caused by rotatory artifacts produced by regions of high absorbance³⁰. The values of specific rotation were calculated using the molar concentrations determined spectrophotometrically and a value of 40,200 for the molecular weight of HRP¹².

The HRP-F complex was studied at pH 4.3 in a solution which was 10^{-2} M with respect to KF; HRP-CN at pH 6.0 with 10^{-4} M KCN; HRP-OH at pH 11.3 obtained by addition of KOH; and HRP-N₃ at pH 4.3 with 0.5 M NaN₃. From the dissociation constants of the complexes^{16, 41, 67}, it was estimated that the HRP-CN, HRP-F, and HRP-N₃ complexes represented greater than 95 % of the total HRP in solution, and that HRP-OH was about 75 % formed. The limiting factor for HRP-OH formation is the instability of the protein at high pH³⁰.

Techniques for splitting the heme group from the protein moiety of HRP have been described in a series of papers by Maehly³⁰⁻³². For this study, HRP was split by making the solution acidic and allowing it to react at room temperature for several hours. The splitting reaction, followed by taking absorption spectra of the solution³⁰, was not complete in 26 hours at pH 3.0, but appeared to be

complete after 12 hours at pH 2.75. No precipitate of heme or denatured protein was observed during the course of the splitting experiments.

A solution of hemin was prepared in an ethanol-water mixture containing 44.5 weight percent ethanol, a medium in which hemin is soluble and stable. The final solution was 1.5×10^{-5} M in hemin, and 1.7×10^{-4} M in NaOH.

Results

Figure 21 shows the ORD curves for HRP and split HRP from 215 m μ to 350 m μ , plotted as specific rotation vs. wavelength. Within experimental error, the ORD curves of the hydroxide, fluoride, and cyanide complexes of HRP are the same as that of pure HRP. The ORD of HRP-N₃ could not be obtained in this region due to the high absorbance of azide. The curves in Figure 21 show a minimum at 233 m μ which is characteristic of the conformation-dependent trough in the negative intrinsic Cotton effect centered at 225 m μ . For a quantitative measure of the amplitude of this trough, the reduced mean residue rotation, $[R']_{233}$, has been used, as suggested by Simmons, et al.⁷² The values of $[R']_{233}$ for HRP, its cyanide, fluoride, and hydroxide complexes and for split HRP were calculated from the formula:

$$[R']_{233} = \frac{3M_R[\alpha']_{233}}{100(n_{233}^2 + 2)} \quad (2)$$

where the refractive index for water, n_{233} , was taken as

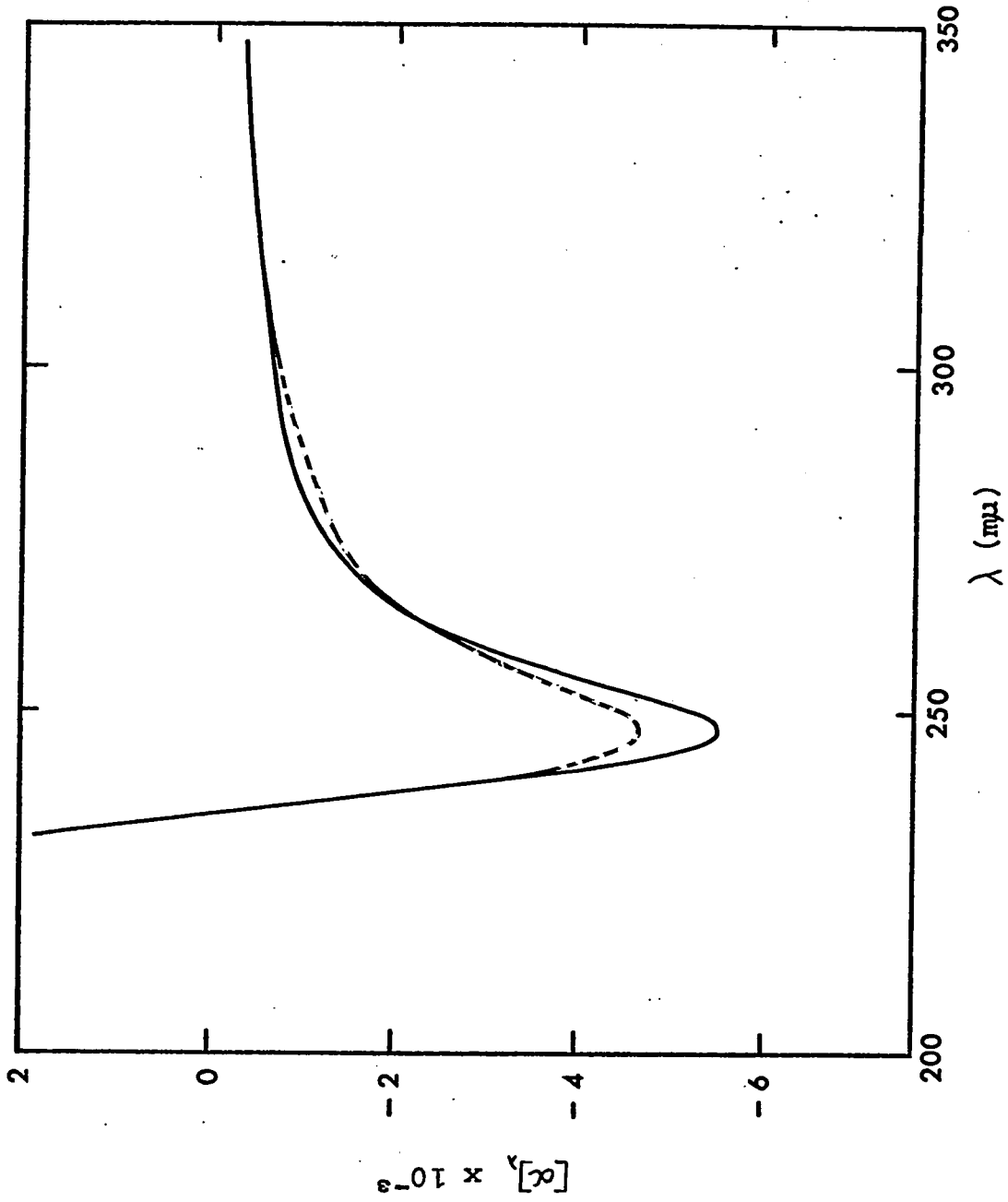


Figure 21. ORD curves of HRP (—) and split HRP (---) in the UV region.

1.39⁶¹, and the mean residue molecular weight, M_R , as 115⁶⁰. It is reasonable to assume that the rotation observed at 233 m μ is caused by protein only. Since there is 18 weight percent carbohydrate material present in HRP^{10,13}, a corrected specific rotation, $[\alpha']_{233}$, was used in eq 2, based on an effective protein molecular weight of 40,200 x 0.82. Table VIII summarizes the results for HRP, its complexes and split HRP, where the tabulated value of $[R']_{233}$ represents the mean and the error limit the mean deviation of the determinations. Multiple determinations were carried out for two reasons: to ascertain the reproducibility of the ORD spectrum for a given sample, and to check on the variation of $[R']_{233}$ with change in concentration of the protein. Although the variation in HRP concentration was greater than a factor of two, small mean deviations of $[R']_{233}$ were obtained. In addition, the $[R']_{233}$ data showed no trend with concentration; only a random scatter about the mean was observed. The lack of concentration dependence of $[R']_{233}$ is indicative that the Cotton effect observed is genuine⁶⁰.

Figure 22 shows the extrinsic Cotton effects associated with the heme Soret bands of HRP and its fluoride, cyanide, and hydroxide complexes. Similarly, Figure 23 shows the ORD curves for HRP-N₃, completely split HRP, and HRP which was partially split by reacting it at pH 3.0 for 20 hours. The ORD curve of the 1.5×10^{-5} M hemin solution

Table VIII

Reduced mean residue rotation at 233 m μ for horseradish peroxidase, its hydroxide, cyanide, fluoride and azide complexes, and for split HRP.

Species	$-[R^1]_{233} \times 10^{-3}$	Number of Determinations
HRP	6.0 \pm 0.2	7
HRP-OH	6.0 \pm 0.1	3
HRP-CN	5.9 \pm 0.1	3
HRP-F	5.9 \pm 0.1	3
split HRP	5.1 \pm 0.1	2

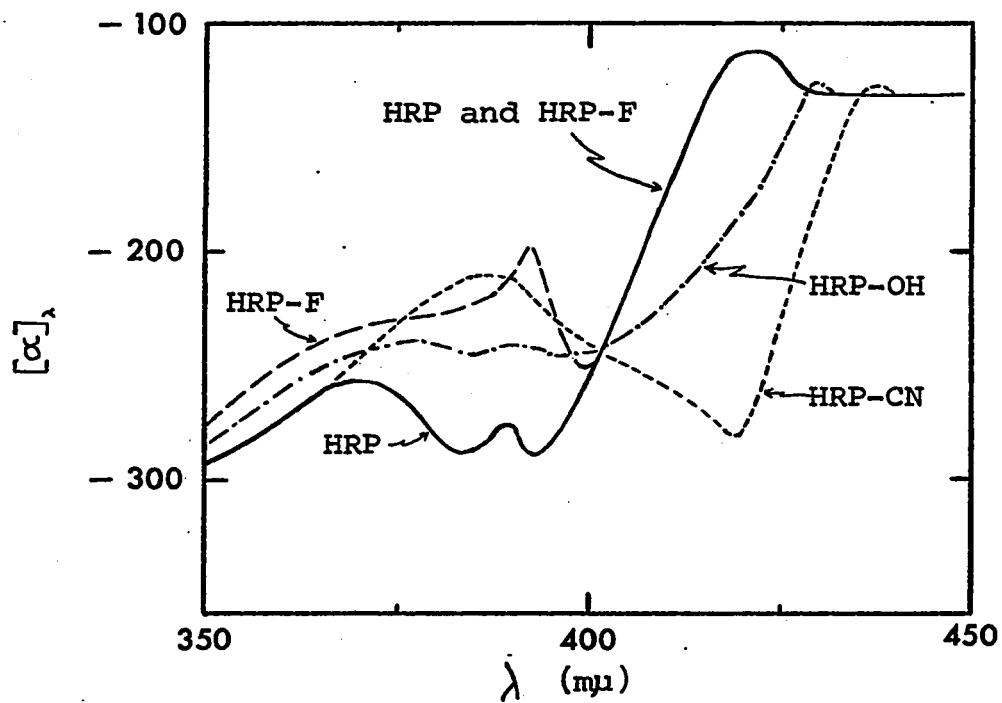


Figure 22. ORD curves in the visible region for HRP and its fluoride, cyanide and hydroxide complexes.

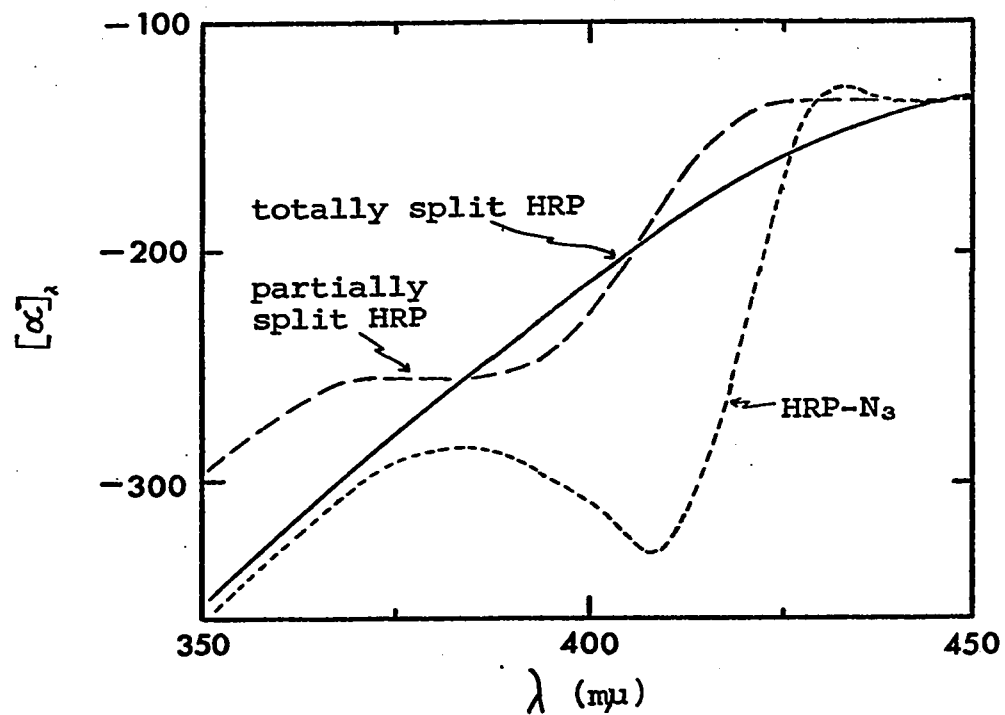


Figure 23. ORD curves in the visible region for the azide complex of HRP and for HRP which has had the heme group partially and totally split from the protein.

was examined in the region 365-450 m μ . The optical rotation was constant in that wavelength region, with no evidence of a Cotton effect at the Soret band of the hemin.

Discussion

Although $[R']_{233}$ for the HRP-ligand complexes appears smaller than for pure HRP, the difference is within experimental error. This same result was observed in the case of myoglobin and its complexes⁷⁸. It can therefore be concluded that the binding of ligands to HRP has less than 2 % effect on the amount of α -helical conformation of the protein.

Splitting the heme from the protein portion of HRP results in a 15 % decrease in $[R']_{233}$. This result agrees with the difference found between the values of $[R']_{233}$ for apomyoglobin and metmyoglobin^{78,82}, and supports the suggestion that the heme binding stabilizes the molecule as a whole²⁰. Inspection of Figure 21 shows that the ORD curve of split HRP is lower than that of HRP in the region 250-320 m μ , a result which was not observed in similar studies on myoglobin and apo-myoglobin^{78,82}, but comparison of the ORD curves of catalase and acid-denatured catalase shows the same phenomenon⁷⁸. This would indicate that for HRP, there may be other Cotton effects from the heme group which affect the ORD in this region, and although no such fine structure was observed in the present study, results

from a recent study of the CD of HRP showed the presence of bands at 282, 335, and 370 $m\mu^{83}$.

The value of $[R']_{233} = -6000$ for HRP indicates that it has less helical content than myoglobin, catalase, or hemoglobin, all of which have values of $[R']_{233}$ of about $-9000^{75, 76, 78, 82}$ and that HRP has a greater helical content than cytochrome c, which has a value of $[R']_{233}$ of about -4400^{84} . Use of $[R']_{233}$ to calculate the helical content of proteins seems to result in an underestimate in many cases⁸⁰, which may be a result of the fact that fully coiled PGA has been used as the standard for 100 % helicity. Although there seems to be agreement that for random PGA, $[R']_{233} = -2000$, there is a wide disparity in the reported values for fully coiled PGA^{72, 74, 76}. Further, there seems to be an optical anomaly associated with what had been supposed to be the fully coiled form^{85, 86}. Thus, it appears that a better estimate of the helical content of HRP can be made using the value of $[R']_{233}$ for myoglobin as a secondary standard, since X-ray crystallographic studies have shown that it contains 77 % α -helix^{87, 88}. Using $[R']_{233}$ equal to -2000 for 0 % helix and $-9200^{72, 75, 78, 82, 89}$ for 77 % helix, and assuming that the heme Cotton effects make a negligible contribution to $[R']_{233}$, HRP is calculated to contain 43 % α -helical structure, which is reduced to 33 % for split HRP. This estimate of the helical content of HRP agrees with a value of 40 % helical content

found in a study of the CD of HRP⁸³.

The ORD curves for HRP and HRP-CN in the visible region agree with those found previously⁷⁹. The curves for HRP-F, HRP-OH, and HRP-N₃ are also of the same sign and order of magnitude as HRP and HRP-CN, thus leading to the conclusion that the orientation of the heme with respect to the protein is the same for HRP and its ligand complexes. While the ORD curve of HRP in the visible region is very similar to those of hemoglobin and myoglobin⁸⁰, it differs significantly from those of catalase⁷⁹ and ferricytochrome c^{84,80,81}. Further, the ORD curves of HRP-CN, ferricytochrome c-cyanide⁸¹ and ferrimyoglobin-cyanide⁷⁸ are all similar to each other, but as a group are quite different from that of catalase-cyanide⁷⁹. It is known that the heme iron of cytochrome c has histidine and methionine bound in the fifth and sixth coordination positions and that hemoglobin and myoglobin have histidine and water in the fifth and sixth positions⁸². A comparison of absorption spectra, magnetic moments, and reduction potentials of the heme proteins led Brill and Williams to conclude that HRP "is an amino-carboxylate, or less probably a water-amino complex, and that catalase is a dicarboxylate or less probably a carboxylate-water complex"⁸³. However, Brill and Sandberg later concluded that for HRP, histidine is in the fifth position⁸⁷. The results of the present study, when compared with the ORD curves of the other heme proteins as mentioned above, indicate that

HRP is probably similar to myoglobin and hemoglobin, with histidine in the fifth position and water in the sixth position.

The results on HRP-OH disagree with an earlier finding that upon the formation of alkaline HRP, the ordered structure of the protein is destroyed^{9a}. The results of the present studies, both at 233 m μ and in the Soret region, indicate little difference between the structures of HRP and HRP-OH. Osbahr and Eichhorn reached their conclusion from ORD measurements of an extrinsic Cotton effect associated with the absorption peak at 640 m μ in HRP. This Cotton effect disappeared upon raising the pH from 7.2 to 11.0, a result which can alternatively be interpreted as being due to the disappearance of the absorption peak at 640 m μ when HRP-OH is formed⁸.

Inspection of Figure 23 shows that as the heme splits from the protein, the positive Cotton effect in the visible region broadens and diminishes in magnitude, and then disappears altogether when the heme has been completely split from the protein. This result, along with the observed lack of any Cotton effect for the hemin solution, confirms the contention that the extrinsic Cotton effect arises from the interaction of the heme with an asymmetric site on the protein^{7a}.

In a recent study on the inactivation of HRP when treated with azide¹⁶, Brill and Weinryb concluded that

azide was attacking a methionine residue at the active site. Evidence from the present study suggests instead that the observed inactivation was due to the splitting of the heme from the protein. Their experiment in which HRP was inactivated by reacting it with azide at pH 5.2 and 42° for five hours was repeated in this study. After removal of the azide by dialysis, the Soret absorption spectrum and the ORD curves of the solution at both the UV and Soret regions were found to be the same as those of partially split HRP. Although they ran a control in the absence of azide at pH 5.2 and found no inactivation, it is known that splitting occurs faster at a given pH in the presence of ligands such as fluoride, cyanide, and azide³². Finally, they reported recovery of some of the activity of the inactivated samples after dialysis. This can be explained on the basis that the splitting is reversible, with the recombined HRP exhibiting normal peroxidatic activity³².

CHAPTER 5. THE EFFECTS OF TEMPERATURE AND IONIC STRENGTH
ON THE FORMATION OF THE HYDROXIDE COMPLEX OF HRP

Introduction

It is widely accepted that HRP, like hemoglobin and myoglobin, contains water in the sixth coordination position of the heme ferric iron^{5,19,24}, although the suggestion has been made that the heme of HRP lies in a crevice with both the fifth and sixth positions occupied by protein residues²⁶. When a solution of HRP is made alkaline, there are accompanying changes in the spectrum of HRP⁵, and its magnetic moment changes from 5.45 to 2.66 Bohr magnetons²⁴, indicating the formation of a new species, HRP-OH*. The pK for hydroxide formation has been measured to be 10.9 by spectrophotometry and 11.3 by use of a magnetic balance²⁴, and 10.6 by a study of the reduction potentials of HRP¹⁹, but these studies were not carried out at constant ionic strength. A study of the kinetics of cyanide binding to

*Abbreviations used in this chapter: P, refers specifically to a form of HRP in which it is assumed that water is in the sixth coordination position; HRP-OH or POH, hydroxide form of HRP; \bar{P} , \overline{POH} , H^+ , equilibrium values of P, POH, and H^+ ; K_c , apparent equilibrium constant defined in terms of concentrations, and hence not a true thermodynamic constant.

HRP at an ionic strength of 0.11 yielded a value of 10.8 for this pK (Chapter 3). This chapter contains a report on a spectrophotometric study of the formation of HRP-OH at 25.0° for seven values of ionic strength over the range 0.02 to 0.20 and also at 18.0° and 35.0° with $\mu = 0.11$.

Experimental

Two grades of HRP were obtained from Boehringer-Mannheim Corp., N. Y.: "analytical reagent grade" (RZ = 2.9 lot 6485206) and "purified lyophilized powder" (RZ = 0.8). All HRP was exhaustively dialyzed against conductivity water and centrifuged before use. Analytical reagent grade KNO_3 (Mallinckrodt) and KOH (B.D.H.) were used without further purification.

Some of the "purified" HRP was treated by passage through a 1.1 x 50 cm column of C-50 CM Sephadex cation exchange gel. The HRP was eluted using pH 6.2 phosphate buffer, with the ionic strength increasing from 0.1 to 0.2 during the course of the elution. A single passage through the column resulted in the recovery of a fraction of RZ = 2.7 which represented 65 % of the initial "purified" HRP as determined by absorbance measurements at 497 $m\mu$. This purification procedure is described in detail in Appendix II. Absorbance measurements were made with a Beckman DU spectrophotometer which had the cell compartment thermostated to $\pm 0.1^\circ$. A Beckman Expandomatic pH meter was used for

all pH measurements.

For a typical experiment, an appropriate amount of 1 M KNO_3 and enough stock HRP to make a final HRP concentration of about 1.7×10^{-5} M were pipetted into a 10 ml volumetric flask, which was then filled to the mark with water. The 10 ml of solution was transferred to a 30 ml beaker which was covered with Parafilm and placed in a constant temperature bath. A Beckman 39183 combination pH electrode, a Teflon syringe needle, and a platinum stirring wire were inserted through slits in the Parafilm. The pH was measured and was found typically to have a value of 5.5. A three ml aliquot of the solution was transferred with a syringe to a cuvet and the HRP concentration was determined by measuring the absorbance of the solution at 497 m μ where the molar absorptivity coefficient is⁵ $1.00 \times 10^4 \text{ M}^{-1} \text{ cm}^{-1}$. The absorbance of the solution was then measured at 416 m μ , the wavelength corresponding to the maximum of the Soret peak of HRP-OH⁵. A second HRP solution of about pH 5.5 was prepared to use as a blank in the spectrophotometer. Its concentration was such that the difference in absorbances between the blank and the experimental solution was about 0.1 at 416 m μ , thus keeping the absorbance readings during the course of the titration in the range 0.1 - 0.6, which includes the region of minimum error due to instrumental uncertainty⁵⁹. The experimental HRP solution was returned to the beaker and the pH was raised by the addition from

a 10 μ l Hamilton syringe of a few μ l of approximately 1 M KOH, an amount small enough that no volume correction was necessary. The solution was stirred, the pH was remeasured, the absorbance of an aliquot was measured at 416 m μ in a capped cuvet, and the aliquot was returned to the beaker. Nine to eleven points were obtained this way, with the titration being carried out to about pH 11.35. Above this pH, the heme splits from the protein at an appreciable rate³⁰. After each increase in pH, the beaker was flushed gently with nitrogen so that there would be no change in pH or ionic strength due to absorption of carbon dioxide from the atmosphere, a problem encountered particularly above pH 10. This method was effective as proved by the pH stability of the solution at any given pH over a period of 15 minutes.

While it is true that the addition of KOH to the solution contributes to the ionic strength, this contribution is negligible for most cases. At pH 11.3, the KOH added results in an increase in ionic strength of 0.002. This means that the greatest effect due to the added base would be a 10 % increase in the ionic strength for the last point taken in the experiment performed at $\mu = 0.02$.

Temperature-jump kinetic experiments were carried out on the apparatus which was described in Chapter 2. A temperature jump of about 6° was applied to a 5.18×10^{-6} M solution of "analytical reagent grade" HRP at 25° with pH = 11.0 and $\mu = 0.11$. The photomultiplier output voltage

corresponding to a change in absorbance at 416 m μ with time was displayed on an oscilloscope. Estimation of a maximum relaxation time for the equilibration of the HRP - HRP-OH mixture was made by examination of photographs of the oscilloscope traces.

If it is assumed that a water molecule is in the sixth coordination position of the heme iron of HRP; its ionization can be represented by:



Charges on the protein species have been omitted since they are not known. The reversibility of the process represented in eq 1 was tested in the following experiment. The absorbance curve of the Soret peak of an HRP solution at pH 5.5 was taken, the pH raised to 11, then readjusted to pH 5.5 and the spectrum was remeasured.

Results

The reversibility of hydroxide formation was demonstrated by the invariance of the spectrum of HRP at pH 5.5 within instrumental error (<0.5 %) before and after adjustment of the pH to 11.

The total absorbance of the solution at any pH is the sum of the absorbances due to the P and POH species, which for a 1 cm cell is given by:

$$A = \epsilon_p [P] + \epsilon_{POH} [POH] \quad (2)$$

where ϵ_p and ϵ_{POH} are the molar absorptivities of P and POH

at 416 m μ . The value of ϵ_{POH} cannot be determined directly because it is not possible to raise the pH of the solution high enough to form 100 % POH without causing irreversible changes in the enzyme. The equilibrium constant corresponding to eq 1 is given by:

$$K_c = \frac{[\text{POH}][\text{H}^+]}{[\text{P}]} \quad (3)$$

Equations 2 and 3 can be combined to give the expression:

$$\Delta A = [\text{P}]_0 \Delta \epsilon - \frac{[\text{H}^+]\Delta A}{K_c} \quad (4)$$

where $\Delta A = A - A_0$, where A_0 is the absorbance of the solution when all HRP is in the P form; $[\text{P}]_0$ is the initial concentration of HRP; and $\Delta \epsilon = \epsilon_{\text{POH}} - \epsilon_{\text{P}}$. The value of $[\text{H}^+]$ is obtained from the equation:

$$\text{pH} = -\log[\text{H}^+] \quad (5)$$

The validity of eq 5 will be discussed later.

From eq 4, it follows that a plot of ΔA vs. $[\text{H}^+]\Delta A$ should yield a straight line, with a slope of $-1/K_c$ and an intercept of $[\text{P}]_0 \Delta \epsilon$. Such a plot is shown in Figure 24, the data being from an experiment using "analytical reagent grade" HRP at 25.0° and $\mu = 0.14$. It is obvious from Figure 24 that the experimental data do not fit eq 4. The deviation from eq 4 is indicative that at least a second process is occurring. It was found that the deviation from the expected straight line was smallest when "analytical reagent grade" HRP was used, greater for Sephadex-treated

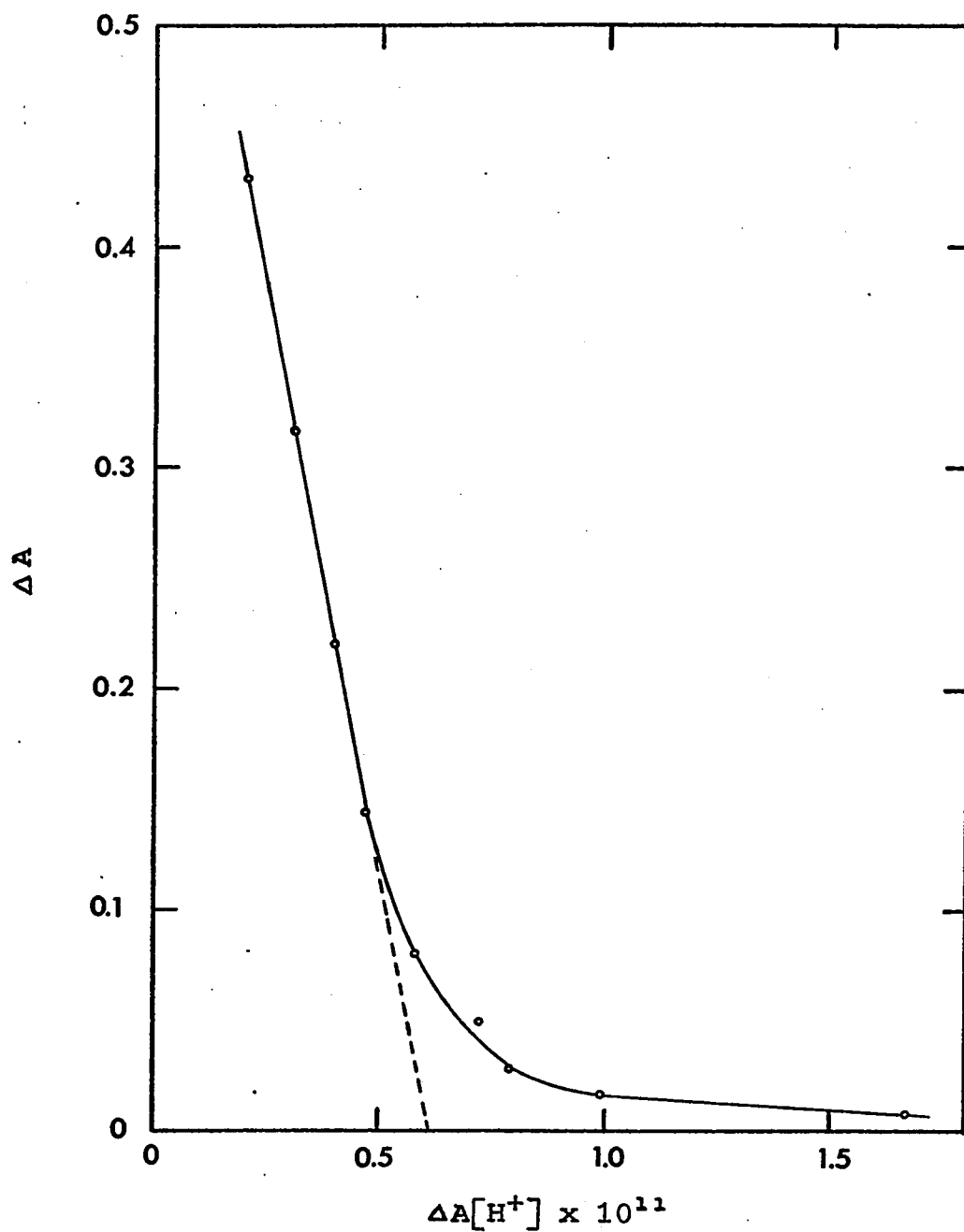


Figure 24. Plot of ΔA vs. $\Delta A[H^+]$ for a spectrophotometric titration of pure horseradish peroxidase at 25.0° and $\mu = 0.14$. The lack of linearity can be interpreted to mean that more than one ionization is taking place.

"purified" HRP and greatest for "purified" HRP.

From the temperature-jump experiments it was not possible to determine exactly the relaxation time constant, τ , for the reaction being observed since the relaxation appeared to be instantaneous on the fastest time scale which could be used. The time scale is limited by the instrument response time determined by the photomultiplier load resistor setting, which must be large enough to obtain sufficient sensitivity to observe the absorbance change accompanying the chemical relaxation. However, examination of photographs of the oscilloscope traces indicated that τ must be less than 30 psec using the solution and experimental conditions described in the previous section.

Discussion

Among the possible explanations which could account for the observed deviation from linearity shown in Figure 24, one of the simplest might be that a heme-linked ionizable group with a pK roughly in the range 9-10 is present on HRP and that its ionization gives rise to another spectroscopically distinguishable species. However, this possibility is ruled out since the amount of deviation from linearity of plots of ΔA vs. $\Delta A[\bar{H}^+]$ varies with the nature of the preparation. A more plausible explanation is that the observed effect might be due to the presence of more than one isozyme of HRP in the preparations used, and that

the amount of the minor constituent varies with the preparation^{10,11}.

If there are two isozymes present which have the same absorption spectrum for the P species but which have different equilibrium constants for the ionization of P to form POH, one can derive an equation analogous to eq 4:

$$\Delta A = \frac{\Delta\epsilon_1[P]_0 f}{1 + \frac{[H^+]}{K_{c1}}} + \frac{\Delta\epsilon_2[P]_0(1-f)}{1 + \frac{[H^+]}{K_{c2}}} \quad (6)$$

where f is the fraction of HRP present as isozyme 1, the subscripts indicate isozyme 1 or isozyme 2, and the other symbols have the same meaning as before. Equation 6 can be used with a nonlinear least-squares computer program (Appendix I) to yield best-fit values of $\Delta\epsilon_1 f$, K_{c1} , $\Delta\epsilon_2(1-f)$, and K_{c2} . The value of f cannot be separated from that of $\Delta\epsilon$. By use of eq 6, it is possible to obtain a good fit to the experimental titration data as shown in Figure 25. The circles in Figure 25 show experimental values of ΔA as a function of pH while the solid line is the theoretical curve obtained from use in eq 6 of the computer best-fit values of $K_{c1} = 3.7 \times 10^{-9}$ M, $\Delta\epsilon_1 f = 5.3 \times 10^3$ M⁻¹ cm⁻¹, $K_{c2} = 9.1 \times 10^{-12}$ M, and $\Delta\epsilon_2(1-f) = 3.9 \times 10^4$ M⁻¹ cm⁻¹.

Table IX summarizes the results of the computer analysis of the experimental titration data using eq 6. These results were all obtained using "analytical reagent grade" HRP. The error limits shown on the results are either

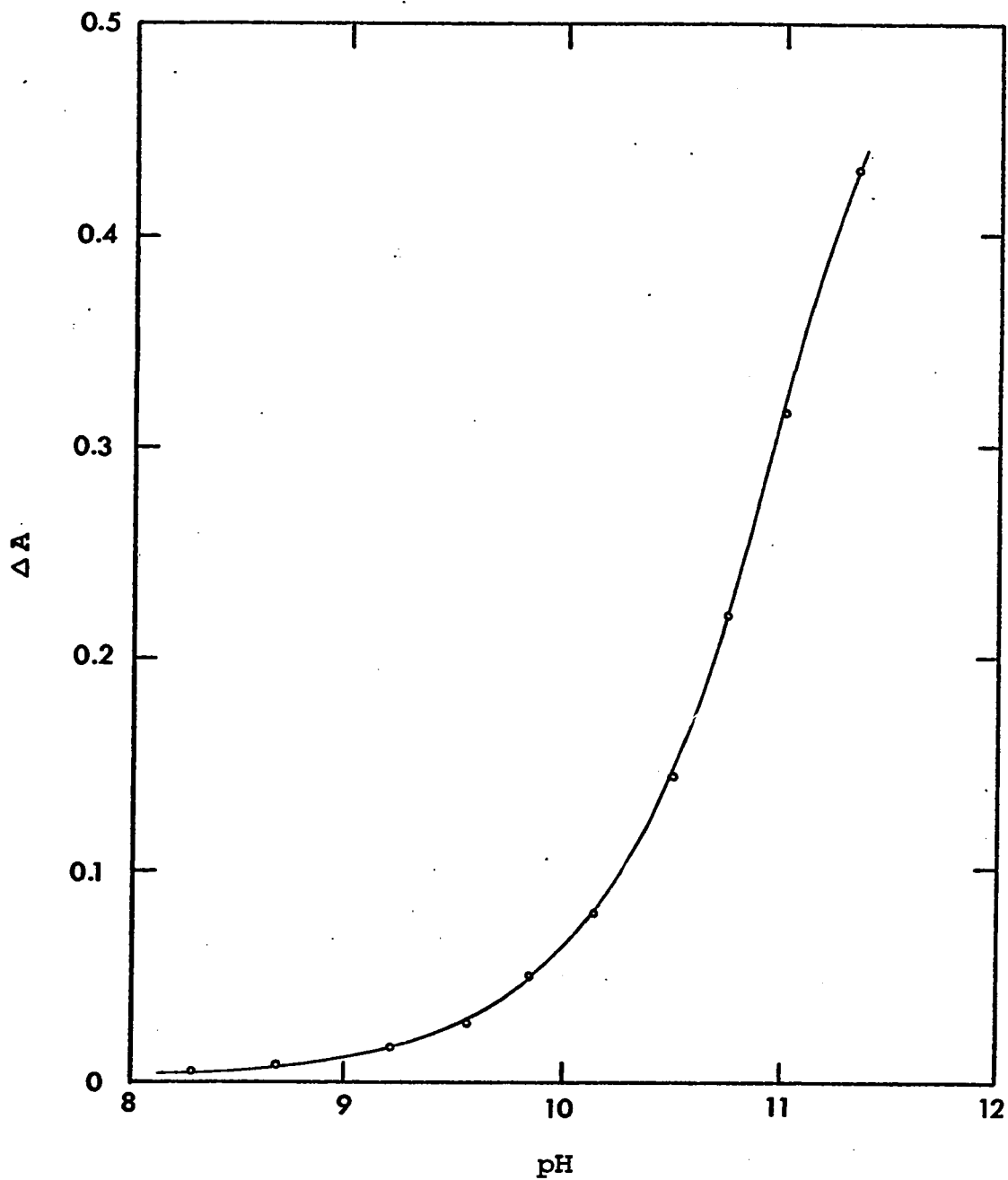


Figure 25. Plot of ΔA vs. pH for a spectrophotometric titration of pure horseradish peroxidase at 25.0° and $\mu = 0.14$. The solid line is calculated using computer best-fit parameters in eq 6.

Table IX

Summary of Results of Computer Analysis of
Experimental Titration Data Using eq. 6

μ	$t, ^\circ\text{C}$	$\Delta\epsilon_1 f \times 10^{-2}$ ($\text{M}^{-1} \text{cm}^{-1}$)	$K_{c1} (M)$	$\Delta\epsilon_2 (1-f) \times 10^{-4}$ ($\text{M}^{-1} \text{cm}^{-1}$)	$K_{c2} (M)$
0.02	25.0	7.0 ± 1.4	$(2.9 \pm 1.6) \times 10^{-9}$	3.7 ± 0.1	$(1.47 \pm 0.07) \times 10^{-11}$
0.05*	25.0	3.4 ± 1.4	$(6.2 \pm 5.0) \times 10^{-9}$	3.6 ± 0.1	$(1.17 \pm 0.10) \times 10^{-11}$
0.08	25.0	7.6 ± 1.9	$(1.7 \pm 1.0) \times 10^{-9}$	3.8 ± 0.2	$(9.4 \pm 0.6) \times 10^{-12}$
0.11*	25.0	6.5 ± 1.3	$(1.8 \pm 0.4) \times 10^{-9}$	3.9 ± 0.1	$(1.00 \pm 0.05) \times 10^{-11}$
0.14	25.0	5.3 ± 1.6	$(3.8 \pm 2.5) \times 10^{-9}$	3.9 ± 0.2	$(9.1 \pm 0.6) \times 10^{-12}$
0.17*	25.0	3.8 ± 1.6	$(4.5 \pm 2.5) \times 10^{-8}$	3.7 ± 0.1	$(9.1 \pm 0.3) \times 10^{-12}$
0.20*	25.0	4.1 ± 0.7	$(3.2 \pm 3.0) \times 10^{-7}$	3.7 ± 0.1	$(8.8 \pm 0.2) \times 10^{-12}$
0.11	18.0	9.8 ± 3.0	$(1.4 \pm 0.5) \times 10^{-10}$	3.3 ± 0.2	$(7.5 \pm 0.5) \times 10^{-12}$
0.11	35.0	4.0 ± 1.1	$(7.6 \pm 2.0) \times 10^{-9}$	3.4 ± 0.1	$(1.48 \pm 0.06) \times 10^{-11}$

* Duplicate experiments performed for these conditions.

standard deviations obtained from the computer analysis, or in the case of duplicate runs, the mean deviation, although for the duplicate runs the two types of errors were about equal. The values of $\Delta\epsilon_{1f}$ and $\Delta\epsilon_{2(1-f)}$ show no variation with change of temperature or ionic strength; the mean and mean deviation of all the values found for these parameters are: $\Delta\epsilon_{1f} = (5.4 \pm 1.6) \times 10^3 \text{ M}^{-1} \text{ cm}^{-1}$ and $\Delta\epsilon_{2(1-f)} = (3.7 \pm 0.1) \times 10^4 \text{ M}^{-1} \text{ cm}^{-1}$. The error limits quoted for $\Delta\epsilon_{1f}$ and K_{c1} are considerably larger than those for $\Delta\epsilon_{2(1-f)}$ and K_{c2} , which is a consequence of the relative contributions of the two terms on the right side of eq 6. Although the two terms are typically about equal at pH 8.5, the second term is ten times larger than the first at pH 10.5, and 50 times larger at pH 11.3. Thus it takes a relatively large change in trial values of $\Delta\epsilon_{1f}$ or K_{c1} to influence the overall fit of eq 6 to the experimental data.

The existence of several isozymes of HRP has been known for some time⁷⁻⁹, and recently the properties of the individual isozymes have been studied in detail^{10,11}. Shannon, et al. reported that two types of isozymes, which they designated as A-1 and C, had different spectral properties¹⁰. They showed the spectra of the two isozymes at pH values ranging from 4.4 to 10.5. In neutral or acid solution, the Soret absorption bands of the two isozymes are almost identical. The spectrum of the C isozyme at pH 9.6 is the same as that near pH 7. However, the maximum of the Soret peak

of the A-1 isozyme at pH 9.6 shows a shift to higher wavelength, and its overall absorption spectrum appears to be typical of that of partially formed HRP-OH. At pH 10.5 both isozymes display spectra which are characteristic of HRP-OH⁵.

On the basis of these findings, it appears probable that the Boehringer-Mannheim "analytical reagent grade" HRP used for this study consists of a minor component of the A-1 type of isozyme, and a major component of the C type isozyme, corresponding to the designations "isozyme 1" and "isozyme 2" used in eq 6. Assuming that the spectra of the P and POH species of the two isozymes are the same, the relative amounts of the two isozymes present can be estimated from the mean values of $\Delta\epsilon_1 f$ and $\Delta\epsilon_2(1-f)$. If $\Delta\epsilon_1$ and $\Delta\epsilon_2$ are equal, then $(1-f)/f = 3.7 \times 10^4 / 5.4 \times 10^2$ and $f = 0.014$, thus indicating that 1.4 % of the "analytical reagent grade" HRP used was isozyme of the A-1 type, and the rest was of the C type. This calculation also allows determination of the value of the molar absorptivity coefficient of HRP-OH at 416 m μ . The ratio A_{403}/A_{416} was measured for an "analytical reagent" HRP solution at pH 7, and the result 0.668 was obtained, which yielded a value of $\epsilon_{p416} = 6.08 \times 10^4 \text{ M}^{-1} \text{ cm}^{-1}$ from Keilin and Hartree's value⁵ of $\epsilon_{p403} = 9.1 \times 10^4 \text{ M}^{-1} \text{ cm}^{-1}$. From $\Delta\epsilon_2 = \epsilon_{pOH416} - \epsilon_{p416} = 3.74 \times 10^4 \text{ M}^{-1} \text{ cm}^{-1}$, a value of $\epsilon_{pOH416} = 9.82 \times 10^4 \text{ M}^{-1} \text{ cm}^{-1}$ is then obtained, which differs from the previously reported

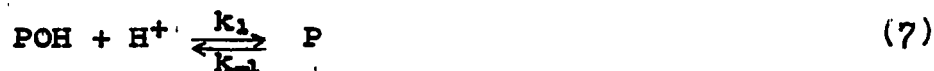
value⁵ of $\epsilon_{\text{POH}416} = 8.85 \times 10^4 \text{ M}^{-1} \text{ cm}^{-1}$. However, Keilin and Hartree determined their value from a spectrum of HRP at pH 11.4, where the formation of HRP-OH is not complete.

Data from an experiment using "purified grade" HRP indicates that there is about 12 % A-1 type isozyme present in that preparation. Since most of the kinetic study of the binding of cyanide to HRP described in Chapter 3 was carried out using "purified" HRP, the question is raised as to whether the presence of two isozymes would affect the interpretation of the results. It was reported that experiments repeated at three pH values ranging from 4.2-8.5 using "analytical reagent" HRP gave, within experimental error, the same observed binding rate constants as those from experiments using "purified" HRP. Therefore, over the pH range of the duplicate experiments, the presence of two isozymes did not affect the kinetic results since the rate constants did not vary with the relative amounts of the two isozymes present. At higher pH values, the experimental data from the cyanide binding study was fit by a mechanism in which it was postulated that the rate of binding of cyanide to POH was negligible. The amount of POH present at any pH is dependent on the pK for its formation, which the present study has shown to be different for the two isozymes. The computer best-fit value for the equilibrium constant for POH formation obtained in the cyanide study was $(1.4 \pm 0.4) \times 10^{-11} \text{ M}$ at 25° and $\mu = 0.11$, while under the

same conditions and using the same definition of pH, the present study yields the values $K_{c1} = (1.8 \pm 0.4) \times 10^{-9}$ M and $K_{c2} = (1.00 \pm 0.05) \times 10^{-11}$ M. Thus, the equilibrium constant for hydroxide formation from the kinetic study, which according to the present interpretation must be a weighted mean value for the two isozymes, agrees within experimental error with K_{c2} for the predominant isozyme 2. As a further check of possible errors in the previous analysis, the nonlinear least-squares analysis of the forward rate equation, given by equation 35 in Chapter 3, was repeated with terms included which allowed for 12 % isozyme of the A-1 type. This meant that the term containing one equilibrium constant for POH formation was replaced with two terms containing as fixed constants the values of K_{c1} and K_{c2} at $\mu = 0.11$ found in the present study. The usual iterative procedure then found the best-fit values for the other rate and equilibrium constants. Those constants were all found to agree within 5 % of the values found in the previous study, so that the presence of two isozymes in the preparation used does not affect the previous interpretation of the results within experimental error.

Although a precise relaxation time was not determined for the reaction involving the formation of POH, it is possible to establish limits for the rate constants involved. Since the experiments were performed using "analytical reagent grade" HRP, the effect of the small amount

of isozyme A-1 will be ignored. If the reaction is written as an association:



then the reciprocal relaxation time, $1/\tau$, is given by⁵⁸:

$$\frac{1}{\tau} = k_1([\overline{\text{POH}}] + [\overline{\text{H}^+}]) + k_{-1} \quad (8)$$

A lower limit for k_1 can be obtained from eq 8 by introducing the relationship $k_{-1} = k_1 K_{c1}$, and the values of $[\overline{\text{POH}}] = 2.6 \times 10^{-5} \text{ M}$, $[\overline{\text{H}^+}] = 10^{-11} \text{ M}$, and $\tau < 30 \text{ } \mu\text{sec}$. Therefore, $3.3 \times 10^4 \text{ sec}^{-1} < k_1 (2.6 \times 10^{-5} \text{ M})$, or $k_1 > 1.3 \times 10^{10} \text{ M}^{-1} \text{ sec}^{-1}$ at 31° . This result compares with values found by Eigen and co-workers for other protonation reactions, such as the combination of a hydrogen ion with a hydroxide ion, which has a rate constant of $1.3 \times 10^{11} \text{ M}^{-1} \text{ sec}^{-1}$ ⁹⁵, or protonation of anions such as formate, benzoate, substituted benzoates and phenolates, all of which have rate constants in the range $2 \times 10^{10} \text{ M}^{-1} \text{ sec}^{-1}$ to $6 \times 10^{10} \text{ M}^{-1} \text{ sec}^{-1}$ at 25° ^{96,97}.

If the reaction is written as a displacement by hydroxide ion:



introduction of $K_w = 10^{-14} \text{ M}^2$ and analogous treatment to that above allows the calculation that $k_2 > 1.6 \times 10^7 \text{ M}^{-1} \text{ sec}^{-1}$. The value of k_2 appears to be quite large in comparison with the specific rate constants for fluoride and cyanide binding to HRP with the two most acid heme-linked

groups ionized⁶⁷, and although the process represented by eq 9 cannot be ruled out on this basis, the apparent agreement of k_1 with specific rate constants for other protonation reactions is evidence that the proton transfer process is the one being observed in this study.

The effect of ionic strength on the values of K_{c1} and K_{c2} can be treated on the basis of the theory of the secondary salt effect. For a reaction of the type:



where Z is the charge on the undissociated acid, the concentration equilibrium constant, K_c , is related to the thermodynamic equilibrium constant, K_T , by the expression:

$$\log K_c = \log K_T + 2(1 - Z)D \quad (11)$$

The symbol D in the above equation stands for a portion of the extended Debye-Hückel expression due to Davies⁶⁸, which at 25° and with water as the solvent is given by:

$$D = 0.509 \left(\frac{\sqrt{\mu}}{1 + \sqrt{\mu}} - 0.20 \mu \right) \quad (12)$$

The experimental data were analyzed using eq 6 and by assuming that eq 5 is valid. However, the definition of pH is an operational one. The term pH does not have a simple meaning; it is not a true measure of either the hydrogen ion concentration or hydrogen ion activity, but probably of a quantity between the two⁶⁸. If it were a measure of hydrogen ion activity, then for this study, eq 8 would take the form:

$$\log K_{obs} = \log K_T + (1-2Z)D \quad (13)$$

where K_{obs} is the same as K_c except that hydrogen ion concentration is replaced by hydrogen ion activity.

Figures 26 and 27 are plots of $\log K_{c1}$ vs. D and $\log K_{c2}$ vs. D , respectively. There is too much scatter in the data in Figure 26 to try to interpret quantitatively the results for isozyme 1. However, inspection of Figure 26 shows that the plot of $\log K_{c1}$ vs. the ionic-strength-dependent term goes through a minimum; this behavior is opposite to that found in corresponding studies on the formation of ferri-myoglobin hydroxide⁹⁹ and ferrihemoglobin hydroxide¹⁰⁰. The data shown in Figure 27, for isozyme 2, fits a straight line with a slope of -2.9 ± 0.4 as determined by linear least-squares analysis. This slope may be used to predict the effective charge on the P species, but the accuracy of this prediction depends on the interpretation of pH and hence on whether eq 11 or eq 13 is more valid. If eq 11 were obeyed, the slope of Figure 27 would be expected to be -2 for $Z = +2$ and -4 for $Z = +3$, while if eq 13 were the more valid equation, the slope would be -3 for $Z = +2$. Thus, it appears that the slope of -2.9 obtained from the plot in Figure 27 is indicative of an effective charge of between $+2$ and $+3$ on the P species.

The heat of ionization can be obtained from a linear plot of $\log K_T$ vs. $1/T$; the slope of such a plot is $-\Delta H^\circ/2.303R$. The ionic strength dependence of K_{c2} at 25.0°

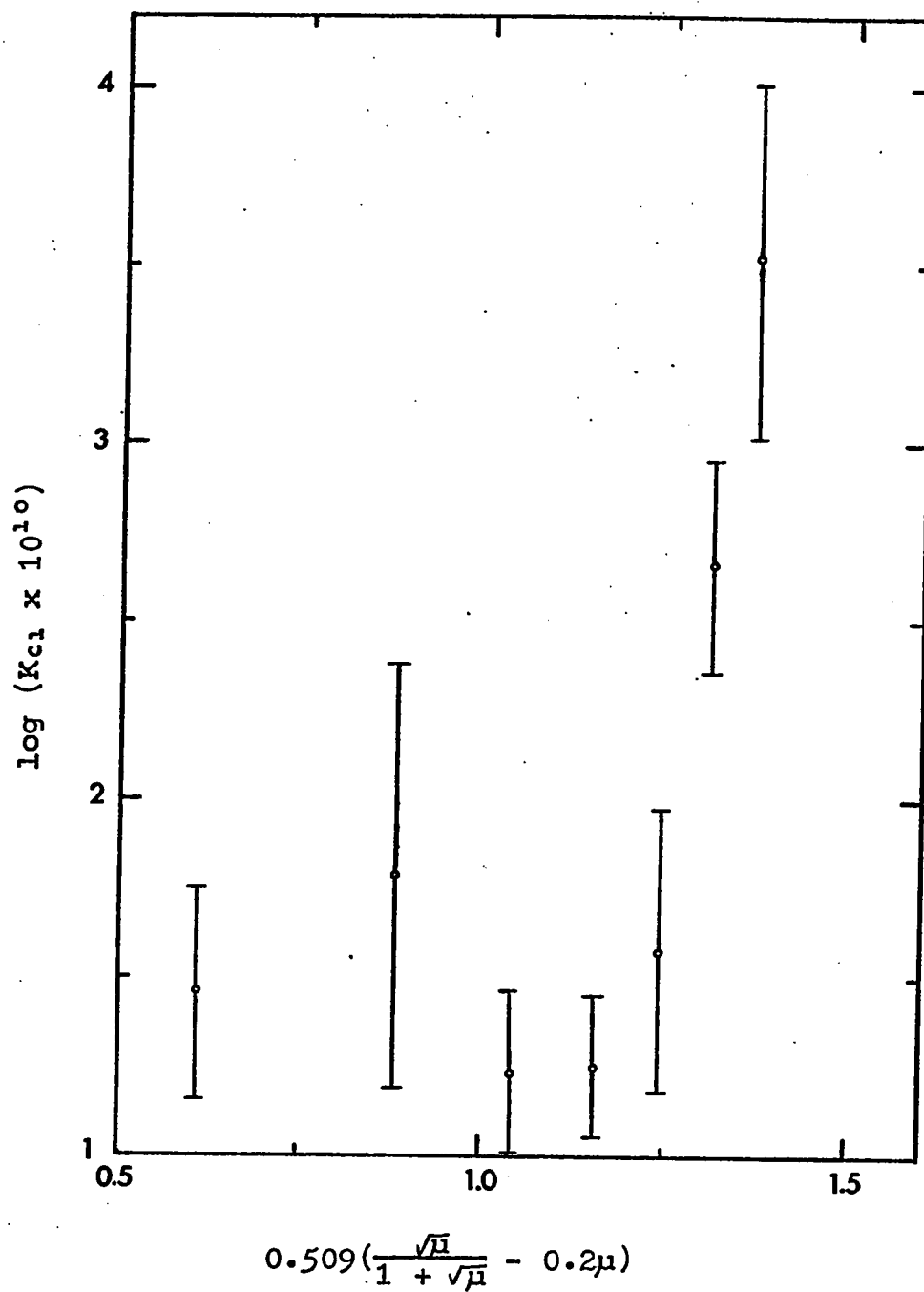


Figure 26. Plot of $\log K_{c1}$ vs. $0.509 \left(\frac{\sqrt{\mu}}{1 + \sqrt{\mu}} - 0.20\mu \right)$ showing the ionic strength dependence of K_{c1} at 25.0° .

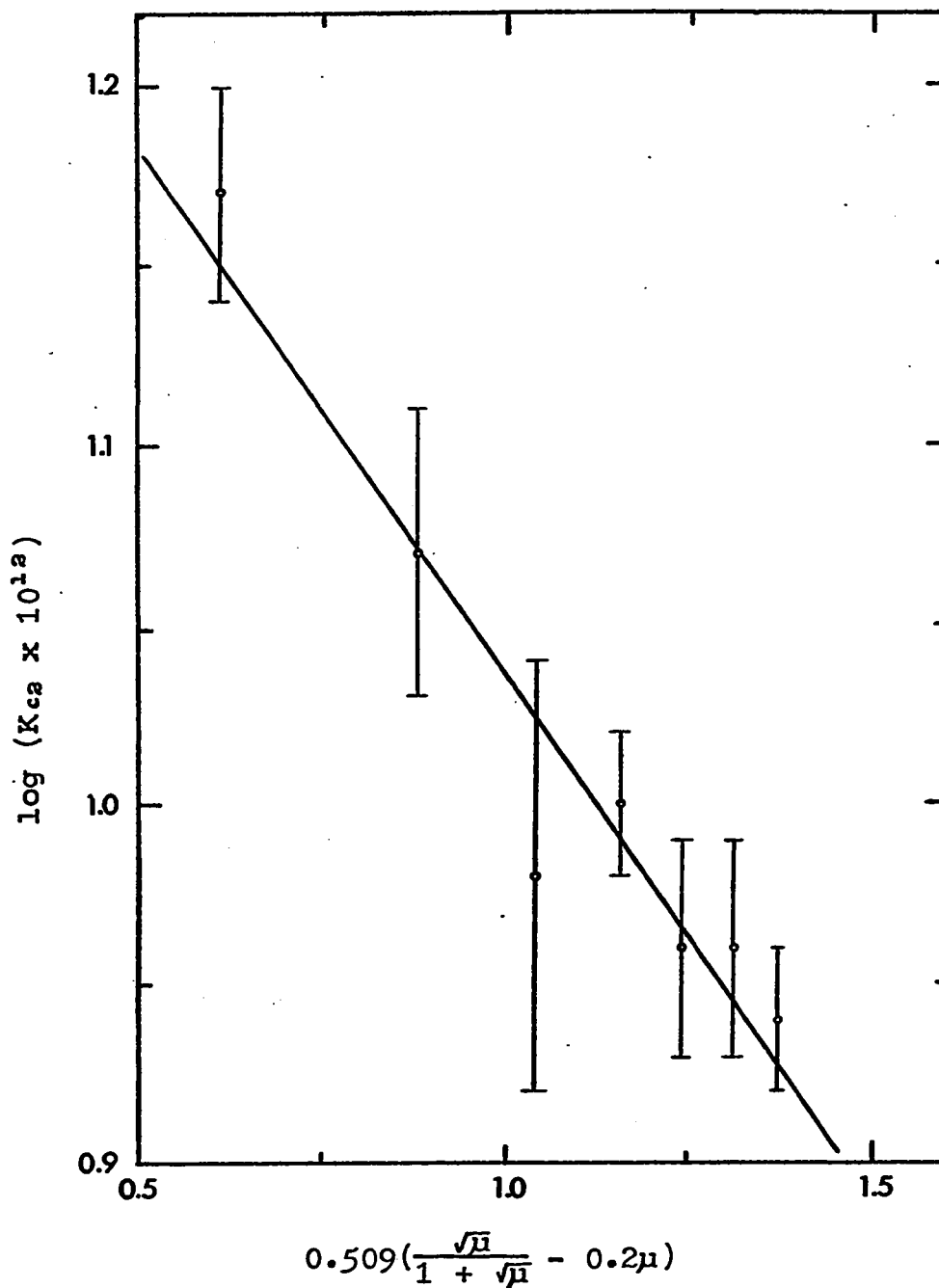


Figure 27. Plot of $\log K_{ca}$ vs. $0.509\left(\frac{\sqrt{\mu}}{1 + \sqrt{\mu}} - 0.20\mu\right)$ showing the ionic strength dependence of K_{ca} at 25.0° .

is well enough defined that the intercept of the straight line in Figure 27 can be used to obtain a value of $K_{T_2} = (2.14 \pm 0.25) \times 10^{-11}$ M. Values of K_{T_2} at 18.0° and 35.0° , calculated from eq 11, using a value of -2.9 for the slope and with appropriate correction for the change in the Debye-Hückel constant with temperature, are $(1.58 \pm 0.10) \times 10^{-11}$ M and $(3.33 \pm 0.67) \times 10^{-11}$ M, respectively. The logs of these values vs. $1/T$ are plotted in Figure 28; from linear least-squares analysis, ΔH_2° is found to equal 7.8 ± 0.1 kcal/mole. From the value of ΔH_2° , additional thermodynamic quantities can be calculated for the ionization of isozyme 2 (type C) at 25.0° :

$$\Delta G_2^\circ = -RT \ln K_{T_2} = 14.6 \pm 0.1 \text{ kcal/mole}$$

$$\Delta S_2^\circ = \frac{\Delta H_2^\circ - \Delta G_2^\circ}{T} = -22.6 \pm 1.0 \text{ e.u.}$$

These values may be compared to the corresponding thermodynamic quantities for other ionizations of water in different environments, shown in Table X. As can be seen in that table, the thermodynamic constants for the ionization of water in the sixth position of the heme proteins are not too different from one another, but as a group they differ from either the ionization of water alone or on $\text{Fe}(\text{OH}_2)_6^{3+}$, showing the considerable effect of the protein-heme structure on the nature of the hydrogen-oxygen bond in the water molecule.

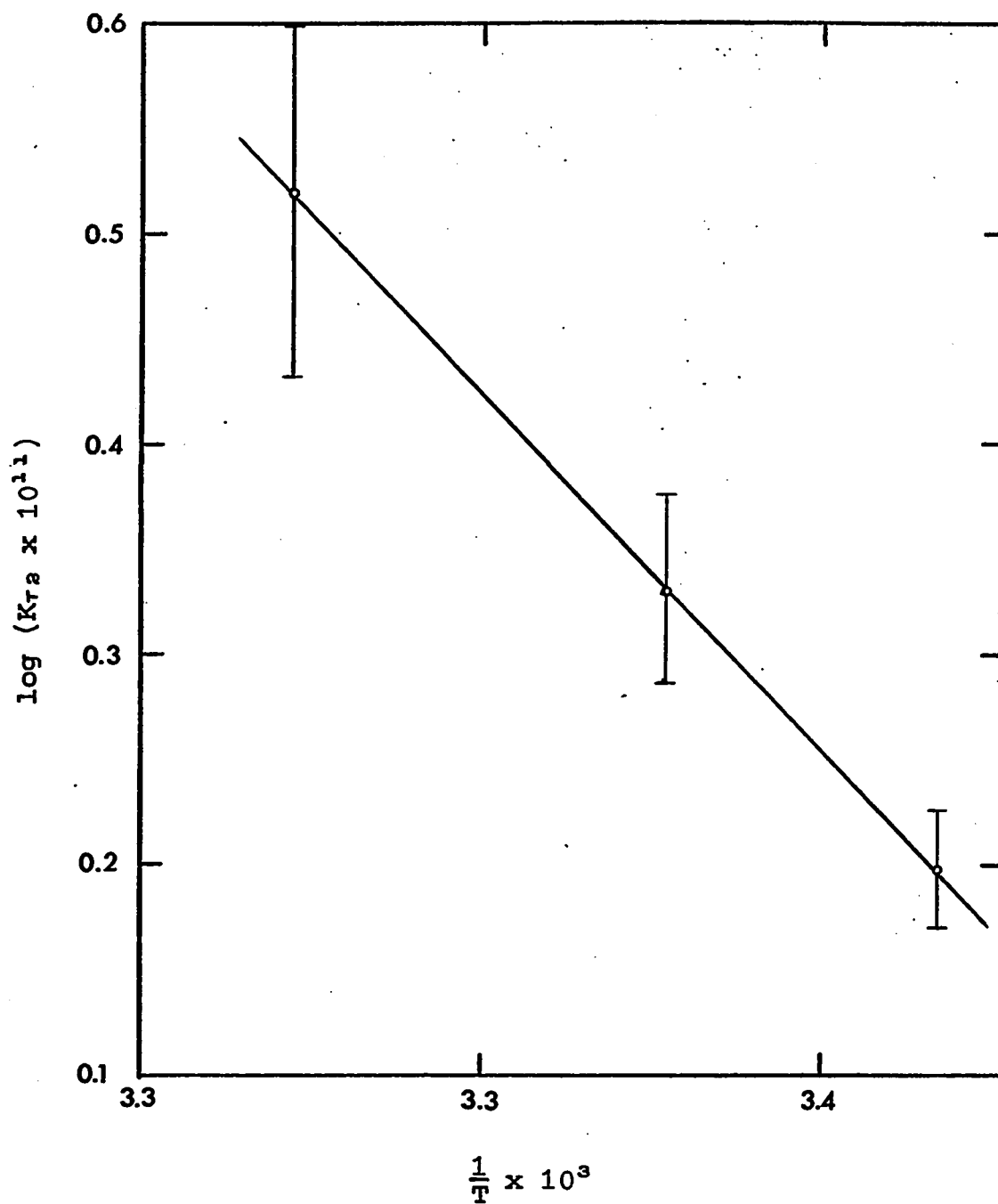


Figure 28. Plot of $\log K_{ra}$ vs. $1/T$ for experiments performed at $\mu = 0.11$. The slope is $-H_2^{\circ}/2.303R$.

Table X
 Thermodynamic Constants for the Ionization of Water,
 and Water Coordinated to Various Fe^{III} Complexes, at 25.0°.

Species	ΔG° (kcal/mole)	ΔH° (kcal/mole)	ΔS° (e.u.)	Reference
H ₂ O	19.1	13.5	-18.7	101
Fe(OH ₂) ₆ ³⁺	2.96 ± 0.04	10.4 ± 0.2	25.0 ± 0.7	102
Ferrihemoglobin	11.90 ± 0.03	3.91 ± 0.49	-27.3 ± 1.8	100
Ferrimyoglobin	12.12 ± 0.04	5.75 ± 0.67	-21.7 ± 2.4	99
Ferri-HRP ¹	14.6 ± 0.1	7.81 ± 0.14	-22.6 ± 1.0	this study

¹ Refers to isozyme 2 or C-Type isozyme found in this study

CHAPTER 6. STUDIES ON HEME PROTEINS USING THE NMR HALIDE
ION PROBE TECHNIQUE

The use of halide ions as probes for nuclear magnetic resonance studies of proteins has been the subject of several recent papers¹⁰³⁻¹⁰⁷. This chapter is a report on the use of the halide ion probe technique to study four heme proteins: bovine hemoglobin, sperm whale myoglobin, bovine liver catalase, and horseradish peroxidase*.

Theory

Nuclei which have a quadrupole moment can interact with a fluctuating electric field gradient to provide an effective nuclear relaxation mechanism. For ³⁵Cl, which has a nucleus of spin 3/2, the contribution to the nuclear resonance linewidth from quadrupole relaxation is¹⁰⁸:

$$\Delta\nu = \frac{2\pi}{5}(e^2qQ)^2 \tau_c \quad (1)$$

where $\Delta\nu$ is the linewidth in Hz at half-height; the

.....

*Abbreviations used in this chapter: Hb, ferrihemoglobin; Mb, ferrimyoglobin; Cat, catalase; PCMB, p-chloromercuribenzoate; $\Delta\nu_{obs}$, total observed ³⁵Cl linewidth; $\Delta\nu'$, total ³⁵Cl linewidth minus the contribution from the NaCl present in the solution; Hz, Hertz, or cycles/sec.

quantity (e^2qQ), known as the quadrupole coupling constant, consists of e , the charge on the electron, q , the electric field gradient at the nucleus, and Q , the quadrupole moment of the nucleus; τ_c is the rotational correlation time. A large range of linewidths is possible, since both τ_c and the quadrupole coupling constant can vary greatly for different molecules. Dilute aqueous solutions of chloride ion give linewidths of about 15 Hz, a result of the fact that the chloride ion is essentially symmetrically solvated, which produces a field gradient of almost zero at the nucleus. If the chlorine atom is involved in covalent bonding, a large value of the coupling constant, and hence, a large linewidth results. For example, the linewidth for CCl_4 would be of the order of 14.5 kHz^{103} .

If there are several sites available for the chlorine, and if the exchange between them is slow, the resulting spectrum will contain lines characteristic of the different environments, with the areas proportional to the concentrations of the various sites. If the exchange between the sites is fast compared to the reciprocal of the width of the broadest line, a single composite line is observed with the observed linewidth, $\Delta\nu_{obs}$, given by:

$$\Delta\nu_{obs} = \sum \Delta\nu_i P_i \quad (2)$$

where $\Delta\nu_i$ is the natural linewidth of ^{35}Cl in the i th environment and P_i is the probability that the chlorine is at the i th site.

Experimental

Heme proteins used in this study were: bovine Hb (2X cryst., A grade, lot 64385) from Calbiochem; sperm whale Mb from Mann Research Laboratories; analytical reagent grade HRP (RZ = 2.9, lot 6485206) and purified grade HRP (RZ = 0.8) from Boehringer-Mannheim Corp., N. Y.; and bovine liver catalase from Pierce Chemicals (RZ = 0.1) and from Boehringer-Mannheim Corp., N. Y. (analytical reagent grade, RZ = 0.9, lot 6028247). Protein solutions were dialyzed against water and centrifuged before use. All other chemicals used in this study were reagent grade and were used without further purification. Concentrations of the heme proteins were determined from absorbance measurements using either a Beckman DU or a Cary Model 14 spectrophotometer, along with literature values for the molar absorptivity coefficients^{5, 56}. Measurements of pH were made with a Beckman expanded scale pH meter.

The catalase from Pierce Chemicals was further purified by ammonium sulfate precipitation (50 % saturation) and dialysis, followed by passage through a 2.5 cm x 50 cm column of G-200 Sephadex gel. The catalase was eluted using pH 6.4 phosphate buffer of ionic strength equal to 0.1. The purest fraction resulting from a single passage through the column had a RZ value of 0.5.

The apoprotein of HRP was isolated by cleaving analytical reagent grade HRP at pH 2.5 using Yonetani's

modification¹⁰⁹ of Teale's 2-butanone method¹¹⁰. Spectrophotometric measurements at 403 m μ , the maximum of the Soret peak of HRP, indicated that less than 2.5 % of the native HRP was present in the isolated apo-HRP.

PCMB titrations of analytical reagent grade catalase and analytical reagent grade HRP were carried out at pH 6.0 using the method of Boyer¹¹¹. Samples were allowed to stand at room temperature for 24 hours to ensure that the reaction was complete before measurements were made on the Cary Model 14.

The ³⁵Cl spectra were obtained at 5.9 MHz using a Varian VF16 wide line NMR spectrometer equipped with a V4012A high resolution 12" magnet. A Varian V3521 integrator or a Princeton Applied Research JB-4 lock-in amplifier were used for field modulation and detection. Linewidths were calibrated from sidebands of a saturated aqueous NaCl solution. A Hewlett-Packard 241A oscillator supplied the sideband frequency, which was measured using a Hewlett-Packard 521C counter. All spectra were obtained at room temperature using 5 ml of liquid in a sample tube of 15 mm diameter. Linewidths reported in this chapter were measured as the distance between the turning points of dispersion mode spectra and are the average of at least five spectra. Error limits reported are mean deviations. Representative spectra are shown in Figure 29.

For each experiment, spectra were taken of a NaCl

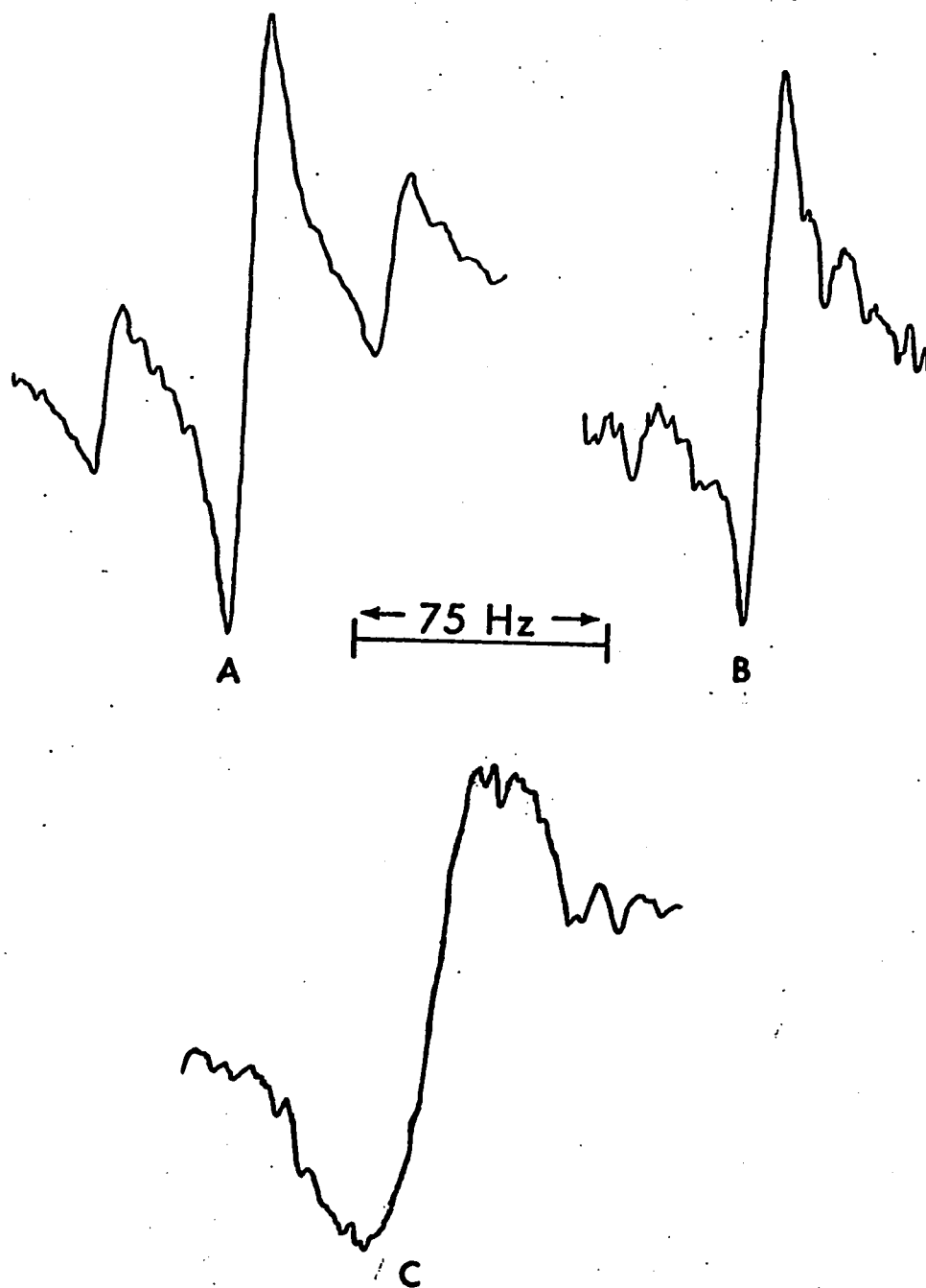


Figure 29. Representative NMR spectra. A. Saturated NaCl with 75 Hz sidebands. B. 3.4×10^{-5} M Hb in 0.5 M NaCl; linewidth is 15 Hz. C. Broad signal with a linewidth of 65 Hz.

solution of a molarity equal to that in the experimental solution. In the case of the experiments involving titration with HgCl_2 , a solution of protein was prepared which was either 0.5 M or 1.0 M in NaCl and was titrated with μl volumes of a solution of HgCl_2 which was about 100 times more concentrated than the protein. This procedure eliminated the necessity for a correction due to increase in total volume, since the maximum increase in volume due to added titrant was less than 5 %.

Results

For solutions used in the present study, eq 2 can be written as:

$$\Delta\nu_{\text{obs}} = \Delta\nu_{(\text{Cl}^-)}P_{(\text{Cl}^-)} + \sum \Delta\nu_j P_j \quad (3)$$

in which the contribution to the total linewidth from the chloride ion in solution is separated from that from chloride in the other possible environments. Because the chloride ion concentration was at least 10^4 times that of the protein, $P_{(\text{Cl}^-)}$ is close to unity and eq 3 can be simplified to:

$$\Delta\nu' = \Delta\nu_{\text{obs}} - \Delta\nu_{(\text{Cl}^-)} = \sum \Delta\nu_j P_j \quad (4)$$

Further, the assumption that $P_{(\text{Cl}^-)} \approx 1$ implies that the P_j s are independent of each other. All linewidths obtained from protein solutions will henceforth be expressed in terms of $\Delta\nu'$, i.e., the linewidth of the experimental solution minus the linewidth of a solution containing only NaCl of the same concentration as that in the experimental solution.

The ^{35}Cl linewidth of a solution of either 0.5 M NaCl or 1 M NaCl at pH 6.5 was found to be 14 ± 2 Hz, which was not changed by lowering the pH to 2.0. Addition of HgCl_2 to a solution of NaCl broadened the line linearly; a 0.5 M NaCl solution which was 2×10^{-4} M with respect to HgCl_2 gave a linewidth of 25 ± 2 Hz.

This study resulted in the first observation, by the NMR halide ion probe technique, of direct chloride binding to a protein. Figure 30 shows the effect of pH on $\Delta\nu'$ for solutions of 7.3×10^{-5} M analytical reagent grade HRP and apo-HRP, both 1 M in NaCl. HRP precipitated below pH 3 and apo-HRP below pH 3.5, thus setting the lower limits of pH at which the study could be carried out. Significant broadening due to chloride ion binding to catalase was observed for solutions of catalase obtained from Pierce Chemicals. A 4.1×10^{-5} M solution of catalase at pH 6.5 which was 0.5 M in NaCl gave a value of $\Delta\nu' = 50 \pm 5$ Hz. The amount of broadening was the same for solutions of catalase from the same source, but which had been further purified. The broadening was less by an order of magnitude for a solution of the analytical reagent grade catalase; for 2.8×10^{-5} M analytical reagent grade catalase at pH 6.8 and which was 0.5 M in NaCl, $\Delta\nu' = 6 \pm 1$ Hz.

Curves showing the titrations of analytical reagent grade HRP, Hb, and analytical reagent grade catalase with HgCl_2 , a reagent which is quite specific for sulfhydryl

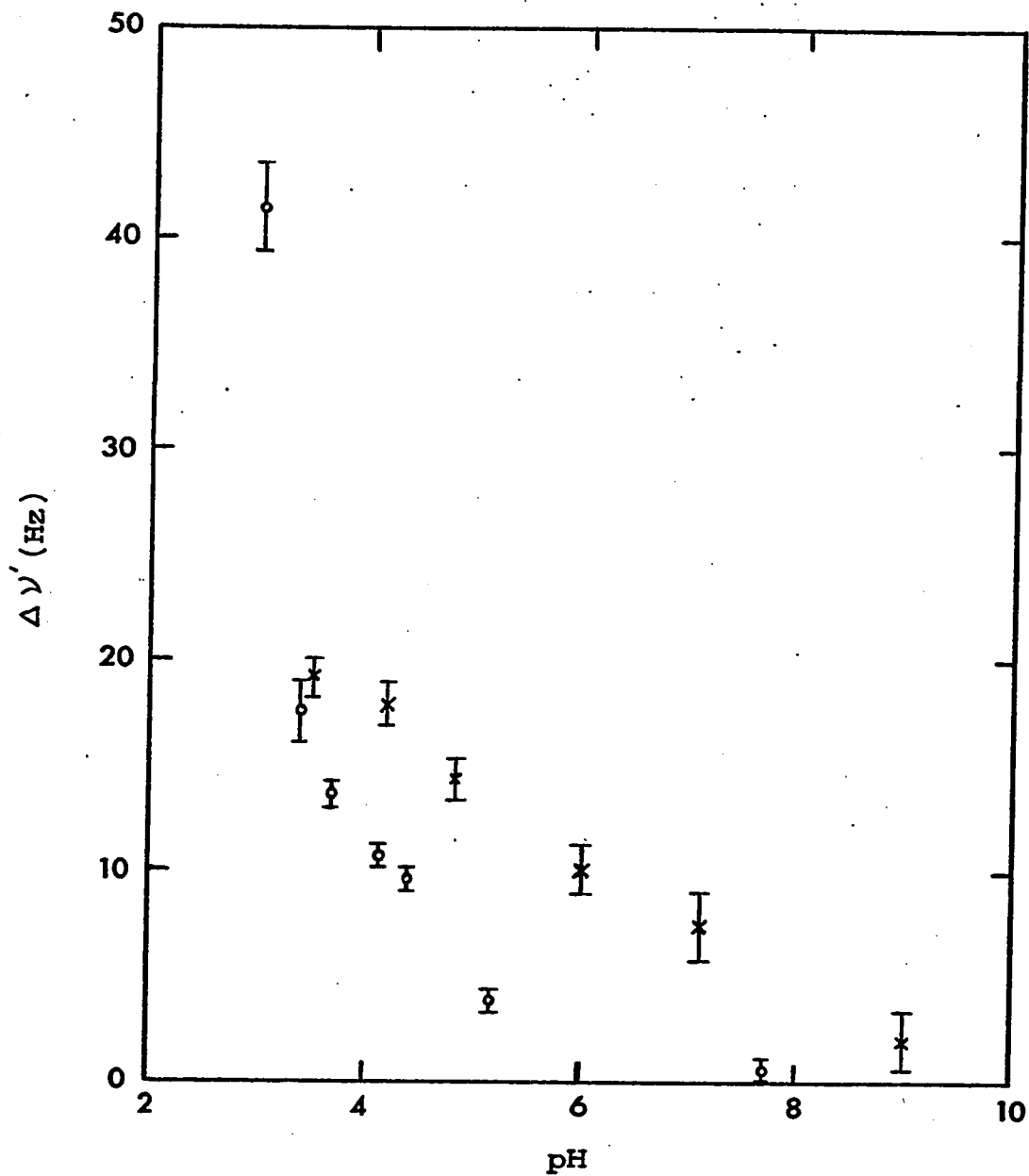


Figure 30. Plot of line broadening vs. pH for a solution of 7.3×10^{-5} M HRP (o) and 7.3×10^{-5} M apo-HRP (x), both 1 M in NaCl.

groups¹¹², are shown in Figures 31, 32, and 33, with the results plotted as $\Delta \nu'$ vs. $[\text{HgCl}_2]/[\text{protein}]$. The titration curves of HRP and catalase indicate the presence of one and two sulfhydryl groups, respectively; the titration curve of Hb is not as well defined, appearing to break between $[\text{HgCl}_2]/[\text{Hb}]$ ratios of one and two. The HgCl_2 titration curve for purified grade HRP was identical to that of analytical reagent grade HRP. Spectrophotometric titration of analytical reagent grade HRP and analytical reagent grade catalase with PCMB indicated the presence of 1.0 ± 0.2 and 4.5 ± 0.5 sulfhydryl groups, respectively.

The results of the titration of 4.46×10^{-5} M Mb at pH 7.9 and $[\text{Cl}^-] = 1\text{M}$ with HgCl_2 are shown in Figure 34. The dashed line in that figure shows the broadening expected from the addition of HgCl_2 alone, i.e., if there were no interaction between the HgCl_2 and the myoglobin. For a given amount of HgCl_2 added to the Mb solution, the line-width was found to be pH dependent. This is illustrated in Figure 35, which is a plot of $\Delta \nu'$ vs. pH for a sample containing 1 M NaCl, 4.5×10^{-5} M Mb, and 1.1×10^{-4} M HgCl_2 . The broadening expected if there were no interaction between Mb and HgCl_2 is again shown by a dashed line. There appears to be no break indicating the presence of an end point in Figure 34; another titration carried out to a ratio of $[\text{HgCl}_2]/[\text{Mb}]$ of greater than 10 also indicated no break. The reversibility of the reaction between HgCl_2

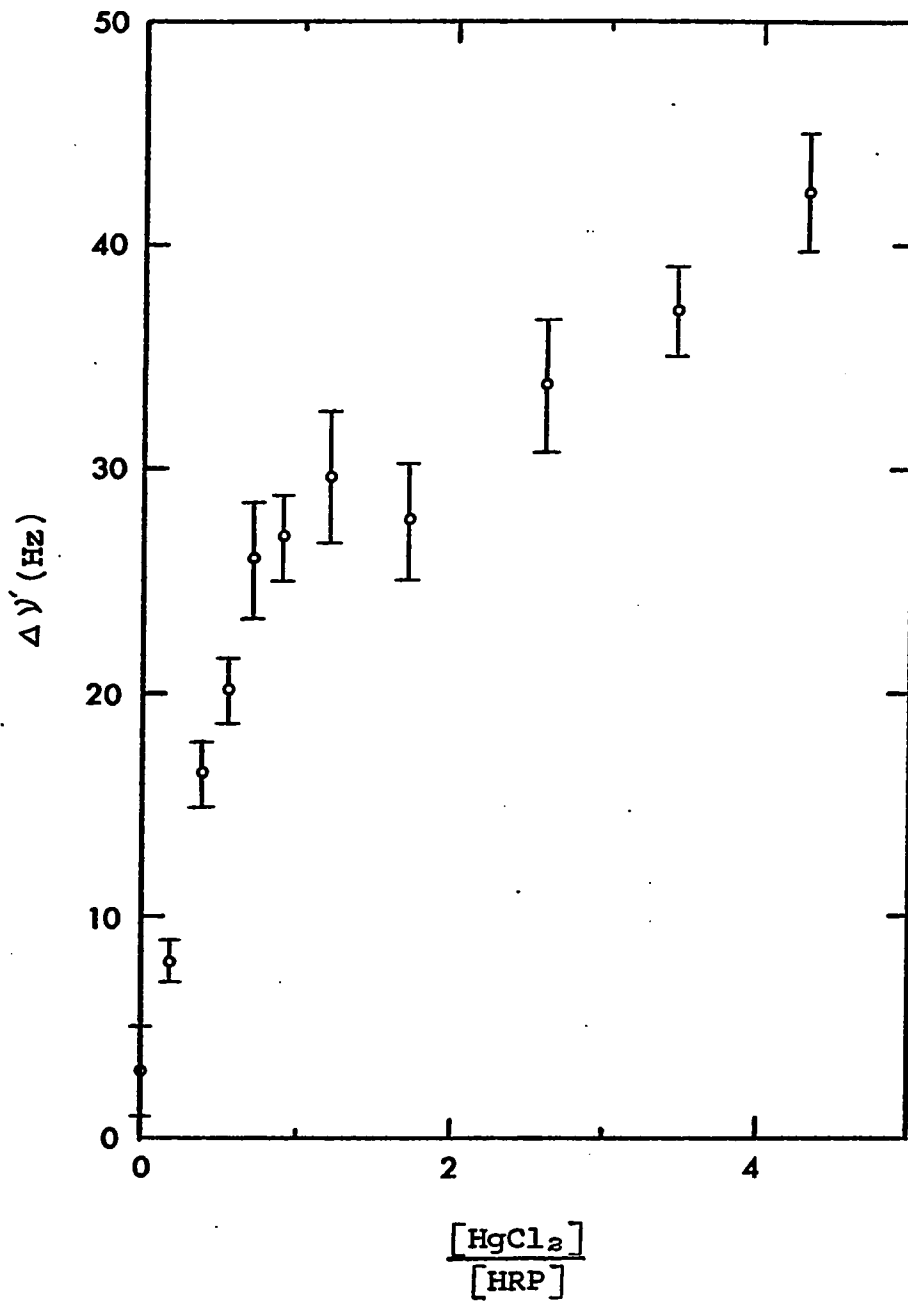


Figure 31. Curve showing the titration of 5.8×10^{-5} M HRP with HgCl_2 ; pH = 7.0, $[\text{Cl}^-] = 0.5$ M.

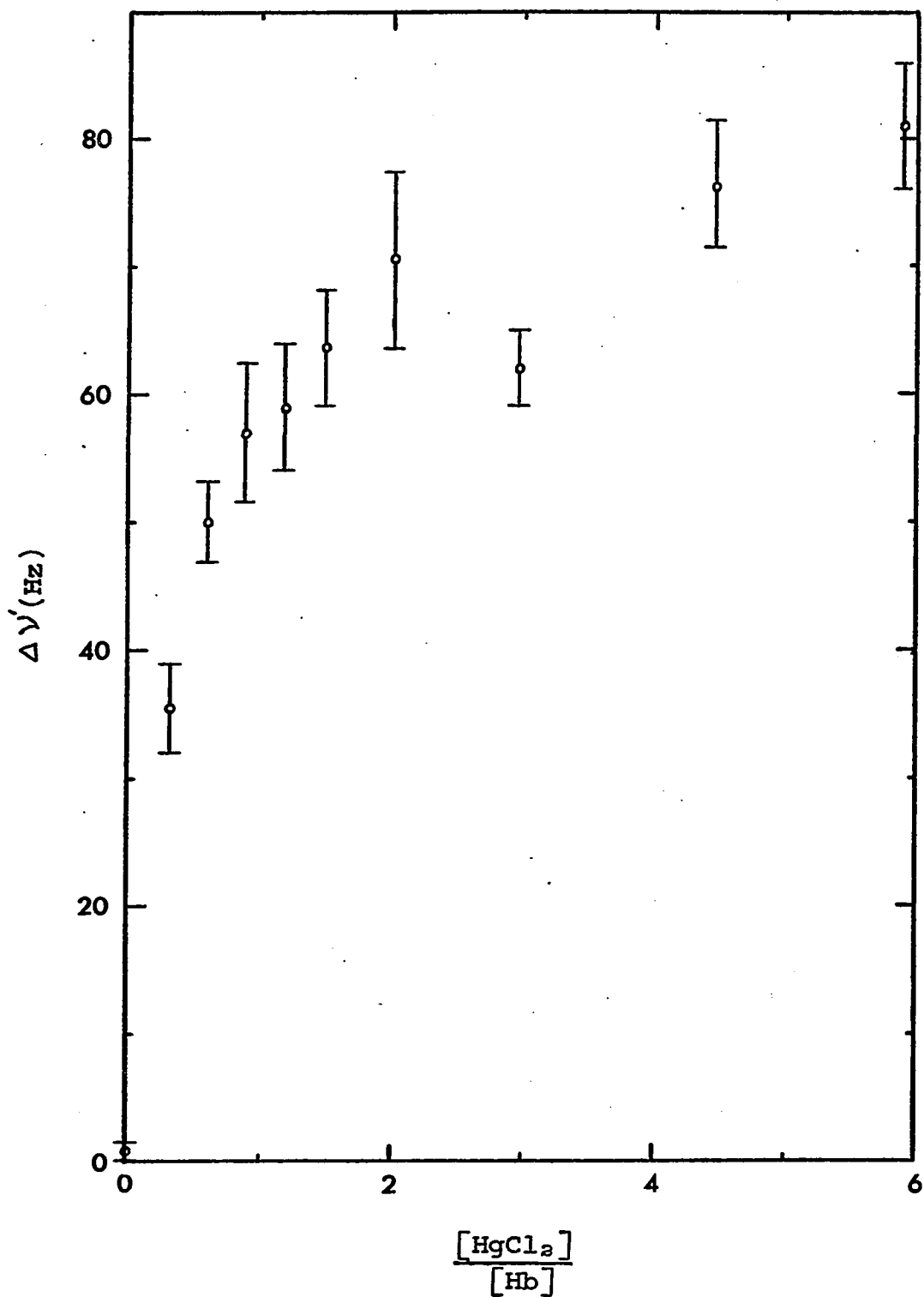


Figure 32. Curve showing the titration of 3.4×10^{-5} M Hb with HgCl_2 ; pH = 6.3, $[\text{Cl}^-] = 0.5$ M.

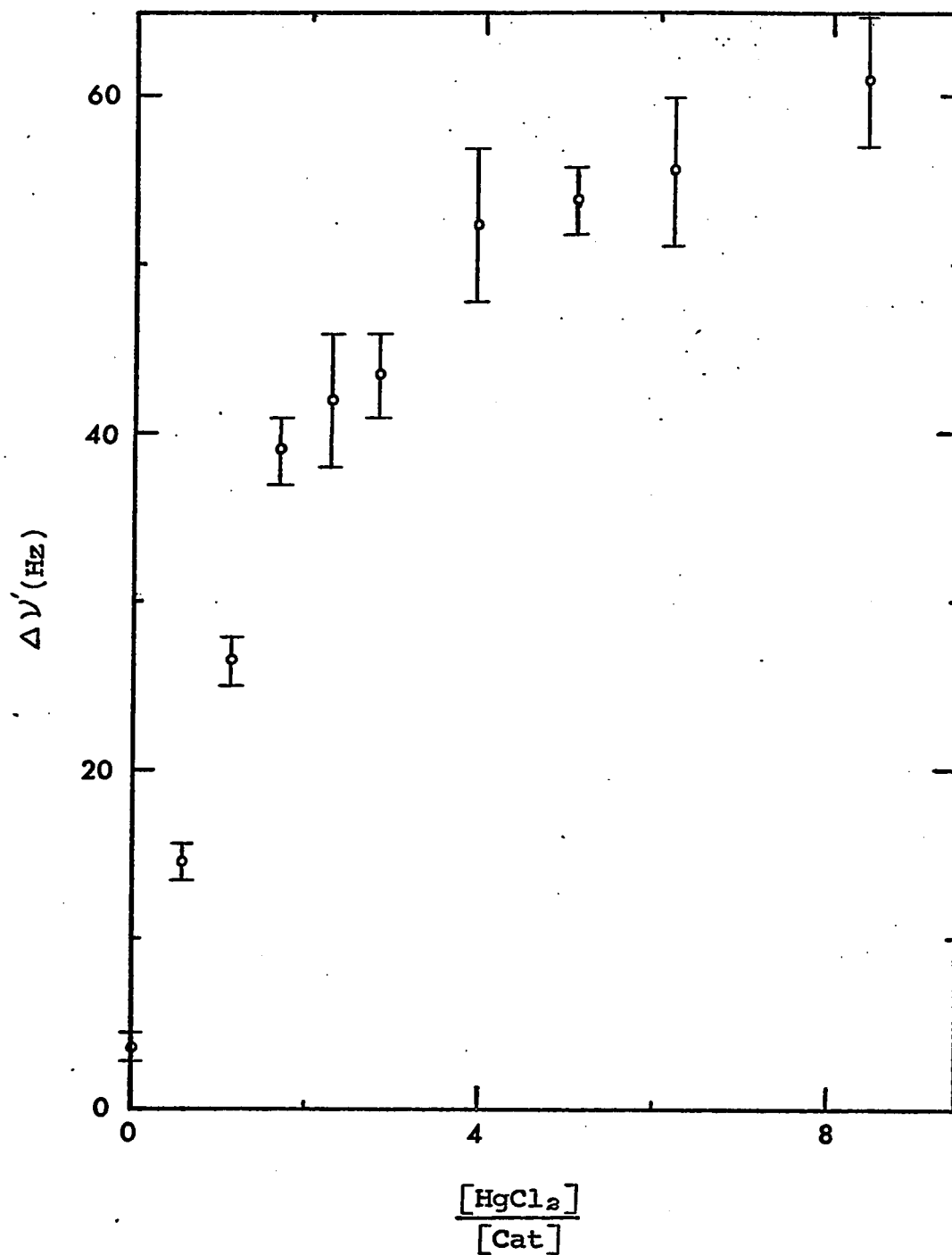


Figure 33. Curve showing the titration of 1.0×10^{-5} M catalase with HgCl_2 ; pH = 6.6, $[\text{Cl}^-] = 1 \text{ M}$.

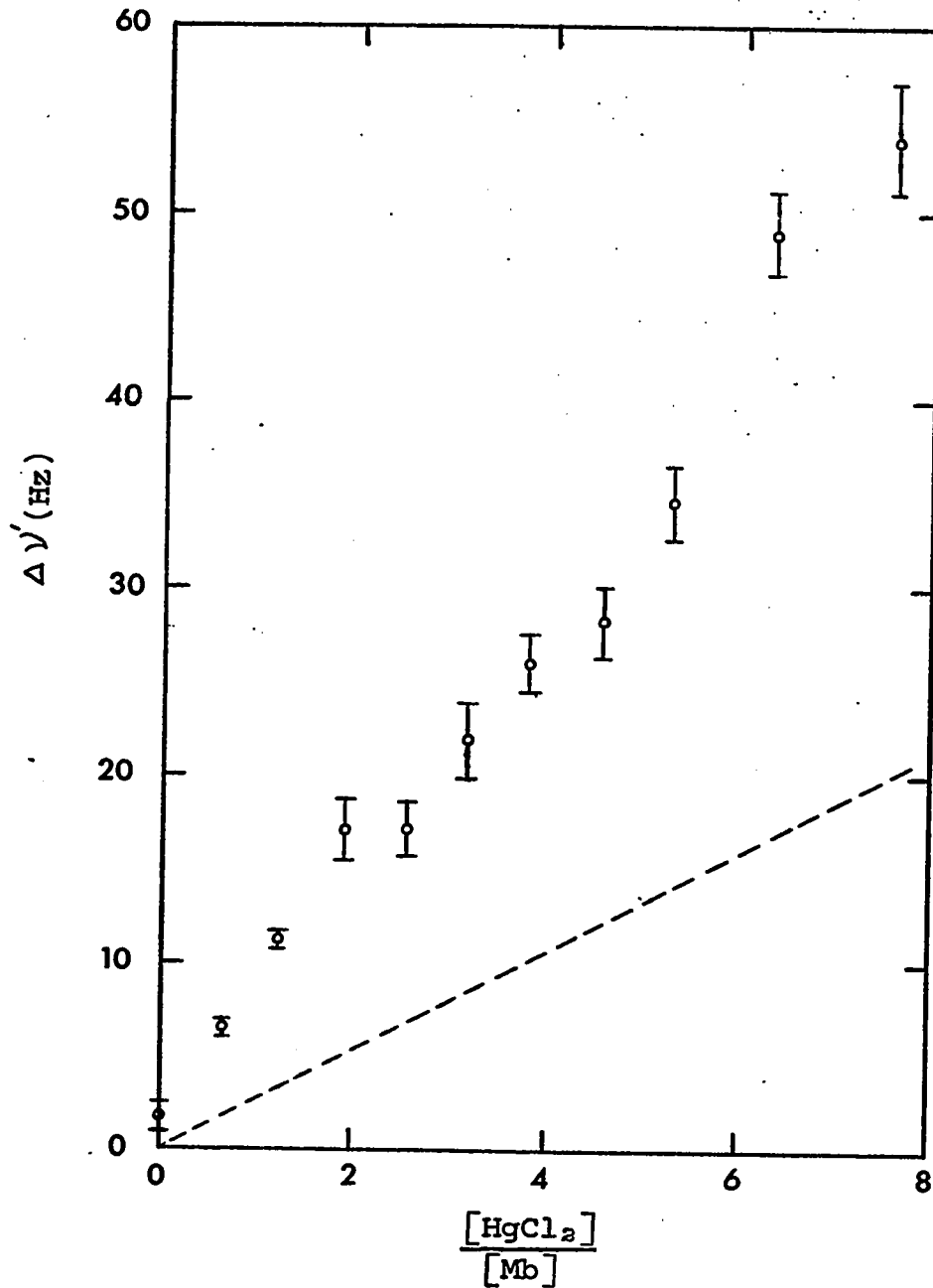


Figure 34. Curve showing the titration of 4.46×10^{-5} M Mb with HgCl_2 ; pH = 7.9, $[\text{Cl}^-] = 1$ M. The dashed line shows the broadening expected if there were no interaction between the Mb and the HgCl_2 .

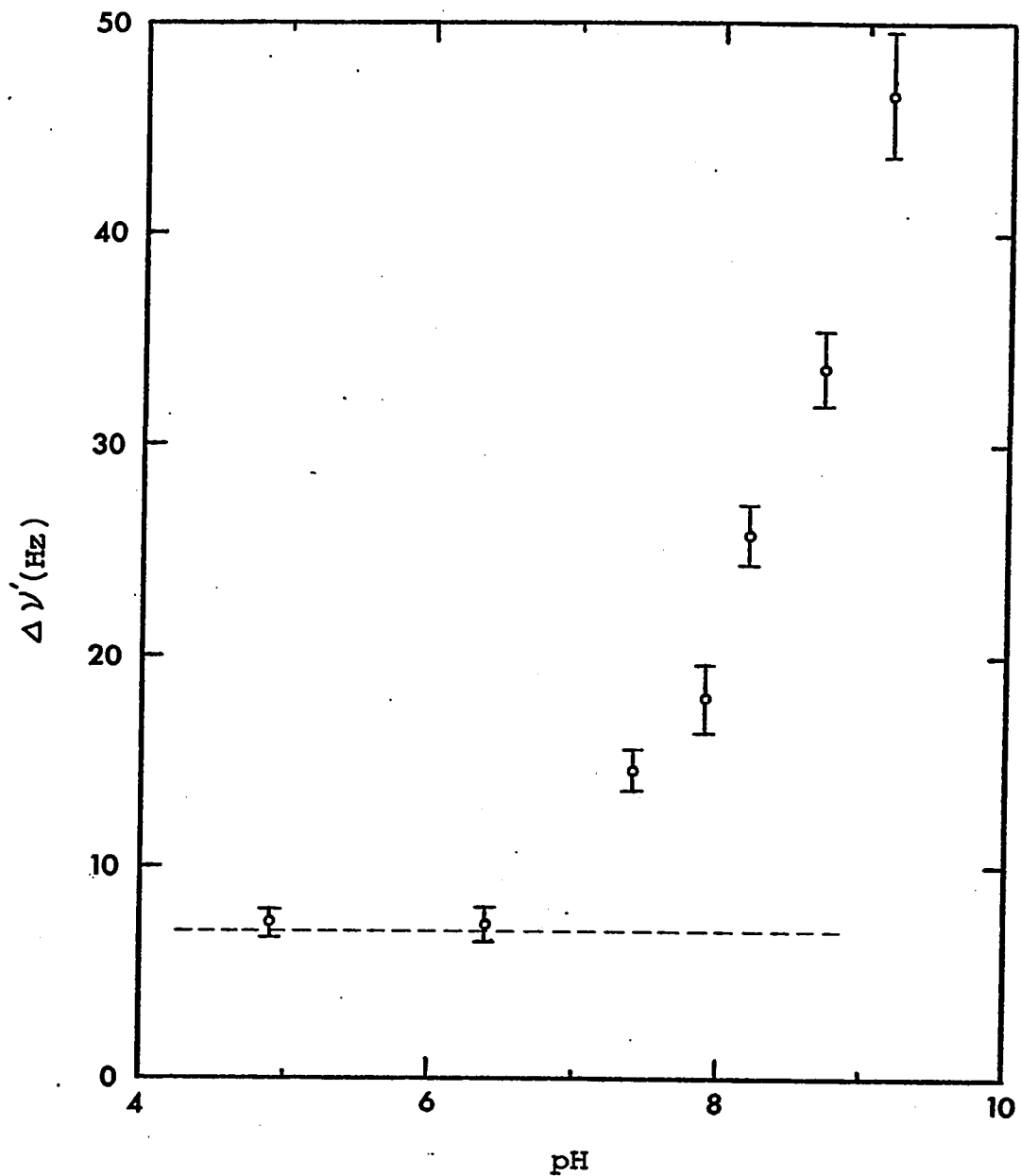


Figure 35. Plot of line broadening vs. pH for a solution of 4.5×10^{-5} M Mb; $[\text{HgCl}_2] = 1.1 \times 10^{-4}$ M; $[\text{Cl}^-] = 1$ M. The dashed line shows the broadening expected if there were no interaction between the Mb and the HgCl_2 .

and Mb was demonstrated by lowering the pH of a solution containing 1 M NaCl, 2.1×10^{-5} M Mb, and 2.1×10^{-4} M HgCl₂ from pH 9.2 to 5.8. This resulted in $\Delta\nu'$ decreasing from 56 ± 5 Hz to 11 ± 1 Hz, the value expected from the presence of unreacted HgCl₂.

The reactivity of HgCl₂ with methionine and imidazole was investigated at pH values of 7 and 10 by observing the linewidths of solutions of 1 M NaCl containing 3.4×10^{-4} M HgCl₂ with and without the presence of either 4×10^{-4} M methionine or 4×10^{-4} M imidazole. No evidence of interaction between HgCl₂ and either compound was observed.

Discussion

The observed binding of chloride ions to catalase and analytical reagent grade HRP demonstrates the potential usefulness of the halide ion probe technique as a tool for observing protein-chloride interaction. Since it has been reported that the Soret absorption peak of HRP undergoes a spectral change at low pH in the presence of chloride, a result which was attributed to the binding of chloride to the heme ferric iron of HRP³⁰, one might expect that the observed line broadening was due to chloride exchange at the sixth coordination position of the iron, and that the observed pH dependence is correlated with the pH dependence of the equilibrium constant for HRP-chloride formation. However, this explanation cannot be correct, since the pH

dependence of chloride binding to apo-HRP is similar to that of native HRP, as can be seen in Figure 30. The results of this study do not rule out the possibility that chloride binds to the heme, since $\Delta\nu$ for the heme-chloride site could simply be too small to result in a contribution to the total linewidth, as expressed in eq 2. The pH dependence of the chloride binding could be explained if the chloride were binding electrostatically and nonspecifically in regions of appreciable positive charge, since the net positive charge on the protein would increase as the pH was lowered due to protonation of various groups. This hypothesis is substantiated by the fact that the amount of broadening at a given pH is greater for apo-HRP than it is for native HRP. An ORD study has shown that as the heme is split from the protein of HRP, the protein becomes less helical (Chapter 4 of this thesis), thus the greater chloride binding for apo-HRP could be a result of the partial unfolding of the protein and the exposure of more binding sites. One can also see in Figure 30 that the amount of line broadening for HRP increased appreciably below pH 3.4, which might be due to the rapid splitting of the heme from the protein of HRP³⁰.

The results of the study of chloride binding to catalase are difficult to explain, since they varied with the source of the catalase. There are two possibilities which could account for the observed results. The first is that

there is some impurity capable of binding chloride present in the catalase preparation obtained from Pierce Chemicals. If this is the case, the impurity must be protein material, since it was not removed by exhaustive dialysis. However, further purification of that preparation increased the ratio of absorbances of the maxima of the heme and protein peaks (RZ) by a factor of five, indicating that a considerable amount of protein was removed during the further purification. Thus, if the observed results are due to a protein impurity, the protein must have a molecular weight similar to that of catalase since the same line broadening was observed before and after additional purification. An alternative explanation would be that the isolation procedure used by Pierce Chemicals resulted in a change in the protein such that groups capable of binding chloride were exposed.

This investigation also included studies of the behavior of Hg^{2+} as a sulfhydryl reagent when the halide ion probe method is used as a means of detection. The titration of HRP with HgCl_2 has a well-defined end point indicating one sulfhydryl group, as is shown in Figure 31. The positive slope beyond the end point in Figure 31 is due to the contribution from uncomplexed HgCl_2 . The presence of one sulfhydryl group in HRP was confirmed by the spectrophotometric titration using PCMB. No previous quantitative study has been made on the sulfhydryl groups of HRP, but

qualitative amino acid analysis has shown the presence of cysteine¹⁵. Although purified grade HRP contains a greater amount of protein material than does the analytical reagent grade HRP, as evidenced by its considerably lower RZ value, results from the two protein preparations were the same, indicating the presence of no additional reactive sulfhydryl groups in the protein impurities present.

It had previously been reported that good results were obtained using this method for the titration of equine and human hemoglobin¹⁰⁴. However, the HgCl₂ titration curve for bovine Hb, shown in Figure 32, is difficult to interpret. It is obvious that there is at least one sulfhydryl group, and probable that there is a second, since the titration curve has a slope characteristic of HgCl₂ alone only after a [HgCl₂]/[Hb] ratio of two. Direct comparison of this curve with those obtained by Stengle and Baldeschwieler¹⁰⁴ cannot be made for two reasons. First, their data is for equine and human Hb, while this study was carried out using bovine Hb, and although they found the same number of sulfhydryl groups for both of those hemoglobins (two), there could be a species difference between those two types and bovine Hb. Second, their published curves show points only at integral [HgCl₂]/[Hb] ratios, so any anomalous behavior might not show up due to a lack of sufficient points. The simplest explanation for the behavior shown in Figure 32 is that there are two reactive

sulfhydryl groups in bovine Hb, but that they are in environments of different accessibility. Thus, if the second site is less accessible and has a smaller τ_c than the first, the slope of the titration curve of the second site would be less than that of the first, as predicted by eq 1.

The results of the HgCl_2 titration of catalase, which indicate that there are two reactive sulfhydryl groups, disagree with the results of the PCMB titration which indicates 4.5 ± 0.5 reactive sulfhydryl groups, and both of these disagree with the findings of Samejima and Yang¹¹³, who found six reactive groups in catalase by titration with PCMB. The disagreement between the results obtained from the two methods could be due to the nature of the action of the two different sulfhydryl reagents. HgCl_2 reacts rapidly and perhaps only with the most accessible sulfhydryl groups. PCMB reacts slowly with catalase, and it has been suggested that in such cases, some type of bond has to be broken before the sulfhydryl groups can react¹¹³, thus the PCMB could be reacting with additional, less reactive sulfhydryl groups. The slow reaction of PCMB with catalase could also explain the difference between the results of this study and those obtained by Samejima and Yang. Those authors did not tell under what conditions they found the six titratable groups, and since they found an additional

ten sulfhydryl groups upon denaturation of the catalase, it is possible that there exists in catalase sulfhydryl groups of many degrees of reactivity, and that Samejima and Yang's conditions for the PCMB titration were such that more groups could react than under the conditions used in this study. However, as pointed out in the review by Cecil and McPhee¹¹², results of determinations of the number of sulfhydryl groups of proteins often differ depending upon the sulfhydryl reagent used, and also that different investigators frequently obtain conflicting results using the same sulfhydryl reagent.

The results of the titration of Mb with HgCl_2 are quite surprising because Mb is known to contain no cysteine or cystine¹¹⁴. Since mercury is a member of the same group as zinc, and since Zn^{2+} is known to bind to imidazole residues in Mb^{115,116}, there is a possibility that Hg^{2+} might also react with imidazole. Likewise, since methionine contains sulfur, which although incapable of forming a complex of the type R-S-Hg-Cl , might nevertheless be capable of forming a complex with mercury through one of its unshared electron pairs. However, some evidence against either imidazole or methionine residues providing binding sites is furnished by the lack of reactivity of HgCl_2 with either compound. The lack of any break in Figure 34 indicates that either (a) the number of binding sites is large, or (b) the equilibrium constant for the formation of the

mercury-protein complex is very small.

It is interesting to note that Figure 35 looks much like a mirror image of Figure 30. Therefore, one might postulate that the observed pH dependence shown in Figure 35 is a result of Hg^{2+} binding to anionic sites on the protein, and that the number of anionic sites increases as the pH is raised.

This study has shown the halide ion probe technique to be a very sensitive method for detecting the binding of Cl^- or Hg^{2+} to proteins. When used as a means of detection for titrations with HgCl_2 to determine the sulfhydryl content of proteins, this method has the advantages of speed and simplicity and offers the possibility of distinguishing sulfhydryl sites of different accessibility. Judgment of the relative merit of this means of determining the sulfhydryl content of proteins, as compared with older techniques, must await further studies.

LITERATURE CITED

1. Report of the Commission on Enzymes of the International Union of Biochemistry, Pergamon Press, Oxford, 1961.
2. Saunders, B.C., Holmes-Siedle, A.G., and Stark, B.P., "Peroxidase", Butterworths, London, 1964.
3. Bach, R., and Chodat, A., Ber. dtsh. chem. Ges. 36, 606 (1903).
4. Theorell, H., Enzymologia 10, 250 (1942).
5. Keilin, D., and Hartree, E.F., Biochem. J. 49, 88 (1951).
6. Paul, K.G., Acta Chem. Scand. 12, 1312 (1958).
7. Theorell, H., Arkiv Kemi Mineral. Geol. 16A, No. 2 (1942).
8. Jermyn, M.A., and Thomas, R., Biochem. J. 56, 631 (1954).
9. Klapper, M.H., and Hackett, D.P., Biochim. Biophys. Acta 96, 272 (1965).
10. Shannon, L.M., Kay, E., and Lew, J.Y., J. Biol. Chem. 241, 2166 (1966).
11. Kay, E., Shannon, L.M., and Lew, J.Y., J. Biol. Chem. 242, 2470 (1967).
12. Maehly, A.C., Methods in Enzymology II, 801 (1955).
13. Theorell, H., and Akeson, A., Arkiv Kemi Mineral. Geol. 16A, No. 8 (1942).
14. Theorell, H., and Maehly, A.C., Acta Chem. Scand. 4, 422 (1950).
15. Maehly, A.C., and Paleus, S., Acta Chem. Scand. 4, 508 (1950).
16. Brill, A.S., and Weinryb, I., Biochemistry 6, 3528 (1967).

17. Keilin, D., and Mann, T., Proc. Roy. Soc. B122, 119 (1937).
18. Theorell, H., Arkiv Kemi Mineral. Geol. 14B, No. 20 (1940).
19. Harbury, H.A., J. Biol. Chem. 225, 1009 (1957).
20. Watson, H.C., in "Hemes and Hemoproteins", Ed. by Chance, B., Estabrook, R.W., and Yonetani, T., Academic Press, N.Y., 1966, pp. 63-66.
21. Stryer, L., Kendrew, J.C., and Watson, H.C., J. Mol. Biol. 8, 96 (1964).
22. Hoard, J.L., in "Hemes and Hemoproteins", Ed. by Chance, B., Estabrook, R.W., and Yonetani, T., Academic Press, N.Y., 1966, pp. 9-24.
23. Brill, A.S., and Williams, R.J.P., Biochem. J. 78, 246 (1961).
24. Brill, A.S., Comp. Biochem. 14, 447 (1966).
25. Nicholls, P., Biochim. Biophys. Acta 60, 217 (1962).
26. George, P., and Lyster, R.L.J., Proc. Nat. Acad. Sci. U.S. 44, 1013 (1958).
27. Brill, A.S., and Sandberg, H.E., Proc. Nat. Acad. Sci. U.S. 57, 136 (1967).
28. Theorell, H., and Paul, K.G., Arkiv Kemi Mineral. Geol. 18A, No. 12 (1944).
29. Maehly, A.C., Nature 192, 630 (1961).
30. Maehly, A.C., Biochim. Biophys. Acta 8, 1 (1952).
31. Maehly, A.C., Arch. Biochem. Biophys. 44, 430 (1953).
32. Maehly, A.C., Arch. Biochem. Biophys. 56, 507 (1955).
33. Watson, H.C., and Chance, B., in "Hemes and Hemoproteins", Chance, B., Estabrook, R.W., and Yonetani, T., Eds., Academic Press, N.Y., 1966, pp. 149-153.

34. Theorell, H., Arkiv Kemi Mineral. Geol. 16A, No. 3 (1942).
35. Wittenberg, J. B., Noble, R.W., Wittenberg, B.A, Antonini, E., Brunori, M., and Wyman, J., J. Biol. Chem. 242, 626 (1967).
36. Keilin, D., and Hartree, E.F., Biochem. J. 61, 153 (1955).
37. Chance, B., Arch. Biochem. Biophys. 40, 153 (1952).
38. Chance, B., J. Cell. and Comp. Physiol. 22, 33 (1943).
39. George, P., in "Currents in Biochem. Research", Ed. by Green, D.E., Interscience, Inc., N.Y., 1956, p. 338.
40. Chance, B., in "Hemes and Hemoproteins", Ed. by Chance, B., Estabrook, R.W., and Yonetani, T., Academic Press, N.Y., 1960, p. 339.
41. Dunford, H.B., and Alberty, R.A., Biochemistry 6, 447 (1967).
42. Caldin, E.F., "Fast Reactions in Solution", John Wiley and Sons, N.Y., 1964, p. 2.
43. Eigen, M., Discuss. Faraday Soc. 17, 194 (1954).
44. Hartridge, H., and Roughton, F.J.W., Proc. Roy. Soc. A104, 376 (1923).
45. Chance, B., J. Franklin Inst. 229, 455, 613, 737 (1940).
46. Gibson, Q.H., J. Physiol. 117, 49P (1952).
47. Gibson, Q.H., and Milnes, L. Biochem. J. 91, 161 (1964).
48. Sturtevant, J.M., in "Rapid Mixing and Sampling Techniques in Biochemistry", Chance, B., Eisenhardt, R.H., Gibson, Q.H., and Longberg-Holm, K.K., Eds., Academic Press, N.Y., 1964, pp. 89-102.
49. Ver Ploeg, D.A., and Alberty, R.A., J. Biol. Chem. 243 435 (1968).

50. Reference 42, p. 59.
51. Czerlinski, G.H., "Chemical Relaxation", Marcel Dekker Inc., N.Y., 1966.
52. Eigen, M., and De Maeyer, L., in "Technique of Organic Chemistry", Vol. VIII, Pt. II, Ed. by Weissberger, A., Interscience, N.Y., 1963, pp. 895-1051.
53. Czerlinski, G., and Eigen, M., Z. Electrochem. 63, 652 (1959).
54. Reference 52, p. 969.
55. Reference 51, p. 221.
56. Diven, W.F., Goldsack, D.E., and Alberty, R.A., J. Biol. Chem. 240, 2437 (1965).
57. Chowdhury, D.M., personal communication.
58. Reference 51, pp. 218-227.
59. Strobel, H.A., "Chemical Instrumentation", Addison-Wesley, Reading, Mass., 1960, p. 165.
60. King, E.L., "How Chemical Reactions Occur", Benjamin, N.Y., 1964, p. 131.
61. Frost, A.A., and Pearson, R.G., "Kinetics and Mechanism", 2nd Ed., John Wiley and Sons, N.Y., 1961, p. 187.
62. Izatt, R.M., Christensen, J.J., Pack, R.T., and Bench, R., Inorg. Chem. 1, 828 (1962).
63. Davies, C.W., J. Chem. Soc. 1938, 1093.
64. Jones, L.H., Inorg. Chem. 2, 777 (1963).
65. Griffith, W.P., Quart. Rev. (London) 16, 188 (1962).
66. Dixon, M., and Webb, E.C., "Enzymes", 2nd Ed., Longmans, London, 1964, pp. 123-125.
67. Ellis, W.D., and Dunford, H.B., Biochemistry 7, 2054 (1968).

68. Alberty, R.A., and Massey, V., *Biochim. Biophys. Acta* 13, 347 (1954).
69. Alberty, R.A., and Hammes, G.G., *J. Phys. Chem.* 62, 154 (1958).
70. Blout, E.R., *Biopolymers, Symp.*, No. 1, 397 (1964).
71. Ulmer, D.D., and Vallee, B.L., *Advan. Enzymol.* 27, 37 (1965).
72. Simmons, N.S., Cohen, C., Szent-Gyorgi, A.G., Wetlaufer, D.B., and Blout, E.R., *J. Am. Chem. Soc.* 83, 4766 (1961).
73. Samejima, T., and Yang, J.T., *J. Mol. Biol.* 8, 863 (1964).
74. Jirgensons, B., *J. Biol. Chem.* 240, 1064 (1965).
75. Breslow, E., Beychok, S., Hardman, K.D., Gurd, F.R.N., *J. Biol. Chem.* 240, 304 (1965).
76. Yang, J.T., and Samejima, T., *J. Biol. Chem.* 238, 3262 (1963).
77. Beychok, S., *Biopolymers* 2, 575 (1964).
78. Brunori, M., Engel, J., and Schuster, T.M., *J. Biol. Chem.* 242, 773 (1967).
79. Ulmer, D.D., and Vallee, B.L., *Biochemistry* 2, 1335 (1963).
80. Urnes, P., and Doty, P., *Advan. Protein Chem.* 16, 401 (1961).
81. *International Critical Tables*, Vol. III, McGraw-Hill, N.Y., 1930, p. 13.
82. Harrison, S.C., and Blout, E.R., *J. Biol. Chem.* 240, 299 (1965).
83. Strickland, E.H., *Biochim. Biophys. Acta* 151, 77 (1968).
84. Ulmer, D.D., *Biochemistry* 4, 902 (1965).

85. Tomimatsu, Y., Vitello, L., and Gaffield, W.,
Biopolymers 4, 653 (1966).
86. Cassim, J.Y., and Yang, J.T., Biochem. Biophys. Res.
Commun. 26, 59 (1967).
87. Kendrew, J.C., Dickerson, R.E., Strandberg, B.E.,
Hart, R.G., Davies, D.R., Phillips, D.C., and Shore,
V.C., Nature 185, 422 (1960).
88. Kendrew, J.C., Watson, H.C., Strandberg, B.E.,
Dickerson, R.E., Shore, V.C., and Phillips, D.C.,
Nature 190, 666 (1961).
89. Beychok, S., and Blout, E.R., J. Mol. Biol. 3, 769
(1961).
90. Urry, D.W., Proc. Nat. Acad. Sci. U.S. 54, 640 (1965).
91. Myer, Y.P., and Harbury, H.A., Proc. Nat. Acad. Sci.
U.S. 54, 1391 (1965).
92. Caughey, W.S., Ann. Rev. Biochem. 36, 611 (1967).
93. Osbahr, A.J., and Eichhorn, G.L., J. Biol. Chem. 237,
1820 (1962).
94. Blumberg, W.E., Peisach, J., Wittenberg, B.A., and
Wittenberg, J.B., J. Biol. Chem. 243, 1854 (1968).
95. Eigen, M., and De Maeyer, L., Z. Electrochem. 59, 986
(1955).
96. Eigen, M., and Kustin, K., J. Amer. Chem. Soc. 82,
5952 (1960).
97. Eigen, M., and Eyring, E.M., J. Amer. Chem. Soc. 84,
3254 (1962).
98. Gould, V., "pH Measurements", John Wiley and Sons,
N.Y., 1956, pp. 34-45.
99. George, P., and Hanania, G., Biochem. J. 52, 517 (1952).

100. George, P., and Hanania, G., *Biochem. J.* 55, 236 (1953).
101. Clever, H.L., *J. Chem. Ed.* 45, 231 (1968).
102. Milburn, R.M., *J. Amer. Chem. Soc.* 79, 537 (1957).
103. Stengle, T.R., and Baldeschwieler, J.D., *Proc. Nat. Acad. Sci. U.S.* 55, 1020 (1966).
104. Stengle, T.R., and Baldeschwieler, J.D., *J. Amer. Chem. Soc.* 89, 3045 (1967).
105. Bryant, R.G., *J. Amer. Chem. Soc.* 89, 2496 (1967).
106. Haughland, R.P., Stryer, L., Stengle, T.R., and Baldeschwieler, J.D., *Biochemistry* 6, 498 (1967).
107. Ward, R.L., and Happe, J.A., *Biochem. Biophys. Res. Commun.* 28, 785 (1967).
108. Abragam, A., "The Principles of Nuclear Magnetism", Clarendon Press, Oxford, 1961, p. 314.
109. Yonetani, T., *J. Biol. Chem.* 242, 5008 (1967).
110. Teale, F.W.J., *Biochim. Biophys. Acta* 35, 543 (1959).
111. Boyer, P.D., *J. Amer. Chem. Soc.* 76, 4331 (1954).
112. Cecil, R., and McPhee, J. R., *Advan. Protein Chem.* 14, 255 (1959).
113. Samejima, T., and Yang, J.T., *J. Biol. Chem.* 238, 3256 (1963).
114. Edmundsen, A.B., and Hirs, C.H.W., *J. Mol. Biol.* 5, 663 (1962).
115. Breslow, E., and Gurd, F.R.N., *J. Biol. Chem.* 238, 1332 (1963).
116. Banaszak, L.J., Watson, H.C., and Kendrew, J.C., *J. Mol. Biol.* 12, 130 (1965).

APPENDIX I. COMPUTER PROGRAMS

This appendix contains user information and listings of the two basic computer programs used throughout the course of the investigations reported in this thesis.

Nonlinear Least-Squares

A nonlinear least-squares program is invaluable for the fitting of data to equations, such as eq 35 of Chapter 3, which contain a large number of adjustable parameters. A nonlinear least-squares program was obtained from the IBM Share Library (SDA 3094) and was modified to use double precision throughout and to run on the University of Alberta IBM 360 computer.

The program contains three subroutines for which the user must supply appropriate Fortran statements. Immediately after the data is read into the computer, the program calls subroutine SUBZ, which may either be left blank or used at the option of the programmer. This subroutine can be used to calculate constants needed in the model equation, or to perform auxiliary calculations, such as conversion of pH to $[H^+]$, before the main program is executed.

Subroutine F CODE contains the model equation to which the data is to be fit. The model must be of the form $F = f(X(I,1), X(I,2), \dots; B(1), B(2), \dots)$, where F predicts the value of the dependent variable Y(I); X(I,1), X(I,2),...

are the independent variables; and $B(1), B(2), \dots$ are the adjustable parameters or the unknown constants of the model equation.

The subroutine P CODE evaluates the analytic derivatives of the model function for the same point just processed by F coding. If analytic derivatives are not supplied, i.e., if P CODE is left blank (and ISW2 is set equal to 1 in input item number 2), the program will estimate values of $\partial F_i / \partial B(I)$ using finite-difference approximations. Initial guesses for the parameters must be different from zero if estimated derivatives are used.

Once the subroutines have been set up, the data cards are prepared as follows:

<u>Input Item Number</u>	<u>Fortran Label</u>	<u>Format</u>	<u>Comment</u>
1	N	I3	no. of data points ($N_{MAX} = 500$)
	K	I3	total no. of parameters ($K_{MAX} = 25$)
	IP	I3	must be zero
	M	I3	no. of independent variables ($M_{MAX} = 10$)
2	ISW1	I3	must be zero
	ISW2	I3	=0, analytic derivatives =1, estimated derivatives
	ISW3	I3	=0, abbreviated print out =1, detailed print out

Detailed print out gives a complete statement of observed

and predicted values of the dependent variables for each new choice of trial values for the parameters.

<u>Input Item Number</u>	<u>Fortran Label</u>	<u>Format</u>	<u>Comment</u>
3	B(1)	D10.0	initial guesses for parameters, 7 per card
	B(2)	D10.0	
	etc.	D10.0	

4. This item consists of N sub-items. Each sub-item is the input data for one observation, punched according to the format 8D10.0. The sequence of variables in a sub-item must be Y(I), X(I,1), X(I,2),... through X(I,M). Each Y(I) must begin on a new card.
5. Any case data read in from subroutine SUBZ should go here.
6. Sequential cases may be stacked by repeating items 1 through 5. A blank card after the last case will cause a normal stop without an error message.

Weighting Modification of the Nonlinear Least-Squares Program

If the observed values of the dependent variable vary by more than one order of magnitude, a "skewed" fit to the data may result if the program is used in its original form. This problem can best be understood by looking at an example. Suppose a series of apparent rate constants exist which are to be fit by a model equation and which vary from

$k(1) = 1.0 \times 10^4$ to $k(10) = 1.0 \times 10^6$, with the experimental errors of all the points equal at about $\pm 10\%$. If the model assumes trial values of the parameters such that the predicted rate constants are $k(1) = 1.1 \times 10^5$ and $k(10) = 1.1 \times 10^6$, the difference between the observed and predicted values in each case is 1.0×10^5 . It is the sum of the squares of these residuals which the program attempts to minimize. However, in the case above, it can be seen that the predicted value of $k(1)$ is 10 times the observed value, but the predicted value of $k(10)$ agrees within 10 % of the observed value. A simple remedy for this inequitable weighting is the following DO loop which is to be inserted into subroutine SUBZ. For this example, it is assumed that the Nth observed dependent variable is the largest and that there is only one independent variable.

```
DO 1 I=1,N
  X(I,2) = Y(N)/Y(I)
1 Y(I) = Y(I)*X(I,2)
```

By this means, we have created a second independent variable which is in reality a weighting factor.

Now, immediately following the statement defining the model in subroutine F CODE should go the statement:

```
F = F*X(I,2)
```

Thus, both the observed and the predicted values have been multiplied by the weighting factor (or in this case, more properly, a normalizing factor). This weighting method is

also applicable if the user wishes to weight the data points according to their experimental uncertainties, etc. One then merely needs to have the weighting factor read in as an independent variable and to use the statements described above, but omitting the middle card of the DO loop.

A listing of the nonlinear least-squares program and its subroutines is found on the following pages.

Polynomial Least-Squares

A polynomial least-squares program, obtained from Dr. J. A. Plambeck, was used for all linear least-squares analyses which were performed. This program is found following the listing of the nonlinear least-squares program; the listing contains user instructions in comment statements at the beginning.

```

C NONLINEAR LEAST SQUARES
C BY D. W. MARGUARDT
C PROGRAMMED BY T. BAUMEISTER III,
C J. ANA SHELDON AND RUBY M. STANLEY
C CONDENSED TO FIT U. OF A. 360 BY W. D. ELLIS

```

```

C DOUBLE PRECISION USED THROUGHOUT
C
C IBKT=1 MEANS USE UPPER A MATRIX
C
C

```

```

C IMPLICIT REAL*8(A-H,O-Z)
C DIMENSION FMT(12),PKNT(5),SPRN(5)
C DIMENSION BS(50),DB(50),BA(50),G(50),W(51),IB(49),SA(50),P(50),A(5
C IC,51),b(50)
C DIMENSION X(500,10),Y(500)

```

```

C -----
C MAX NO OF PARAMETERS IS K=25
C MAX NO OF IND VARS IS M=10
C MAX NO OF OBSERVATIONS IS N=500
C IWHK = -1 MEANS DO ANY SPECIAL INITIALIZING FOR CASE
C IWHK = 0 MEANS START NEW CASE OR END RUN
C IWHK = 1 MEANS GET P S AND F
C IWHK GREATER THAN 1 MEANS GET F ONLY

```

```

C
C NPRNT=0
C 650 IWHK = 0
C 652 GO TO 4
C 653 IWHK = IWHK
C IF (IWHK.GT.C)GO TO 654
C IF (IWHK.EQ.C)GO TO 660

```

```

C 651 CONTINUE
C
C CODING FOR CASE INITIALIZING GUES HERE
C .....
C CALL SUBZ(Y,X,b,PKNT,NPRNT,N)
C .....
C IF (IBOUT.EQ.0) GO TO 652

```

```

0020
0030
0040
0050

```

```

0060
0080

```

```

0090
0100
0110
0120
0130
0140

```

```

0150
0160
0170
0180
0190
0200

```

```

0210
0220
0230
0240
0250
0260
0270

```

```

0280
0290
0300
0310
0320
0330

```



```

C          END OF LAST PROBLEM
C          CUB IN INPUT CONSTANTS IF NOT SUPPLIED
C          ( XL IS CHECKED IN FIRST ITERATION )
0770
1010
1020
1040
1060
1080
1100
1120
1170
1190
1210
1220
1230
1240
1250
1270
1280
1290
1300
1310
1320
1330
1340
1350
1390
1400
1410
1420
1430
1440
1450
1500
1510
1520

C          FF=4.CCCCC0000
C          E=.CCCC05000C
C          TAU=.CC1CC0CC0000
C          T=2.CC00CC00C
C          IBKT=1
C          GAMCK = 4D.
C          DEL=.CC001
C          ZETA=.1E-30
C          XKDB = 1.
C          CONTINUE

C          READ IN INITIAL B GUESSES 7 TO THE CARD
C          READ (5,901)(B(I),I=1,K)
C          DO 50 I=1,N
C          READ (5,931)Y(I),(X(I,L),L=1,M)
C          IWHEK=-1
C          GU TO 653
C          IBKA=1
C          .....
C          START THE CALCULATION OF THE PTP MATRIX
C          .....
C          WRITE (6,907)N,K,IP,M,IFP,GAMCK,DEL,FF,I,E,TAU,XL,ZETA
C          CONTINUE
C          DO 62 I=1,K
C          G (I) =0.CCCCC0000
C          DO 62 J=1,K
C          A (I,J)=C.CC0CC0000
C          GU TO (63,65,65),IBKA
C          IF (1WS5.EQ.0)GU TO 630
C          IFSS3=1WS3
C          IFSS2=1WS2
C          GU TO 70

```

```

1550
1560
1570
1580
1620
1700
1740
1750
1760
1770
1780
1790
1800
1810
1820
1870
1880
1890
1900
1910
1920
1930
1960
2010
2020
2050
2040
2050
2060
2070
2100
2120
2150
2160

65 IFSS2=0
   GO TO 70
69 IFSS3=1
70 WRITE (6,908)(B(J),J=1,K)
   IF (IFSS3.EQ.C)GO TO 73
68 WRITE( 6,910)
73 I=1
   PHJ=0.00000000
   IF (IFSS2.EQ.0) GO TO 57
   GO TO 600
72 IF (IFSS2.EQ.1)GO TO 602
   THIS IS THE ANALYTICAL P S ROUTINE
C
57 IWHER=1
   GET P S AND F
   GO TO 653
75 GO TO 80
C
C
C ..... THIS IS THE ESTIMATED P S ROUTINE .....
600 CONTINUE
602 IWHER=3
   GO TO 653
606 FWS=F
   J=1
618 CBW=B(J)*DEL
   TWS=B(J)
   B(J)=B(J)+CBW
   IWHER=4
   GO TO 653
620 B(J)=TWS
   P(J)=(F-FWS)/CBW
622 J=J+1
   IF ((J-K).LE.0) GO TO 618
624 F=FWS
C
C ..... END OF ESTIMATED P S ROUTINE .....

```

```
C      80 DO 82 JJ=1,K
      G(JJ)=G(JJ)+(Y(I)-F)*P(JJ)
      DO 82 II=JJ,K
      A(II,JJ)=A(II,JJ)+P(II)*P(JJ)
      82 A(JJ,II)=A(II,JJ)
      318 WS=Y(I)-F
      IF (IFSS3.EQ.0) GO TO 314
      310 WRITE (0,525)Y(I),F,WS
      314 WS=Y(I)-F
      PHI=PHI+WS*WS
      I=I+1
      IF (I.LE.N) GO TO 72
      88 GO TO (90,7C4,7C6),IBKA
      C      SAVE SQUARE ROOTS OF DIAGONAL ELEMENTS
      50 DO 52 I=1,K
      52 SA(I)=DSQRT(A(I,I))
      DO 106 I=1,K
      DO 100 J=1,K
      WS = SA(I)*SA(J)
      IF(WS.GT.0.) GOTO 98
      96 A(I,J) =C.CCCCC000
      GO TO 100
      98 A(I,J)=A(I,J)/WS
      100 CONTINUE
      IF(SA(I).GT.0.) GOTO 104
      102 G(I)=C.CCCCC000
      GO TO 106
      104 G(I)=G(I)/SA(I)
      106 CONTINUE
      DO 110 I=1,K
      110 A(I,I)=1.00000000
      PHIZ=PHI
      C      WE NOW HAVE PHI ZERU
      1132 DO 1133 II=1,K
      2170
      2180
      2190
      2200
      2210
      2220
      2900
      2910
      2930
      3020
      3030
      3040
      3050
      3130
      3140
      3150
      3160
      3170
      3180
      3190
      3200
      3210
      3220
      3230
      3240
      3250
      3260
      3270
      3280
      3290
      3300
      3310
      3320
      3330
      3380
```

```
III=II+25
DO 1133 JJ=1,K
1133 A(III, JJ)=A(II, JJ)
C .....
IF (ITCT.GT.C)GO TO 163
C FIRST ITERATION
150 CONTINUE
152 XL=C.OCCCCOCCCO
154 ITCT=1
DO 161 J=1,K
161 BS(J)=B(J)
C BS(J) CORRESPONDS TO PHIZ
163 IBKI=1
WS=N-K+IP
SE=DSVRT(PHIZ/WS)
IF (IFSS3.GT.C)GO TO 165
162 IF (IFSS2.EQ.C) GO TO 168
167 WRITE (6,911)PHIZ,SE,XLL,GAMMA,XL
GO TO 169
168 WRITE (6,912)PHIZ,SE,XLL,GAMMA,XL
GO TO 169
165 IF (IFSS2.EQ.C)GO TO 1661
166 WRITE (6,903)PHIZ,SL,XL
GO TO 169
1661 WRITE (6,909)PHIZ,SE,XL
169 GO TO 200
164 PHIL=PHI
C WE NOW HAVE PHI LAMBDA
DO 170 J=1,K
IF(DABS(DB(J))/(DABS(B(J))+TAU)).GE.E) GO TO 172
170 CONTINUE
WRITE (6,923)
GO TO 700
172 IF (IWS5.EQ.O)GO TO 172C
1720 IF (IWS4.EQ.O)GO TO 173
IF (IWS4.EQ.1)GO TO 171
```

3390

3400

3410

3420

3440

3450

3460

3470

3480

3490

3500

3510

3520

3530

3540

3550

3560

3570

3610

3620

3660

3670

3680

3720

3730

3770

3780

3790

3800

3810

3820

3830

3870

3880

3910

3920


```

IWS4=IWS4-1
GU TO 173
171 WRITE (6,924)
GC TO 700
173 XKDB = 1.0CCCC000
IF (PHIL.GT.PHIZ)GC TO 190
174 XLS=XL
DU 176 J=1,K
BA(J)=B(J)
176 B(J)=BS(J)
IF (XL.GT..CCCC0001)GU TO 175
1175 DU 1176 J=1,K
b(J)=bA(J)
1176 BS(J)=B(J)
GU TO 6C
175 XL=XL/10.
IBK1=2
GU TO 200
177 PHL4=PHI
C
IF (PHL4.GT.PHIZ) WE NOW HAVE PHI(LAMBDA/10)
GU TO 184
182 DG 183 J=1,K
183 BS(J)=b(J)
GU TO 60
184 XL=XLS
DO 186 J=1,K
BS(J)=BA(J)
186 B(J)=BA(J)
GU TO 60
190 IBK1=4
XLS=XL
XL=XL/10.
DG 185 J=1,K
185 B(J)=BS(J)
GU TO 200
187 IF (PHI.LE.PHIZ)GU TO 196

```

3930
3940
3950
3990
4000
4010
4020
4030
4040
4050
4060
4070
4080
4081
4090
4100
4110
4120
4130
4140
4150
4160
4170
4180
4190
4200
4210
4220
4230
4240
4250
4260
4270
4280
4290
4300

```

191 XL=XL5
    IBK1=3
192 XL=XL*10.
195 DO 193 J=1,K
193 B(J)=BS(J)
    GO TO 200
194 PH14=PH1
C
18C IF (PH14.GT.PH1Z)GO TO 198
196 DO 197 J=1,K
197 BS(J)=B(J)
    GO TO 60
198 IF (GAMMA.GE.GAMCR)GO TO 192
199 XKDB = XKDB/2.
    DO 1199 J=1,K
    IF (PABS(DB(J))/(LABS(B(J))+TAU)).GE.E) GO TO 195
1199 CONTINUE
    DO 1200 J=1,K
1200 B(J)=BS(J)
    WRITE (6,934)
    GO TO 700
C
C .....
C SET UP FOR MATRIX INVERSION
C .....
200 CONTINUE
1102 DO 1103 II=1,K
    III=II+25
    DO 1103 JJ=1,K
1103 A(II,JJ)=A(III,JJ)
1104 DO 202 I=1,K
202 A(I,I)=A(I,I)+XL
C GET INVERSE OF A AND SOLVE FOR DB (J)S
    IBKM=1
C .....
C THIS IS THE MATRIX INVERSION ROUTINE
C K IS THE SIZE OF THE MATRIX

```

4310
4320
4330
4340
4350
4360
4370
4380
4390
4400
4410
4420
4430
4440
4450
4460
4470
4480
4490
4500
4540
4550
4560
4570
4620
4630
4640
4650
4660
4670
4680
4690
4700
4710
4720

```
404 CALL GJR(A,K,ZETA,MSING)
GU TO (415,65C), MSING
415 GU TO (416,71C), IBKM
C      END OF MATRIX INVERSION, SOLVE FOR DB(J)
416 DO 420 I=1,K
      DB(I)=0.0000000
      DO 421 J=1,K
421  DB(I)=A(I,J)*G(J)+DB(I)
420  DB(I)=XKDB*DB(I)
      XLL=C.00000000
      DTG = 0.0000000
      GTG = 0.0000000
      DO 250 J=1,K
      Db(J)=Db(J)/SA(J)
      DTG = DTG + Db(J)*G(J)
      GTG = GTG + G(J)**2
      b(J)=b(J)+DB(J)
250  XLL=XLL+DB(J)*DB(J)
      KIP=K-IP
      IF (KIP.EQ.1) GO TO 1257
      CGAM=DTG/USRT(XLL*GTG)
      JGAM = 1
      IF(CGAM.GT.0) GOTO 253
251  CGAM = DABS(CGAM)
      JGAM = 2
253  GAMMA = 97.2957795*(1.5707268+CGAM*(-0.2121144+CGAM*(0.074261
      1-CGAM*.0187293)))*USRT(1.-CGAM)
      GO TO (257,255), JGAM
255  GAMMA = 180.00000-GAMMA
      IF (XL.LT.1.0)GO TO 257
1255  WRITE(6,922)XL,GAMMA
      GU TO 700
1257  GAMMA=C.0000000
257  XLL=USRT(XLL)
      IBK2=1
      GU TO 300
4730
4740
4750
4760
4770
4780
4790
4800
4810
4820
4830
4840
4850
4860
4870
4880
4890
4900
4910
4920
4930
4940
4950
4960
4970
4980
4990
5000
5010
5020
5030
5070
5080
5090
5100
5110
```

```

252 IF (IFSS3.EQ.0)GU TO 256
254 WRITE (6,904)(DB(J),J=1,K)
      WRITE (6,905)PHI,XL,GAMMA,XLL
256 GU TO (164,177,194,187),IBK1
C
C ..... CALCULATE PHI .....
C
300 I=1
      PHI=0.0000000
      IWBK=2
      IF (IWS5.EQ.0) GU TO 653
302 GU TO 653
304 PHI=PHI+(Y(I)-F)**2
      I=I+1
      IF (I.LE.N) GU TO 302
316 GU TO (252,780,704,760,772),IBK2
C
C ..... THIS IS THE CONFIDENCE LIMIT CALCULATION .....
C
700 DO 702 J=1,K
702 B(J)=BS(J)
      WRITE (6,933)N,K,IP,M,FF,I,E,TAU
      IBKA=2
      GU TO 60
704 GU TO 706
706 WS=N-K+IP
      SE=USGKT(PHI/WS)
      PHIZ=PHI
      IF (IFSS2.EQ.0)GU TO 709
707 WRITE (6,903)PHIZ,SE,XL
      GU TO 708
709 WRITE(6,909) PHIZ,SE,XL
      NOW WE HAVE MATRIX A
C
708 CONTINUE

```

5120
5130
5170
5210

5220
5230
5240
5250
5260
5270

5280
5310
5320
5330
5340
5350

5360
5370
5380
5390
5400
5410

5420
5460
5470

5530
5540
5550
5560
5570
5610
5620

5660

```

1122 DO 1123 I1=1,K
111=I1+25
DO 1123 JJ=1,K
1123 A(I1,JJ)=A(I1,JJ)
1124 IBKM=2
GU TO 404

C
C
C
710 CALL      NGW WE HAVE C = A INVERSE
      PART1(K,A,IBOUT,SA,SE,DS,T,ETEST1,FF,IP)
      IF (ETEST1.EQ.1.0) GU TO 05C

C
      IF (1WS6.EQ.1) GU TO 05C
      WS=K-1P
      WS1=N-K+1P
      PKN=WS/WS1
      PC=PHI/Z*(1.+FF*PKN)
      WRITE (6,920)PC
      WRITE (6,921)
      IFSS3=1
      DO 790 J=1,K
      IBKP=1
      DO 752 JJ=1,K
752  B(JJ)=BS(JJ)
758  UD=-1.00000000
      IBKN=1
      U=DU
      B(J)=BS(J)+U*SA(J)
      IBK2=4
      GU TO 300
762  PH11=PH1
      IF (PH11.GE.PC)GU TO 770
764  U=U+DU
      IF (U/UD.GE.5.)GU TO 788
765  B(J)=BS(J)+U*SA(J)
      IBK2=5
      GU TO 300

```

```

5710
5720
5730
5740
5750
5760
5770
5780
6660
6670
6680
6690
6700
6710
6720
6760
6800
6810
6820
6830
6840
6890
6900
6910
6920
6930
6940
6950
6960
6970
6980
6990
7000
7010

```

766	PHID=PHI	7020
	IF (PHID.LT.PC)GO TO 704	7030
	IF (PHID.GE.PC) GO TO 778	7040
770	D=D/2.	7050
	IF (U/DU.LE..001)GO TO 788	7060
771	B(J)=BS(J)+0*SA(J)	7070
	IBK2=6	7080
	GU TU 300	7090
772	PHID=PHI	7100
	IF (PHID.GT.PC)GO TO 770	7110
778	XK1=PHI2/U+PHI1/(1.-D)+PHID/(D*(D-1.))	7120
	XK2=-((PHI2*(1.+U)/U+D/(1.-D))*PHI1+PHID/(D*(D-1.)))	7130
	XK3=PHI2-PC	7140
	BC=(USGRT(XK2*XK2-4.*XK1*XK3)-XK2)/(2.*XK1)	7150
	GC TU (779,784),IBKN	7160
779	B(J)=BS(J)-SA(J)*BC	7170
	GU TU 701	7180
784	B(J)=BS(J)+SA(J)*BC	7190
781	IBK2=2	7200
	GU TU 300	7210
780	GC TU (782,786),IBKN	7220
782	IBKN=2	7230
	DD=1.C0000000	7240
	BL=B(J)	7250
	PL=PHI	7260
	GU TU 760	7270
786	BU=B(J)	7280
	PU=PHI	7290
	GU TU (783,795,785,769),IBKP	7300
783	WRITE (6,918) J, BL, PL, BU, PU	7310
	GU TU 790	7350
795	WRITE (6,915) J, BU, PU	7360
	GU TU 790	7400
785	WRITE (6,918)J,BL, PL	7410
	GU TU 790	7450
789	WRITE (6,914)J	7510

```

GU TO 790
788 GU TO (791,792),LBKN
C DELETE LOWER PRINT
791 IBKP=2
GU TO 780
792 GU TO (793,794),LBKP
C DELETE UPPER PRINT
793 IBKP=3
GU TO 780
C LOWER IS ALREADY DELETED, SU DELETE BOTH
794 IBKP=4
GU TO 780
790 CONTINUE
GU TO 10
C .....
900 FURMAT (2513)
901 FURMAT (7E10.0)
903 FURMAT (/13X,4H PHI 14X,4H S E 9X,7H LAMBDA 6X,
9031 25H ESTIMATED PARTIALS USED / 5X,2D18.8, D13.3 )
904 FURMAT(/12H INCREMENTS 5D18.8/(12X,5D18.8) )
905 FURMAT (13X,4H PHI 10X,7H LAMBDA 6X,7H GAMMA 6X, 7H LENGTH /
9051 5X, D18.8, 3D13.3)
907 FURMAT( 5H1N = 13,5X,5H K = 13,5X,5H P = 13,5X,5H M = 13,5X,
9071 7H IFF = 13,5X,13HGAMMA CRIT = D10.3,5X,6HDEL = D10.3/6H FF =
9072D10.3,5X,5H I = D10.3,5X,5H E = D10.3,5X,7H TAU = D10.3,5X,6H XL =
9073 D10.3 , 4X, 7HZETA = D10.3 /)
908 FURMAT(/12H PARAMETERS 1P5D18.8/(12X,1P5D18.8))
909 FURMAT (/13X,4H PHI 14X,4H S E 9X,7H LAMBDA 6X,
9091 25H ANALYTIC PARTIALS USED /5X, 2D18.8, D13.3)
910 FURMAT(1H /5X,9X,4H OBS 13X,5H PKED 13X,5H DIFF )
911 FURMAT (/13X,4H PHI 14X,4H S E 11X,7H LENGTH 6X, 7H GAMMA 6X,
9111 7H LAMBDA 6X, 25HESTIMATED PARTIALS USED /5X, 2D18.8, 5D13.3)
912 FURMAT (/13X,4H PHI 14X,4H S E 11X,7H LENGTH 6X, 7H GAMMA 6X,
9121 7H LAMBDA 6X, 24ANALYTIC PARTIALS USED /5X, 2D18.8, 3D13.3)
914 FURMAT(2X,13,12H NONE FOUND )
915 FURMAT(2X,13,36X,2D18.8 )

```

7550

7560

7570

7580

7590

7600

7610

7620

7630

7640

7650

7660

7670

7680

7690

7700

7710

7720

7730

7740

7750

7760

7770

7780

7790

7800

7810

7820

7830

7840

7850

7860

7870

7880

7890

7900

7920

7930

```

518 FORMAT(2X,I3,1P5E16.8)
520 FURMAT(1H/1H/3CH NUNLINEAR CONFIDENCE LIMITS / /
5201 16H PHI CRITICAL = D15.8 )
521 FURMAT(1H / 6H PARA 6X,8H LOWER B 8X,10H LOWER PHI 10X,8H UPPER B
5211 8X,1CH UPPER PHI )
522 FURMAT(18H GAMMA LAMBDA TEST,5X,2E13.3)
523 FURMAT(14H EPSILON TEST )
524 FURMAT(11H FORCE OFF )
525 FURMAT(5X,6E18.8/59X,2D16.8)
529 FURMAT(1CAL)
530 FURMAT(7D16.0)
531 FURMAT(8E16.C)
533 FURMAT(5HIN = I3,5X,5H K = I3,5X,5H P = I3,5X,5H M = I3,5X,
5331 / 6H FF = E10.3,5X,5H T = E10.3,
5332 5X,5H E = D16.3,5X,7H TAU = D10.3 / )
534 FURMAT(19H GAMMA EPSILON TEST )
      END

```

```

7960
6000
8010
8020
6030
6040
6050
8060
6070
8110
8120
8130
8150
6160
6170
8180
8210

```

```

C
SUBROUTINE PART1(K,A,IBOUT,SA,SE,BS,I,LEST1,FF,IP)
THIS SUBROUTINE IS SIMPLY A CHUNK OUT OF THE MAIN
IMPLICIT REAL*8(A-H,U-Z)
DIMENSION A(50,51),SA(50),BS(50)

```

```

710 DO 711 J=1,K
      IF(A(J,J).LT..0) GO TO 713
711 SA(J)=USQRT(A(J,J))
      GO TO 715
713 IBOUT=1
715 KST=-4
      WRITE(6,916)
234 KST=KST+5
      KEND=KST+4
      IF (KEND.LT.K) GO TO 719

```

```

5790
5800
5810
5820
5830
5840
5650
5880
5890
5900

```



```

KEND=K
719 DO 712 I=1,K
712 WRITE (6,916)I,(A(I,J),J=KST,KEND)
IF (KEND.LT.K) GO TO 234
IF (IBOUT.EQ.0) GO TO 717
WRITE (6,936)
EESTI=1.0
GO TO 650
717 DO 718 I=1,K
DO 718 J=1,K
WS=SA(I)*SA(J)
IF(WS.GT. 0.) GOTO 716
714 A(I,J)=C.CCCCCCCC
GO TO 718
716 A(I,J)=A(I,J)/WS
718 CONTINUE
DO 720 J=1,K
720 A(J,J)=1.CCCCCCCC
WRITE (6,917)
KST=-9
721 KST=KST+10
KEND=KST+9
IF (KEND.LT.K) GO TO 722
KEND=K
722 DO 724 I=1,K
724 WRITE (6,935)I,(A(I,J),J=KST,KEND)
IF (KEND.LT.K) GO TO 721
C
GET T*SE*SQRT(C(I,I))
DO 726 J=1,K
726 SA(J)= SE*SA(J)
1112 DO 1113 II=1,K
111=II+25
DO 1113 JJ=1,K
1113 A(II,JJ)=A(II,JJ)
1114 CONTINUE
740 WRITE (6,919)
5910
5920
5960
5970
5980
5990
6020
6030
6040
6050
6060
6070
6080
6090
6100
6110
6120
6130
6170
6180
6190
6200
6210
6220
6260
6270
6280
6290
6300
6350
6360
6370
6380
6390
6400
```

```

WS=K-IP
DO 750 J=1,K
743 HJTL=DSQRT(WS*FF)*SA(J)
STE=SA(J)
CPL=BS(J)-SA(J)*T
CPU=BS(J)+SA(J)*T
SPL=BS(J)-HJTL
SPU=BS(J)+HJTL
WRITE ( 6,927)J,STE,CPL,OPU,SPL,SPU
750 CONTINUE
916 FURMAT(1H /13H PTP INVERSE )
917 FURMAT(1H /30H PARAMETER KORRELATION MATRIX )
918 FURMAT( 2X,15,1P5D18.8)
919 FURMAT( 1H /1H / 13X,4H STD 17X, 16H LNE - PARAMETER 21X,
9191 14H SUPPORT PLANE / 3X, 2H D 7X,6H ERKOR 12X, 6H LOWER 12X,
9192 6H UPPER 12X, 6H LOWER 12X, 6H UPPER )
927 FURMAT(2X,13,1P5D18.8)
935 FURMAT (3X,15,2X,10F10.4)
936 FURMAT (27HC NEGATIVE DIAGONAL ELEMENT )
650 RETURN
END

C
SUBROUTINE GJK(A,N,EPS,MSING)
GAUSS-JORDAN-RUTISHAUSER MATRIX INVERSION WITH DOUBLE PIVOTING.
IMPLICIT REAL*8(A-H,O,R-Z)
DIMENSION A(50,50),B(50),C(50),P(50),Q(50)
INTEGER P,Q
MSING=1
DO 10 K=1,N
C
DETERMINATION OF THE PIVOT ELEMENT
0020
0030
0040
0050
0060
0070
0080
6440
6450
6500
6510
6520
6530
6540
6550
6560
6620
7940
7950
7960
7970
7980
7990
8090
8190
8200

```

```
PIVGT=0.
  DO 20 I=K,N
  DO 20 J=K,N
    IF(DABS(A(I,J))-ABS(PIVGT))20,ZC,30
  30 PIVGT=A(I,J)
    P(K)=I
    W(K)=J
  20 CONTINUE
  IF (ABS(PIVGT)-EPS)40,40,50
  EXCHANGE UP THE PIVOTAL ROW WITH THE NTH ROW
  50 IF(P(K)-K)60,80,60
  60 DO 70 J=I,N
    L=P(K)
    Z=A(L,J)
    A(L,J)=A(K,J)
    A(K,J)=Z
  70 A(K,J)=Z
  EXCHANGE UP THE PIVOTAL COLUMN WITH THE KTH COLUMN
  80 IF(Q(K)-K)85,90,85
  85 DO 100 I=1,N
    L=W(K)
    Z=A(I,L)
    A(I,L)=A(I,K)
    A(I,K)=Z
  90 CONTINUE
  C
  JORDAN STEP
  DO 110 J=1,N
    IF(J-K)130,120,130
  120 B(J)=1./PIVLT
    C(J)=1.00000000
    GO TO 140
  130 B(J)=-A(K,J)/PIVUT
    C(J)=A(J,K)
  140 A(K,J)=0.00000000
  110 A(J,N)=0.00000000
  DO 10 I=1,N
  DO 10 J=1,N
```

```
10 A(I,J)=A(I,J)+C(I)*B(J) 0450
C REORDERING THE MATRIX 0460
  DO 155 M=1,N 0470
    K=N-M+1 0480
    IF(P(K)-K)160,170,160 0490
    160 DO 160 I=1,N 0500
      L=P(K) 0510
      Z=A(I,L) 0520
      A(I,L)=A(I,K) 0530
    180 A(I,K)=Z 0540
    170 IF(Q(K)-K)190,155,190 0550
    190 DO 150 J=1,N 0560
      L=Q(K) 0570
      Z=A(L,J) 0580
      A(L,J)=A(K,J) 0590
    150 A(K,J)=Z 0600
    155 CONTINUE 0610
    151 RETURN 0620
    40 PRINT 40,P(K),Q(K),PIVOT 0630
    45 FORMAT(16HOSINGULAR MATRIX3H I=13,3H J=13,7H PIVOT=D16.8/) 0640
    MSING=2 0650
    GO TO 151 0660
  END 0670
```

```
SUBROUTINE SUBZ(Y,X,B,PRNT,NPRNT,N)
IMPLICIT REAL*8(A-H,O-Z)
DIMENSION Y(500),X(500,10),B(50),PRNT(5)
RETURN
END
```

```
SUBROUTINE FCODE(Y,X,B,PRNT,F,I)
  IMPLICIT REAL*8(A-H,O-Z)
  DIMENSION Y(500),X(500,10),B(50),PRNT(5)
  RETURN
END
```

```
SUBROUTINE PCODE(P,X,B,PRNT,F,I)
  DIMENSION P(50),X(500,10),B(50),PRNT(5)
  RETURN
END
```

```
C THIS IS A GENERAL PROGRAM FOR LEAST SQUARE POLYNOMIAL FIT
C FORTRAN IV MODIFICATION OF OUI LSWI FOR 360 OPERATION
C
C DOUBLE PRECISION USED THROUGHOUT
C
C LIST OF SYMBOLS USED FOR INPUT
C N= NUMBER OF POINTS
C M= NC. OF COEFFICIENTS OF PLY
C N1= NO. OF ADDITIONAL POINTS AT WHICH EVALUATION OF FITTING
C     PLY. IS DESIRED. MAX. N1=50
C L= NC. OF DATA SETS TO BE FIT SIMULTANEOUSLY. L=1-4
C IEVAL= SIGNAL TO OUTPUT. IF IEVAL>0, A TABLE OF THE INPUT
C     DATA WITH PLY EVALUATIONS AND RESIDUALS IS PRINTED
C X= INDEPENDENT VARIABLE
C W= WEIGHTING FACTOR. USE 1.0 FOR EQUAL WEIGHTING
C Y= DEPENDENT VARIABLE
C X1= EXTRA X AT WHICH PLY IS TO BE EVALUATED
C
C IMPLICIT REAL*8(A-H,O-Z)
C DIMENSION A(20,15), B(20,4), X(500), Y(500,4), W(500), SUM(4),
C     X
C     RESID(500,4), STD(15,4), EVAL(500), XI(50)
C
C 1 READ (5,1000) N, M, N1, L, IEVAL
C IF (N) 1,1,2
C DO 3 I = 1,N
C 3 READ (5,2000) X(I), W(I), Y(1,1),Y(1,2),Y(1,3),Y(1,4)
C IF (N1) 5,5,4
C 4 READ (5,2000)(XI(I), I = 1,N1)
C 5 CALL LSWI(X,Y,W,RESID,N,SUM,L,A,B,M)
C     DEG = N - M - 1
C     DO 6 I = 1,M
C     DO 6 J = 1,L
C
C 6 STD(I,J) =DSQRT(SUM(J) * A(I,1)/DEG)
C WRITE (6,3000) N, M, N1, L
C DO 7 I = 1,M
```

```
7 WRITE (6,40CC) (A(I,J), J = 1,M)
DO 8 J = 1,L
WRITE (6,50CC) (B(I,J), STD(I,J), I = 1,M)
WRITE (6,60CC) SUM(J)
IF (IEVAL) 11,11,9
9 DO 10 I = 1,N
10 EVAL(I) = RESID(I,J) + Y(I,J)
WRITE (6,70CC) (X(I),W(I),Y(I,J),EVAL(I),RESID(I,J),I = 1,N)
11 IF (NI) 8,8,12
12 DO 13 I = 1,N1
13 EVAL(I) = PLY(X1(I),M,B,J,20,4)
WRITE (6,80CC) (X1(I), EVAL(I), I = 1,N1)
8 WRITE (6,50C0)
GO TO 1

1000 FURMAT (12I6)
2000 FURMAT (6U12.C)
3000 FURMAT (48H1
LEAST SQUARE POLYNOMIAL FIT USING LSQ1 /
M=12,0H NI=12,5H L=12/13HOLEKKUR MATRIX)
X 3HON=13,5H
4000 FURMAT (1HG1P8U14.5)
5000 FURMAT (37HC
COEFFICIENT ERROR/(1H 1P2D20.7))
6000 FURMAT (36HCWEIGHTED SUM OF SQUARED DEVIATIONS=1PUI3.5)
7000 FURMAT (70HC
X WEIGHT EVALUATI
RESIDUAL/(1F 1P5U14.5))
XLN
8000 FURMAT (29HC EXTRA X EVALUATION/(1H 1P2D14.5))
9000 FURMAT (54H -----)
END
```

```
SUBROUTINE LSQ1(X,Y,W,RESID,N,SUM,L,A,B,M)  
IMPLICIT REAL*8(A-H,O-Z)  
DIMENSION X(500),Y(500,1),RESID(500,1),A(20,15),B(20,1),C(500,15),  
XSUM(1),W(500)
```

C

```
COMMON C
```

C

```
DC 1 I = 1,N  
1 C(I,1) = 1.CCCCCCCCCC  
DO 2 J = 2,M  
DO 2 I = 1,N  
2 C(I,J) = C(I,J - 1) * X(I)  
DO 3 I = 1,M  
DO 3 J = 1,M  
A(I,J) = C.CCCCCCCCCC  
DC 3 K = 1,N  
3 A(I,J) = A(I,J) + C(K,I) * C(K,J) * W(K)  
DO 4 J = 1,L  
DC 4 I = 1,M  
B(I,J) = 0.CCCCCCCCCC  
DO 4 K = 1,N  
4 B(I,J) = B(I,J) + C(K,I) * Y(K,J) * W(K)  
CALL MAINV (A,M,B,L,DETERM)  
DC 6 J = 1,L  
SUM(J) = C.CCCCCCCCCC  
DO 6 I = 1,N  
RESID(I,J) = POLY(X(I),M,B,J,20,1) - Y(I,J)  
6 SUM(J) = SUM(J) + RESID(I,J)**2*W(I)  
RETURN  
END
```



```
C
C MATRIX INVERSION WITH ACCOMPANYING SOLUTION OF LINEAR EQUATIONS
C
C SUBROUTINE MATINV(A,N,B,M,DETERM)
C
C IMPLICIT REAL*8(A-H,U-Z)
C DIMENSION IPIVOT(20), A(20,20), B(20,1), INDEX(20,2), PIVOT(20)
C COMMON PIVOT,INDEX, IPIVOT
C EQUIVALENCE (IRCW,JROW), (ICOLUM,JCOLUM), (AMAX,T,SWAP)
C
C INITIALIZATION
C
C DETERM = 1.00000000
C DO 20 J = 1,N
C 20 IPIVOT(J) = 0
C DO 55C I = 1,N
C
C SEARCH FOR PIVOT ELEMENT
C
C AMAX = 0.00000000
C DO 105 J = 1,N
C IF(IPIVOT(J) - 1) 60,105,60
C 60 DO 100 K = 1,N
C IF (IPIVOT(K) - 1) 80,100,740
C 80 IF(DABS(AMAX) -DABS(A(J,K))) 85,100,100
C 85 IRCW = J
C ICOLUM = K
C AMAX = A(J,K)
C 100 CONTINUE
C 105 CONTINUE
C IPIVOT(ICOLUM) = IPIVOT(ICOLUM) + 1
C
C INTERCHANGE ROWS TO PUT PIVOT ELEMENT ON DIAGONAL
C
C IF (IKOW - ICOLUM) 140,200,140
C 140 DETERM = -DETERM
```

```
DU 200 L = 1,N
SWAP = A(IRLW,L)
A(IRKW,L) = A(ICCLUM,L)
200 A(ICCLUM,L) = SWAP
IF (M) 260,26C,210
210 DO 250 L = 1,M
SWAP = B(IRLW,L)
B(IRKW,L) = B(ICCLUM,L)
250 B(ICCLUM,L) = SWAP
260 INDEX(I,1) = IRKW
INDEX(I,2) = ICCLUM
PIVOT(I) = A(ICCLUM,ICCLUM)
DETERM = DETERM * PIVOT(I)
C
C DIVIDE PIVOT ROW BY PIVCT ELEMENT
C
A(ICCLUM,ICCLUM) = 1.000000000
DU 350 L = 1,N
350 A(ICOLUM,L) = A(ICCLUM,L)/PIVCT(I)
IF (M) 380,38C,360
360 DU 370 L = 1,M
370 B(ICOLUM,L) = B(ICCLUM,L)/PIVCT(I)
C
C REDUCE NONPIVCT ROWS
C
380 DO 550 LI = 1,N
IF(LI - ICCLUM) 400,550,400
400 T = A(LI,ICCLUM)
A(LI,ICOLUM) = 0.0
DU 450 L = 1,N
450 A(LI,L) = A(LI,L) - A(ICCLUM,L) * T
IF (M) 550,55C,460
460 DO 500 L = 1,M
500 B(LI,L) = B(LI,L) - B(ICCLUM,L) * T
550 CONTINUE
C
```

C INTERCHANGE COLUMNS
C

```

DO 710 I = 1,N
L = N + 1 - I
IF (INDEX(L,1) - INDEX(L,2)) 630,710,630
630 JKRW = INDEX(L,1)
JCOLUM = INDEX(L,2)
DO 705 K = 1,N
SWAP = A(K,JKRW)
A(K,JKRW) = A(K,JCOLUM)
A(K,JCOLUM) = SWAP
705 CONTINUE
710 CONTINUE
740 RETURN
END

```

```

REAL FUNCTION PLY(X,M,COEFF,J,MK,MC)
IMPLICIT REAL*8(A-H,O-Z)
DIMENSION COEFF(MK,MC)
PLY = 0.0
DO 1 N = 1,M
MA = M - N + 1
1 PLY = PLY * X + COEFF(MA,J)
RETURN
END

```

APPENDIX II

PURIFICATION OF HRP USING SEPHADEX GELS

The purity of HRP is commonly expressed in terms of a Reinheitszahl, RZ, or purity number, PN. This quantity is determined by taking the ratio of the absorbance of the maximum of the Soret peak (403 m μ) to that of the maximum of the protein peak (280 m μ). The maximum RZ for HRP is 3.04¹⁴. HRP is commercially available from Boehringer-Mannheim Corp., N. Y., in two forms: purified grade, at about \$45.00/g, with an RZ of about 0.8; and analytical reagent grade, at about \$1000.00/g, with an RZ ranging from 2.9 to 3.0. This study was undertaken to provide HRP of an intermediate purity for the studies described in Chapter 5 and to determine if the crude HRP could be economically and easily purified. An earlier qualitative study by another worker in this laboratory, Raymond Segal, indicated that Sephadex gels would provide a useful medium for the purification of HRP.

Preparation of Gels and Columns

Two types of Sephadex gels were used in the purification tests: G-75, a molecular-sieve with a molecular weight fractionation range of 1000-50,000; and C-50 CM-Sephadex, which is a carboxymethyl derivative of Sephadex that functions as a cation exchanger. The two types of Sephadex

were prepared for use in the following manner: 3.5 g of G-75 and 1.5 g of CM were each allowed to swell for 24 hours in about 150 ml of phosphate buffer of pH 6.2 and μ equal to 0.1, with three changes of supernatant liquid to ensure complete equilibration. Approximately 50 ml of each type of swollen gel were obtained.

Chromatographic columns were constructed using 50 ml burets. A small plug of glass wool was placed at the bottom of the column and some 3 mm diameter glass beads were placed on top of the glass wool. The columns were filled by pouring a slurry of the gel into the column. After a layer of gel a few centimeters thick had formed at the bottom, the outlet was opened to aid settling. Each column was filled until it had a bed length of about 50 cm. In the case of the CM column, the bed length was not constant, since the size of the gel network is a function of ionic strength. The columns were flushed with 25 ml of buffer prior to addition of the sample. Because the gel bed compacted, the flow through the column was quite slow even with the stopcocks completely open, and further, it was not completely constant throughout the duration of the separation. These studies were conducted with the stopcocks of the columns completely open, with flow rates of the order of 0.5 ml/min.

Purification and Performance of the Columns

The concentration of the purified grade (RZ = 0.77) HRP was determined spectrophotometrically to be 7.6×10^{-4} M using light of 497 m μ and a molar absorptivity value⁵ of $1.00 \times 10^4 \text{ M}^{-1} \text{ cm}^{-1}$. One ml of the purified grade HRP was added to each column and when the solution drained to the top of the bed, two ml of pH 6.2 phosphate buffer, $\mu = 0.1$, were added. The buffer did not acquire any brownish color characteristic of the HRP solution, which indicated that all of the HRP had been adsorbed on the columns.

The HRP was eluted through the G-75 column entirely with buffer of ionic strength 0.1, but with the CM column, the ionic strength was gradually increased from 0.1 to 0.2 to aid the separation. Fractions of effluent were collected from the columns and the concentration of HRP in each fraction was determined spectrophotometrically. The results of the single column purifications are shown in Tables XI and XII. After the fourth fraction of HRP was collected from the G-75 column, the column showed no brown coloration. However, after the fifth fraction was collected from the CM column, there remained a small brown band at the top of the column, and the entire column had a slightly brownish tinge. The top band started to move only after the ionic strength of the buffer was increased to approximately 0.5 by addition of potassium nitrate. By using buffer of ionic strength up to 0.8, the CM column was completely cleaned of

Table XI

Purification of Crude HRP on a G-75 Sephadex Column

<u>Fraction</u>	<u>Ml</u>	<u>Moles x 10⁸</u>	<u>RZ</u>	<u>% Yield*</u>
1	2.6	5.0	0.4	6.6
2	5.0	52.5	1.6	69.2
3	4.0	14.8	0.9	19.5
4	3.4	2.5	0.2	<u>3.3</u>
				98.6

Table XII

Purification of Crude HRP on a CM-Sephadex Column

<u>Fraction</u>	<u>Ml</u>	<u>Moles x 10⁸</u>	<u>RZ</u>	<u>% Yield*</u>
1	2.7	5.3	1.9	7.0
2	5.6	34.7	2.8	45.8
3	2.9	14.1	2.7	18.6
4	3.0	4.4	1.8	5.8
5	4.6	1.5	0.6	2.0
6	6.0	3.0	0.2	<u>3.9</u>
				83.1

* 7.58×10^{-7} moles of HRP, RZ = 0.77, were added initially.

all traces of brownish material.

After dialysis to get rid of KNO_3 and buffer, the spectrum of fraction number six (the slow fraction) from the CM column was examined. The Soret peak of this fraction had a maximum at the same wavelength (403 m μ) as the other fractions, but exhibited a more gradual decrease of absorbance with decreased wavelength. The higher absorbance on the UV side of the peak may be due to the very intense protein peak in this fraction (RZ = 0.2).

In order to ascertain if this technique can be used to obtain fractions purer than those shown in Tables XI and XII, part of fraction number two from the G-75 column was passed through the CM column. It was felt that the two types of columns used in series might be more effective than a second passage through the same column. 1.16×10^{-7} moles of G-75 fraction number two were added to the CM column and eluted as described above; the results are shown in Table XIII.

Table XIII

Further Purification of G-75 Purified HRP on a CM Column

<u>Fraction</u>	<u>Ml</u>	<u>Moles x 10⁸</u>	<u>RZ</u>	<u>% Yield*</u>
1	2.6	1.92	2.74	16.5
2	2.6	3.22	2.98	27.8
3	2.6	2.15	2.86	18.5
4	2.6	0.75	2.26	<u>6.5</u>
				69.3

* 1.16×10^{-7} moles of HRP, RZ = 1.6, were added initially.

As before, a small band was left at the top of the column. This band was not collected because of its small size. If one calculates the yield from the original crude HRP, fraction number two of the doubly purified HRP amounted to 19.2 % of the original, and fraction number three 12.8 %. These two fractions combined represented 32 % yield from the original purified grade HRP used, with a corresponding purification from $RZ = 0.77$ to $RZ = 2.93$.

Although no attempt was made to maximize either purification or yield through variation of flow rates, column lengths, etc., it has been clearly demonstrated in this study that HRP can be purified easily with good yields using Sephadex gels.